Aus dem Institut für Physik, Universität Potsdam.

Second-order nonlinear optical interactions and cascading effects in thin organic films

Dissertation

zur Erlangung des akademischen Grades

"doctor rerum naturalium"

(Dr. rer. nat.)

in der Wissenschaftsdisziplin

"Physik der Kondensierten Materie"

eingereicht an der
Mathematisch-Naturwissenschaftlichen Fakultät
der Universität Potsdam

von
Viachaslau Ksianzou
Geboren am 21-09-1976 in Zhodino, Belarus

Potsdam, den 21.03.2010

Published online at the
Institutional Repository of the University of Potsdam:
URL http://opus.kobv.de/ubp/volltexte/2010/4918/
URN urn:nbn:de:kobv:517-opus-49186
http://nbn-resolving.org/urn:nbn:de:kobv:517-opus-49186

Introduction

Optical technologies have the exclusive potential to increase the rates of data communication. They are scaling with advances in lasers, optical fibres and optical coding technologies. Bringing the benefits of broadband communications to European citizens presents both the challenge and the rewards for the next generation of photonic systems. Part of the challenges now is to achieve cost, size, integration and performance levels well beyond even today's telecom grade components into datacom footprints and cost range and to make their use simple for the system integrator. This means to implement more intelligent components, so that they can configure themselves, for instance, in wavelength, bit rate and dispersion.

Optical signal processing has the potential to realize high-speed and high capacity processing at speeds which are 100 to 1000 times faster than that achievable with conventional electronic signal processing. This is a key enabling technology for ultra high-speed networks, into the multi-terabit per second regime.

There are two complementary areas of optical signal processing - the realization of "optical in, optical out" network elements such as regenerators of repeaters and the more futuristic optical computing, which could apply to a wide range of applications, including real-time digital signal processing for military and security, real-time video compression, as well as network functions such as header processing and error correction.

One of the core challenges for the realization of all optical networks is the cost effective all optical generator, capable of regeneration, reshaping and retiming (3R). Breakthrough designs and technologies for achieving this in a multiwavelength configuration will have a major impact.

A recent report of Optoelectronics Industry Development Association for 2015 shows:

•The network bit rates will be dominated by 40 Gbps in the core and 10 Gbps in metro areas, while higher rates will go in.

•Total transmission capacity per carrier will be in the 100 Tbps range.

•All optical processing can be viewed as the key enabling technology for very high bit rates beyond 160 Gbps, where electronic solutions will become impractical. Many functional elements are required such as Arrayed Wave Guides (AWGs) and integrated elements for photon control, wavelength/dispersion management and ultimately photon storage, improvements in switching technologies both in the spatial and wavelengths domains. Realisation of a photonic memory may also play a critical role here.

From all those fascinating challenges the present work is addressing mainly aspects of importance for photonic switching.

Photonics as a field of science began in 1960 with the invention of the laser, as well as the invention of the laser diode in 1970 with following development of fibre optic communication systems. Similarly to electronics, photonics can be characterized as a branch of physics and technology associated with radiation detection, behaviour, and consequences of the existence and destruction of photons.

In the last decades, there has been an increase in speed of computers and data lines together with a miniaturization of electronic components. As result, a transition from electronics in direction to photonics is required both in the processing and in the data transfer. The future of photonics lies in the integration of waveguides into silicon chips and the coupling of glass and polymer waveguides to silicon chips for direct transmission of light signals from the laser sources through the optical waveguides to the chip, where the signals are processed. This is incomparably faster than the neat electrical signal processing and resulting information can easily be transmitted through the optical transmission lines into the common data network.

Integrated optics is the technology of integrating various optical devices and components for generating, focusing, splitting, combining, isolating, polarisation, coupling, switching, modulating, and detecting light, all on a single substrate (chip). Optical waveguides provide the connection between these components[1].

In recent years, compact integrated circuits have been developed and implemented in optical information systems where signal transport is realized at optical wavelengths. For instance, automotive industry needs fast, flexible, and lightweight replacements for on-board electronics. In this case, the use of polymer optical fibres (POFs) for data communication between working elements can reduce the weight of cars. For data processing, various integrated photonic components can be combined with optical fibres. Traditionally, such integrated photonic devices are based on nonlinear optical crystals like Lithium Triborate[2,3]. However, many commercial applications require properties that are not realizable by use of nonlinear crystals.

In this work, doped polymer layers were selected as a base for realization of photonic devices. Specially prepared dye-doped polymers can provide much higher second-order nonlinearities in comparison to inorganic crystals. That allows fabrication of small and fast switchers, modulators and logical elements. Reviewing commercial applications one can note an increasing role of small ultrafast devices utilizing poled dye-doped polymers[4-11]. In modern electro-optic devices, data rates above 165 Gbits/s are realized with the help of nonlinear polymer waveguides[12-15].

Cross-phase modulation (XPM) is a nonlinear optical effect where one wavelength of light can affect the phase of another wavelength of light through the optical Kerr effect. XPM can be used as a technique for adding information to a light stream by modifying the phase of a coherent optical beam with another beam through interactions in an appropriate non-linear medium. It is well known that the Kerr effect is a third-order nonlinear optical process. This means it can be observed in media with high value of third-order susceptibility. As a rule to observe third order nonlinear optical effects one needs light intensities higher than in case of linear optics and even higher than in case of second order nonlinear optical processes.

To avoid problems like photochemical degradation connected with high light intensities necessary to induce third-order effects, one can use the concept of parametric multi-step nonlinear processes developed by Armstrong, Blombergen at. al.[16]. This concept is called “cascading” and includes several second-order nonlinear phenomena, which simultaneously appear in media, but which are observed as higher-order effects, e.g. third-order effects. Cascading processes exist in all non-centrosymmetric media like nonlinear crystals, but the most efficient effects are observed in specially prepared inhomogeneous structures. Inducing spatial periodic modulation of second-order susceptibility one can produce special structures, which fulfil the so-called Quasi Phase Matching (QPM) condition. Although QPM is a well-known technique in nonlinear optics[17-20], the particular case of organic nonlinear materials and especially the waveguide geometry have not been investigated extensively. In comparison to bulk materials the waveguide geometry has several advantages: e.g. a high concentration of light energy and a long interaction length allowing the use of light sources with low intensity.

To reach phase matching for ordinary fabricated waveguides one should take care about dispersion and geometrical parameters of the core layer. Nevertheless, QPM allows to fulfil phase and amplitude conditions for any predefined set of waveguide core parameters[21] simultaneously. In this work, own mathematical software was developed and implemented with the aim to optimize QPM properties of waveguides. Using Finite Element Analysis (FEA) the stability of models was analyzed. Numerical simulations were used to understand how perturbations influence the development of phase and amplitude of the travelling waves.

Waveguides used at optical wavelengths are typically dielectric ones. They are structures in which a dielectric material with high refractive index is surrounded by a dielectric material with lower refractive index. Waveguiding is based on the phenomenon of total internal reflection. In the present work, organic waveguides are of special interest. The core material of these waveguides consists of an organic material (most commonly a polymer). The advantages of polymer-made waveguides are their low production costs and their easy processability. In addition, polymers can be used to fabricate different optical elements (prisms, Bragg-mirrors) which makes them very promising for integrated optics[22,23]. Such photonic components made of polymers can be easily combined with elements like optical fibres[24-26].

As was mentioned above, the optical nonlinearity of waveguides can be utilized for realizing ultrafast switching or light modulation. High energy densities necessary for nonlinear applications can easily be provided in the core of waveguides over the whole waveguide length. However, a high energy density includes additional requirements towards material quality. From the fabrication point of view, optical losses and their origin must be investigated and minimized before devices fabrication. A further direction of optimization is the increase of the nonlinearity by use of special materials so that the same effect can be achieved at low light intensities. The optimization process includes at least two different components: molecular engineering of nonlinear active molecules and improvement of the efficiency of wave interaction producing the nonlinearity.

Another direction of research was the application of nonlinear optical effects to the characterization of thin films and interfaces. Since nonlinear properties of materials are defined by their internal structure, they can be considered as sensitive tools for their analysis. For instance, in the present work several new types of vacuum-deposition organic films were developed. Further analysis of the second harmonic generation was used to obtain information about morphology, multilayer formation, microcrystal orientation, types of aggregation, and about charge transport processes[27-30].

The scope of the present work is the investigation of second-order nonlinear optical processes within planar polymer waveguides and interfaces. Both the maximization of efficiency of nonlinear phenomena and the understanding of inter- and intra- molecular processes, which occur within the layers or at their interfaces, have been central issues. The whole work is a combination of theoretical and experimental approaches and can be divided in to three major parts:

Description of linear and second-order-nonlinear properties of the used materials;

Analysis of regularities and attempts to predict characteristics of new compound;

Modelling of light propagation in nonlinear inhomogeneous media with specially fabricated structure, resulting in some unusual properties.

Based on this the present work has the following structure:

In the first chapter, methods of deposition of dye-doped polymer films are discussed. Various techniques are discussed and compared — spin-coating, dip-coating, drop-casting, and vacuum deposition. Although all of these techniques are well known, it remains a challenge to develop the reliable fabrication know-how in processing and patterning of polymeric materials. An important problem, which occurred during preparation of multilayer structures by combining a dip-cast buffer layer and a spin-coated core, results in the penetration of solvent into the lower layer from the upper layer. To overcome this problem, one can deposit the upper layer in vacuum.

The second chapter describes experimental methods of inducing second-order nonlinearities in waveguides as well as relevant properties of waveguides, ranging from optimal poling conditions, second harmonic conversion efficiency to the possibility of pulse shape distortion during high intensity light propagation in the waveguide. Complementary to the experimentally obtained properties of the waveguides, FEA was used to estimate properties of energy exchange between fundamental and second harmonic waves within different kinds of waveguides. In addition, some aspects of electro optics, such as the distribution of the electrical field within integrated photonic elements were investigated.

The third chapter deals with the nonlinear properties of single molecules. Using Ab-initio[31,32] and semi-empirical[33,34] methods of quantum chemistry the charge transfer in donor-acceptor molecular system, in our case dye-polymer systems were investigated. Applying the so-called two-level model[35,36], high-order hyperpolarisabilities responsible for molecular nonlinearities were calculated for a series of dyes. Additional to the widely used inorganic nonlinear materials, various combinations of dyes and polymers have been analyzed e.g. DR1 PMMA (Disperse Red 1; Polymethylmethacrylate) and a series of newly synthesized dyes. From more than twenty of these nonlinear dyes, only three have shown sufficient performance after testing. Some of them, being suitable for use in the infrared range, have shown too high losses in the visible range. A similar situation can be described for the matrix polymers.

In the fourth chapter the improvement of linear and nonlinear optical properties of dye-doped polymer films by means of selection of appropriate matrix polymers is described. It shows that the optimal polymer for poled films must not only be transparent but also have high glass transition temperature and low conductivity even while being doped with dye molecules. The solubility is also important for the formation of smooth layers.

The fifth chapter introduces one of the new techniques of poling: Fibonacci-type poling. This technique is used for a further optimization of light conversion in organic waveguides. The nonlinear optical domains along the waveguide are defined according to the Fibonacci law. In this case, more than one nonlinear optical process can simultaneously be realized.

The sixth chapter describes several devices utilizing the concept introduced in Chapter 5, for instance photonic devices based on the Mach-Zehnder interferometer. The possibility of utilization of new concepts, including Fibonacci-poled waveguide and quasi-phasematching structures is discussed in more details. Nonlinear phase-shift based on second order cascading processes for use in various photonic applications is also analyzed in detail.

A short summary at the end highlights the most important contributions of this work and possible directions of further research based on them.

Preparation, characterization and properties of materials for optical waveguides

Fabrication of transparent polymer films

Vacuum deposition

Vacuum deposition provides good thickness control, optical quality and purity of obtained films. By that technique, one can cover large area substrates. However, only a limited number of polymers is able to form films by means of vacuum deposition. On the other hand, insoluble polymers can be deposited only by this technique. By simultaneous deposition of two materials (co-deposition) with different refractive indices, gradient-index structures can be obtained. Co-deposition is helpful for creating a polymer by polycondensation reaction from precursor units or for forming dye-polymer or dye-metal composite systems, as well. Moreover, it sometimes is the only way to create a buffer between soluble polymer layers in complex multilayer structures. Thermal vacuum deposition is easy to realize: the substrate is placed in a vacuum chamber and a small amount of the coating polymer or its precursors are vaporised into the chamber. The monomeric units, e.g. formed by radical depolymerisation of the polymer, or the co-evaporated precursor units (in case of a polycondensation reaction) condense on the substrate forming a uniform polymer coating. Many of such layers can be built up, with controlled optical properties to produce cladding, core and upper cladding at a single technological process. Combining polymer deposition with deposition of metal electrodes, one can fabricate various electro-optic devices. The vacuum deposition of metals can be described by general thermodynamic rules.

The direction of a physical process (or chemical reaction) at constant pressure and for a given temperature is defined by a free energy change ΔG which must have a negative value to reach a new equilibrium state. The change of free energy at constant pressure and temperature is given by:

$$\Delta G = \Delta H - T\Delta S \qquad [1.1]$$

where ΔH and ΔS are the corresponding enthalpy and entropy changes and T is the absolute temperature. Although during condensation in vacuum $\Delta S < 0$ because fewer atomic configurations exists in the solid, the change of enthalpy ΔH is negative and its absolute value higher than the contribution of the second right hand term. Hence, the net change in ΔG is negative[37].

In this work, two widely used methods of vacuum deposition were used, thermal (resistive) heating and electron-beam evaporation. The metal layers (mostly electrodes) were deposited by thermal deposition. As introduced above, a new technology for vacuum deposition of polymer films was used: vacuum deposition polymerisation (VDP). Thin layers of polytetrafluoroethylene (PTFE) have been prepared by using polymer pieces as solid source of material. Then a combined application of thermal and electron beam evaporation to this solid source led first to decomposition of the polymer via the mechanism of radical depolymerisation, then to electron-beam assisted activation of the formed fragments towards chemically active radicals, and finally to their condensation followed by radical polymerisation to the polymer on the substrate. As a result, thin, pinhole free polymer films have been obtained. Their thickness could be varied between the nm and the μm range.

The uniformity of the obtained films is essential for most optical applications. However, a point source for evaporation can, in case of plane substrates, only produce films having a certain variation of the thickness as schematically shown in Fig. 1.

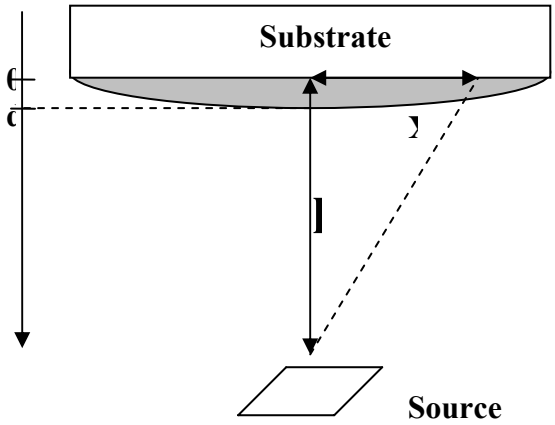

Fig. 1: Film thickness distribution on a substrate as a function of the substrate-source distance and in dependence on source type (point or surface source).

The normalized thickness of the layer for a point source is given by[38] (see Fig. 1):

$$\frac{d}{d_0} = \frac{1}{\left[1+\left(\frac{x}{h}\right)^2\right]^{3/2}} \qquad [1.2]$$

where d_0 is the thickness at the centre of the sample.

Similarly, for a plane surface source with large lateral extension we have:

$$\frac{d}{d_0} = \frac{1}{\left[1+\left(\frac{x}{h}\right)^2\right]^{2}} \qquad [1.3]$$

In this work, the substrate had a square shape with a size of 2.54x2.54 cm^2 (1 sq. inch), and the distance between source and substrate was ca. 10 cm (~4 inches). That gives 97.6% of thickness at the edges of the sample in comparison to the centre of the sample for a point source and 96.9% when the source is of surface-type.

Spin-coating of organic films

Spin coating was the method of choice for polymer film deposition. The polymer was dissolved in a proper solvent, and in case of preparation of polymer chromophore composite films, mixed with a certain amount of chromophore. The polymer solution was spread over the substrate surface. Subsequent fast rotation (spinning) of the substrate forms a thin undoped or doped polymer film which solidifies during spinning by evaporation of the solvent. The properties of the obtained film (specific chromophore concentration and thickness) can precisely be controlled during film deposition and by tuning the rotation speed: the higher the angular speed of spinning, the thinner the film. Commercial spin-coating solutions (usually cladding materials) are supplied with spin-coating curve (layer thickness versus rotation speed)[39].

Preparation by spin coating requires careful post-processing. To remove residual solvent one has to anneal the film at temperatures above the boiling temperature of the solvent (preferably in vacuum). During annealing, one can control the surface quality by means of the

setup shown in Fig. 2, where a sensitive photodiode with large aperture collects scattered light from the annealed sample. A significant reduction of scattered light (10%-15%) was observed for all of the prepared polymer films, during the annealing process.

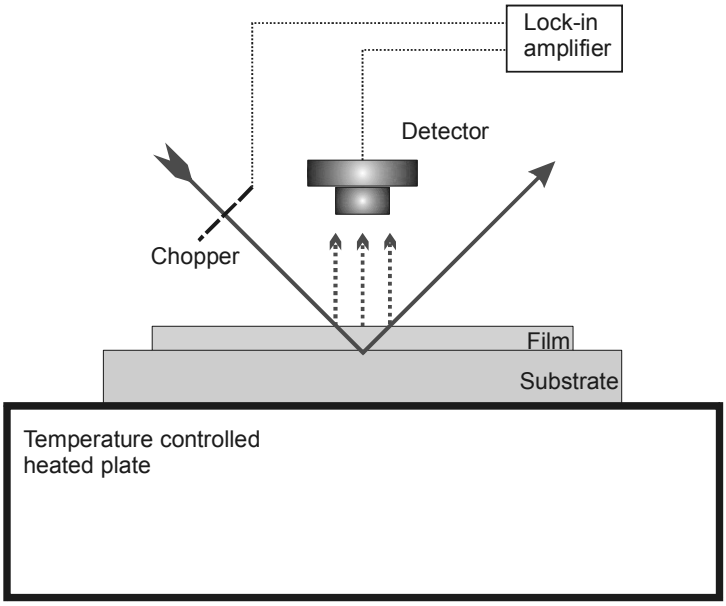

Fig. 2: Setup for control of the annealing process by measurement of scattered light intensity. The detector is thermally isolated (stabilized) to prevent thermal distortions.

The control of the annealing process should prevent undesired thermal decomposition of chromophores or degeneration of the polymer layer by a proper limitation of annealing temperature.

Other techniques

The idea of transferring molecular monolayers from the water-surface to solid substrates was proposed by Dr. Irving in 1917. Eighteen years later, in 1935 Dr. Katherine Blodgett had improved the technique by stacking several monolayers on top of each other so that multilayer films can be created. Since then, Langmuir-Blodgett (LB) films have been used for a wide variety of scientific experimentation for studying of the properties of monolayer of amphiphilic molecules that contain both a hydrophobic and hydrophilic domain (e.g. soaps and detergents). The LB trough allows investigators to prepare a monolayer of amphiphilic molecules on the surface of a liquid, and then compress or expand these molecules on the surface, thereby modifying the molecular density, or area per molecule. The monolayer's effect on the surface pressure of the liquid is measured through use of a Wilhelmy plate, electronic wire probes, or other types of detectors. An LB film can then be transferred to a solid substrate by dipping the substrate through the monolayer.

Complex refractive index of optical materials

Real part of refractive index

One of the main requirements for core materials used in light waveguides, beside transparency, optical homogeneity, thermal and UV-resistance is an appropriate refractive index, higher than that of the used cladding material. In that regime, where absorption can be ne-

glected the optical behaviour of a material is characterized by the real part of the index of refraction. Its dispersion in the VIS-NIR range can be described by the so-called Sellmeier formula:

$$n^2(\lambda) = 1 + \sum_{i=1}^{n} \frac{A_i \lambda^2}{\lambda^2 - B_i} \qquad [1.4]$$

This formula was originally derived by Sellmeier in 1871 as an extension of Cauchy's theory of optical dispersion[40].

As we found from experiment, refractive index of most chromophore-polymer composites in the transparent range (visible-near infrared) can be described by a simplified formula:

$$n^2(\lambda) = n_\infty^2 + \frac{q}{\lambda^2 - \lambda_0^2} \qquad [1.5]$$

Formally, Eq. [1.5] can be derived from Eq. [1.4] by setting $A_i = 0$ for $i > 3$, $B_1 = B_3 = 0$, $A_3 = -A_2$, $1+A_1=n_\infty^2$, $B_2 = \lambda_0^2$, and $A_2 \cdot B_2 = q$. The quantity n_∞ represents the limiting value of refractive index at infinite wavelength, and λ_0 the resonance wavelength. In the approximation of Eq. [1.5] only one resonance is taken into account. In order to perform measurements of dispersion in the range from 532 nm to 1550 nm the values of the refractive index in this region were obtained with a step of 100-150 nm. The Root Mean Square (RMS) deviation Δn_{RMS} between refractive indices n_λ measured and n_λ calculated, respectively, is calculated according to the following formula:

$$\Delta n_{RMS} = \sqrt{\frac{1}{N} \sum_{i=1}^{N} \left(n_{\lambda_i}^{measured} - n_{\lambda_i}^{calculated} \right)^2} \qquad [1.6]$$

The obtained value $\Delta n_{RMS}=0.0005$ is comparable with the precision of the measurements. According to this criterion, a one- resonance model is acceptable. Our system showed a Δn_{RMS} better than 10^{-3}, which corresponds to the precision of the used prism-coupling method.

When the resonance wavelength λ_0 (related to the band gap E_g) for dielectric materials lies in the UV range, the dispersion in the visible range can also be described by the Cauchy formula, which is a particular case of the Sellmeier formula [1.4]:

$$n(\lambda) = n_0 + \frac{n_1}{\lambda^2} + \frac{n_2}{\lambda^4} \qquad [1.7]$$

where n_0, n_1 *and* n_2 are called *Cauchy* parameters.

Another traditional way to quantify the refractive index dispersion of transparent materials is the Abbe number ν_d, defined by

$$\nu_d = \frac{n_d - 1}{n_F - n_C} \qquad [1.8]$$

with n_d, n_F and n_C being the refractive indices at three standard wavelengths (yellow helium d-line at 0.58756 μm, blue hydrogen F-line at 0.48613 μm, and red hydrogen C-line at 0.65627 μm, respectively).

Absorption and imaginary part of refractive index

When absorption cannot be neglected, a more complete description of the optical properties of the material is provided by the complex index of refraction:

$$\tilde{n} = n - i\kappa \qquad [1.9]$$

Where n is the real part of refractive index, describing wave propagation while κ, the imaginary part, describes the attenuation of the wave.

The Kramers-Kronig relations connect the real part of a complex function to an integral containing the imaginary part of this function and vice versa. The relations are named in honour of Ralph Kronig and Hendrik Anthony Kramers. These relations can be used in optics to calculate the refractive index of a material by the measurement of the absorbance, which is better accessible. The Kramers-Kronig relations can be expressed in case of complex refractive index $\tilde{n}$ as[41]:

$$n(\omega) = 1 + \frac{2}{\pi} P\int_0^\infty \frac{\omega'\kappa(\omega')}{\omega'^2 - \omega^2} d\omega' \qquad [1.10]$$

$$\kappa(\omega) = \frac{2\omega}{\pi} P\int_0^\infty \frac{n(\omega') - 1}{\omega'^2 - \omega^2} d\omega' \qquad [1.11]$$

where P stands for the principal value integral.

Forohui and Bloomer[42,43], deduced an expression for the energy dependence of the refractive index $n(E)$ based on a one-electron model extended to amorphous materials.

$$n(E) - n(\infty) = \frac{1}{\pi} P\int_{-\infty}^{\infty} \frac{\kappa(E') - \kappa(\infty)}{E' - E} dE' \qquad [1.12]$$

Here E is the energy of the incoming photon, E' is the integration variable in energy, $n(\infty)$ represents the limiting value of n at high energy, $\kappa(\infty)$ is the respective value of imaginary part of refractive index at high energies, and $\kappa(E')$ is the measured energy dependent κ value. The integration is carried out over the whole energy (wavelength) range covered by the experiment. Energy values and their signs are defined relatively to vacuum level.

In case of thin films, the imaginary part of the refractive index can be obtained as function of angular frequency of light ω according to:

$$\kappa(\omega) = \frac{cA(\omega)}{2d\omega\log_{10} e} \Rightarrow \kappa(\lambda) = \frac{\lambda A(\lambda)}{4\pi d\log_{10} e} = 0.18323\frac{\lambda}{d}A(\lambda) \qquad [1.13]$$

where $A(\omega)$ is the measured absorbance, d is the sample thickness and c is the speed of light.

$$A(\omega) = \log_{10}\frac{I_0(\omega)}{I(\omega)} \qquad [1.14]$$

$I_0(\omega)$ is the light intensity before and $I(\omega)$ at angular frequency behind the sample. For measurements that are more precise the absorbance has to be corrected with respect to losses due to the Fresnel reflection at the interfaces and to scattering losses.

As proposed by Forohui and Bloomer[42,43], $n(E)$ is then found according to a modified formula, which is based on [1.10] and [1.11]:

$$\kappa(E) = \frac{A(E - E_g)^2}{E^2 - BE + C} \qquad [1.15]$$

and

$$n(E)-1=\frac{B_0E+C_0}{E^2-BE+C} \qquad [1.16]$$

where

$$B_0=\frac{A}{Q}\left[-\frac{B^2}{2}+E_gB-E_g^2+C\right] \qquad [1.17]$$

$$C_0=\frac{A}{Q}\left[\left(E_g^2+C\right)\frac{B}{2}-2E_gC\right] \qquad [1.18]$$

and

$$Q=\frac{1}{2}\sqrt{4C-B^2}\ . \qquad [1.19]$$

If E_g, A, B, C, B_0, C_0, are determined from the experimental absorption data and using a nonlinear least-square curve fitting program, the real part of the index of refraction n can be calculated.

The spectral dependence of the dispersion of the index of refraction is usually described as a polynomial in powers of the wavelength by Sellmeir's equation [1.4].

Optical losses in light waveguides

When light propagates within a waveguide, loss of energy certainly occurs. Some of those losses are determined by properties of the bulk materials from which the waveguide is made. This type of losses can be predicted by measurements of bulk material properties (absorption, homogeneity). However, some losses are defined only by geometry of the waveguide.

Attenuation

The loss of light intensity during wave propagation is called *attenuation*. This characteristic quantity includes all types of losses. In any waveguide, attenuation is defined as:

$$L\left[\frac{dB}{cm}\right]=\frac{\alpha}{z}=\frac{1}{z}10\log_{10}\left(\frac{P(z)}{P(0)}\right) \qquad [1.20]$$

where $P(z)$ is the power transmitted over a distance z.

In fact the attenuation expresses only a relation between input and output power without any relation to mechanisms causing the losses. The range of the practically observed values in waveguides is varying from a few dB/cm to several dB/km. As example, the minimum loss in the best silica-glass fibres is 0.3 dB/km at 1.5 μm. Devices, due to their short length (few mm or cm) are not so demanding. Embedding chromophores in a polymer can increase losses from this point of view. We obtained an average loss value of 0.8-0.9 dB/cm at 632 nm for spin-coated guest-host polymer films. The main reason for that are significant absorption and inhomogeneities of the multi-component system. Nonlinear optics requires materials that are even more lossless due to necessity to embed active molecules (chromophores) in polymeric transparent matrices. Second-order nonlinear processes as a rule include two wavelengths. In this case and in case of cascading, where a third wavelength can be involved, the influence of absorption has to be taken carefully into account on each wavelength.

Scattering losses

The origin of scattering losses can be described in a simplified approach by using geometrical optics. Although it is a crude approximation, it allows to explain most of the results and to find ways for reduction of losses. The optical beam performs multiple reflections during propagation as can be seen in Fig. 3. Some part of the energy penetrates into the cladding material through the cladding-core interface. The roughness of this surface decreases the efficiency of total internal reflection and reduces the overall guiding effect.

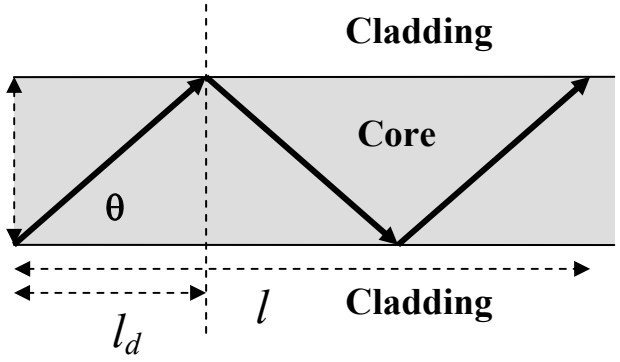

Fig. 3: Light propagation in a waveguide. Geometrical optics description includes multiple reflections at the core-cladding interfaces.

The number of reflections N_r can easily be obtained by simple geometrical considerations and achieves easily a number of a few thousands over several centimetres as can be derived from equation [1.21]. Moreover, scattering occurs at each reflection.

$$N_r = \frac{l}{l_d} = \frac{l}{d}\tan\theta, \;\; with \;\; l_d = \frac{d}{\tan\theta} \qquad [1.21]$$

θ is the so-called bouncing angle, d is the thickness of the core. One has to take into account that scattering occurs at each reflection. The scattering losses on surfaces are described by the Rayleigh criterion[44]:

$$\alpha_1 = \frac{P_{reflected}}{P_{incident}} = \exp\left[\left(\frac{4\pi\sigma}{\lambda}\sin\theta\right)^2\right] \qquad [1.22]$$

where σ is the root mean square (RMS) surface roughness. When a polymer film is deposited on a glass substrate, the roughness σ includes both film surface roughness σ_1 (glass-air border) and glass surface roughness σ_2 (glass-film border) which can be taken into account by the following relation:

$$\sigma = \sqrt{\sigma_1^2 + \sigma_2^2} \qquad [1.23]$$

The bouncing angle θ can be found from the expression:

$$\theta = \arccos\frac{n_{eff}}{n_{core}} \qquad [1.24]$$

For instance, a polyphenylquinoxaline film with thickness of 1 μm and bulk refractive index n=1.76 deposited on BK7 glass has an effective refractive index of 1.74 at 633 *nm* for the

TE0 mode. That corresponds to $\theta = 8.65$ degrees. According to [1.21] the light is reflected N_r=1521 times per *cm* of propagation length. On every reflection, the Rayleigh losses are 0.02%. The average roughness of spin-coated films was determined to be 5 nm. Scattering losses over the distance *l* accumulate as:

$$\alpha = \alpha_1^{N_r} \qquad [1.25]$$

Finally, one can write losses per length as:

$$L = \left[\frac{dB}{cm}\right] = \frac{1}{l} 10 \log_{10} \frac{P(0)}{P(z)} \qquad [1.26]$$

It has to be pointed out that moving into the IR the total amount of the scattering losses is reduced. Our typical value for this type of losses is 1.3 dB/cm at 633 nm. As follows from [1.26] this reduces to approximately 1-1.3 dB/cm at the 3-rd telecommunication window (1550 nm). Therefore, a thick film has fewer reflections than a thin film, and as a result, smaller losses per unit length by Rayleigh scattering at interfaces.

Absorption losses

The absorption of cladding and core material can be taken into account by extending the refractive indices to complex numbers. The effective wave-vector of each mode will contain loss information. The electrical fieldstrength of a travelling wave can be expressed as:

$$E(z,\omega) = Ae^{i(\omega t - \tilde{k}_{eff} z)} + c.c. = Ae^{\mathrm{Im}(\tilde{k}_{eff})z} e^{i(\omega t - \mathrm{Re}(\tilde{k}_{eff})z)} + c.c = A' e^{i(\omega t - \mathrm{Re}(\tilde{k}_{eff})z)} + c.c$$
$$\left[A' = Ae^{\mathrm{Im}(\tilde{k}_{eff})z}, \mathrm{Im}(\tilde{k}_{eff}) < 1\right] \qquad [1.27]$$

where the effective wave-vector $\tilde{k}_{eff}$ includes the refractive index in the real part and losses in the imaginary part:

$$\tilde{k}_{eff} = \mathrm{Re}\left[\tilde{k}_{eff}\right] - i\,\mathrm{Im}\left[\tilde{k}_{eff}\right] = \frac{\omega}{c} n_{eff} - i\delta, \qquad [1.28]$$

where δ is the damping per unit length (attenuation), and ω is the angular eigenfrequency of the waveguide mode. n_{eff} is the real part of the effective refractive index, *A* is the wave amplitude. The complex index of refraction can be obtained by various methods, for instance by means of ellipsometry.

The intensity attenuation in dB per length is calculated using the formula:

$$\left(\frac{\Delta_{dB}}{z}\right) = 20\delta \log_{10} e \qquad [1.29]$$

Often the absorption losses of material are measured directly using a spectrophotometer. Typically, the sample is a slice of the investigated material with a thickness *d*. Then the attenuation δ can be expressed as a value proportional to the absorbance per propagation distance (absorption):

$$\delta = \frac{1}{2\log_{10} e} \frac{A(\lambda_0)}{d} \qquad [1.30]$$

In practice, the values in dB are often in use. Setting *d* = *z* one can rewrite [1.29] as:

$$\left(\frac{\Delta_{dB}}{z}\right) = 10\frac{1}{z}\log_{10}\frac{I_0}{I} = 10\frac{A(\lambda_0)}{z} \qquad [1.31]$$

$A(\lambda_0)$ is the absorbance $A(\lambda) = \log_{10}\frac{I_0(\lambda)}{I(\lambda)}$ at wavelength λ_0.

For measurements with high precision, the Fresnel reflections from both surfaces must be taken into account.

Other types of losses

The cutoff frequency of an electromagnetic waveguide is the lowest frequency for which a waveguide mode will propagate. In fibre optics, it is more common to consider *the cutoff wavelength*, the maximum wavelength that will propagate in an optical fibre or waveguide.

Relatively large dye molecules, sometimes containing several benzene rings, create local inhomogeneities within the polymer matrix having a refractive index different from the rest of the matrix and can convert light frequency, e.g by frequency doubling. In this case, losses occur when some amount of light is converted into other modes either having another bouncing angle or a frequency above the cut-off frequency as shown in (Fig. 4).

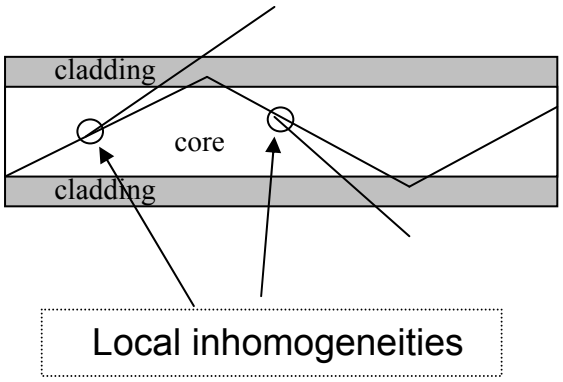

Fig. 4: Local inhomogeneities lead to transfer of energy into higher-order modes that have high losses due to deeper penetration of light into the cladding material. If a deviation of propagation direction is high enough, the condition of total internal reflection is no more valid and waveguiding does not exist for such a beam.

Even high-order modes with frequencies below cut-off frequency as a rule decrease attenuation in the waveguide. As seen in (Fig. 5) a significant part of light energy is concentrated in the cladding and the area around it. When the cladding is thin (for instance in Plastic Optical Fibres – POF) the light intensively scatters on cladding-air interface.

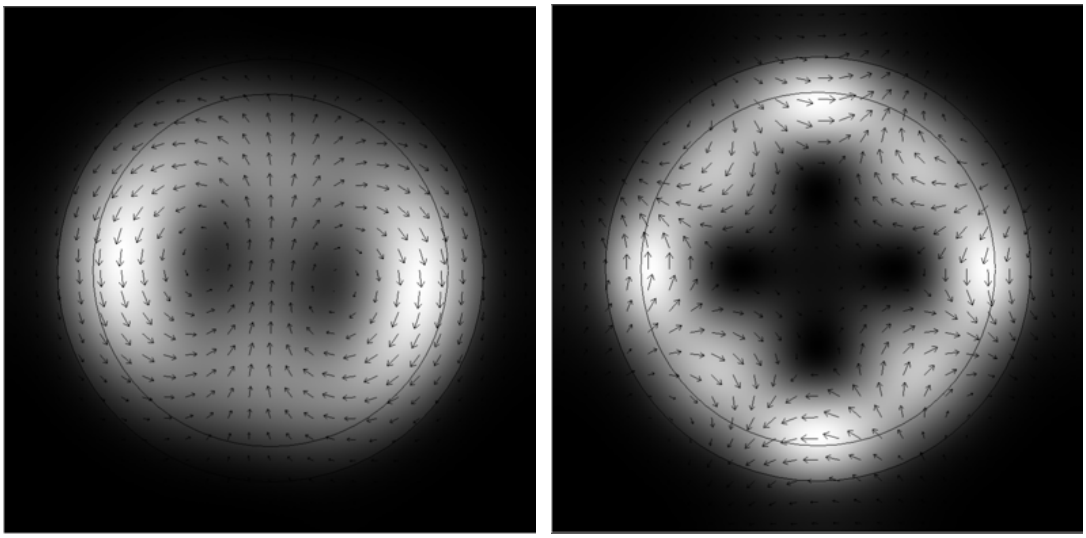

Fig. 5: Intensity distribution of high-order modes in a polymer optical fibre with a circular cross-section. The fibre contains a fused-silica core with n = 1.543 and a diameter of 1 μm. The cladding is 0.1 μm thick, with refractive index n = 1.5. As can be seen, the energy tends to concentrate within the cladding. Part of the field energy is out of the cladding. Hence, high-order modes have high radiation losses. (Arrows show the electrical field vector).

When light propagates in a waveguide (planar, channel) or a fibre the existence of the evanescent field out of the cladding leads to scattering at scratches or dust micro particles that are present on surfaces. Since the number of scattering centres can be quiet large the dissipation of energy cannot be neglected.

As illustrated in Fig. 6, another loss channel is connected to bending losses which occur when a waveguide or a fibre deviates from a strait geometry.

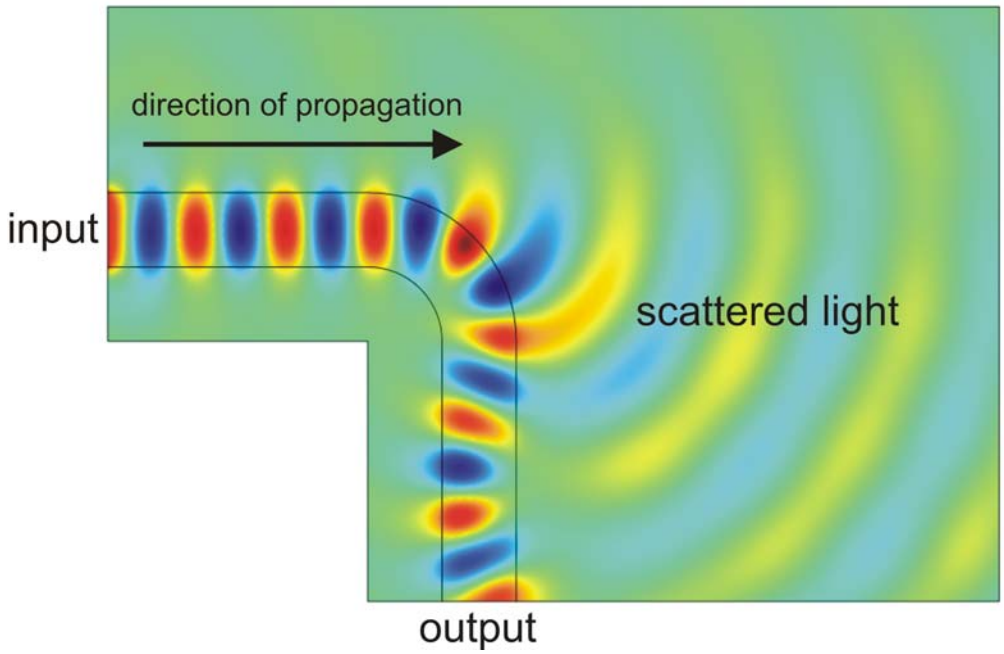

Fig. 6: Electrical field strength of guided modes at a waveguide bend of a planar waveguide with 2 μm width. The electrical field is partially coupled-out in the bending area.

As can be seen in Fig. 6 a part of the field energy is coupling into higher-order modes after passing the bending element. That leads to additional losses due to energy delocalization outside of the waveguide.

Methods of characterization of thin films and interfaces

Ellipsometry

Ellipsometry is a technique developed for surface analysis. The measurement of variation of the polarization state of light after reflection on a surface gives information about the surface material down to a depth of several wavelengths. The non-destructive character of ellipsometry makes it widely used for real-time applications. For instance, the ellipsometric control of thickness can be embedded into vacuum-deposition processes.

Fig. 7 gives an example for such an *in-situ* control. The two ellipsometric angles Ψ and Δ measured during evaporation of a gold layer on a glass substance versus the angle of incidence Φ are plotted for five different layer thicknesses.

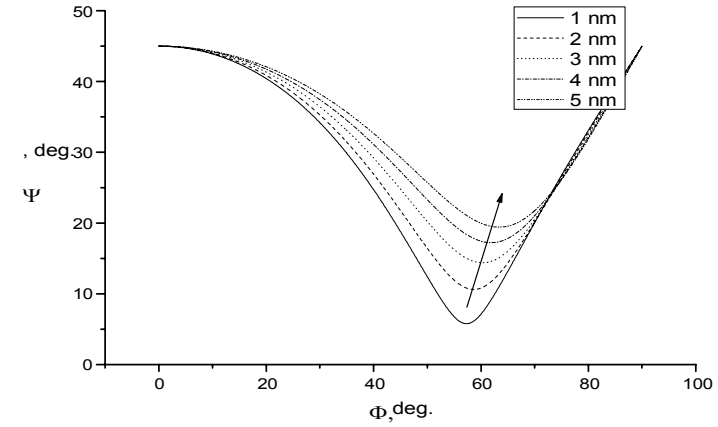

a)

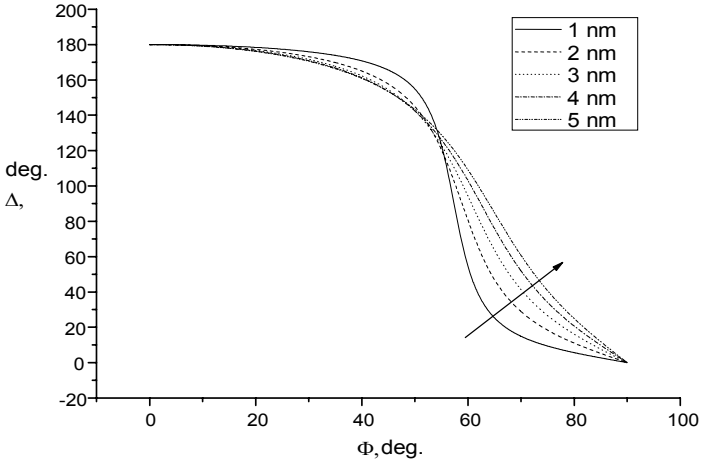

b)

Fig. 7: Ellipsometric angles Ψ (a) and Δ (b) in dependence on the angle of incidence Φ for different layer thicknesses. Changes of thickness of gold in the range 1-5 nm leads to significant changes in the observed ellipsometric parameters Ψ (Φ) and Δ(Φ), where Φ is the angle of incidence. Arrows point into the direction of thickness growth.

The complex ratio ρ of reflection coefficients r_p and r_s, which stand for the reflection coefficients parallel and perpendicular to the plane of incidence, respectively, describes the state of polarization:

$$\rho = \frac{r_p}{r_s} = \tan\Psi e^{i\Delta} \qquad [1.32]$$

Here tan Ψ is the amplitude ratio upon reflection while Δ is the phase shift. These quantities are related to the Fresnel reflection coefficients as illustrated in Fig. 8.

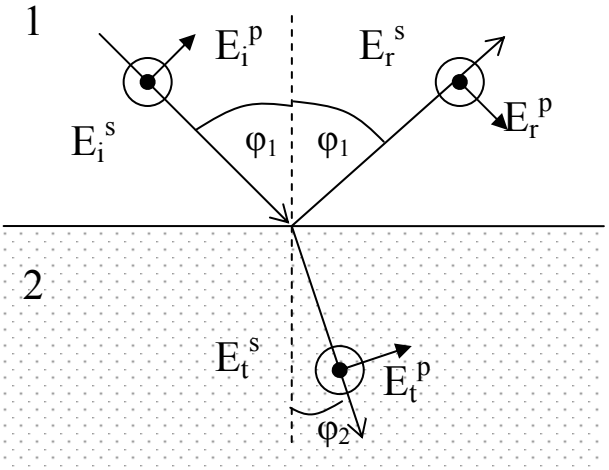

Fig. 8: Reflection and transmission of light at the interface between medium 1 and medium 2. E represents the electrical field vector of light with polarisation parallel (*p*) and perpendicular (s – "senkrecht") to the plane of incidence.

The Fresnel reflection coefficients r^p and r^s, directly related to optical properties of the surface, can be expressed by:

$$r_{12}^p = \frac{E_r^p}{E_i^p} = \frac{\tilde{n}_2\cos\phi_1 - \tilde{n}_1\cos\phi_2}{\tilde{n}_2\cos\phi_1 + \tilde{n}_1\cos\phi_2}$$
$$r_{12}^s = \frac{E_r^s}{E_i^s} = \frac{\tilde{n}_1\cos\phi_1 - \tilde{n}_2\cos\phi_2}{\tilde{n}_1\cos\phi_1 + \tilde{n}_2\cos\phi_2} \qquad [1.33]$$

The ratio t^p and t^s of electric field strengths of transmitted to incoming beam going from medium 1 to medium 2 is defined by equation [1.34] for polarization parallel (*p*) and perpendicular (*s*), respectively.

$$t_{12}^p = \frac{E_t^p}{E_i^p} = \frac{2\tilde{n}_1\cos\phi_1}{\tilde{n}_2\cos\phi_1 + \tilde{n}_1\cos\phi_2}$$
$$t_{12}^s = \frac{E_t^s}{E_i^s} = \frac{2\tilde{n}_1\cos\phi_1}{\tilde{n}_1\cos\phi_1 + \tilde{n}_2\cos\phi_2}, \qquad [1.34]$$

where the subscript "12"stands for the interface between the first and second medium. E_i is the electric field amplitude of the incoming beam in medium 1. E_r is the reflected electrical field amplitude in medium 1 after reflection at medium 2. The equations [1.33] and [1.34] are called *Fresnel equations*.

Ellipsometry found also applications in nonlinear optics[45-47]. So-called null-ellipsometry is mainly used in those cases where the signal polarization from the sample is compensated to be linear by using a compensator (Soleil-Babinet compensator). This signal reduced to null by a crossed analyzer. Then very small deviations in phase, which occur as a result of disturbing the polarization compensation, modulate the intensity at output with a good signal/noise ratio. The scheme of null-ellipsometry is widely used for electro-optics measurements. Applying an AC-electrical field at frequency Ω (kHz-MHz range) the light modulation at Ω gives is a signal due to the Pockels effect while at 2Ω light modulation is caused by the Kerr effect.

A detailed description of the theory of ellipsometry and especially of spectroscopic ellipsometry are available in many sources[48-51].

Prism coupling method

Assuming an optically homogeneous, isotropic transparent layer, the processes going on during propagation within a step-index film can be described by superposition of multiply reflected beams. Involving Fresnel equations for claddings-core interfaces one can write the following dispersion equation[52]:

$$k_x d = (m+1)\pi - \arctan\left(\frac{k_x}{\gamma_0}\right) - \arctan\left(\frac{k_x}{\gamma_2}\right) \qquad [1.35]$$

for s-polarized (Transverse Electrical – TE) modes, and

$$k_x d = (m+1)\pi - \arctan\left(\left(\frac{n_0}{n}\right)^2 \frac{k_x}{\gamma_0}\right) - \arctan\left(\left(\frac{n_2}{n}\right)^2 \frac{k_x}{\gamma_2}\right) \qquad [1.36]$$

for p-polarized (Transverse Magnetic) TM modes, where the coefficients are defined as follows:

$$\begin{aligned} k_x &= k_0\sqrt{n^2 - n_{eff}^2} \\ \gamma_0 &= k_0\sqrt{n_{eff}^2 - n_0^2} \\ \gamma_2 &= k_0\sqrt{n_{eff}^2 - n_2^2} \end{aligned} \qquad [1.37]$$

with $k_0 = \frac{2\pi}{\lambda}$ and n_0, n_2 and n being the refractive indices of substrate, superstrate and core, respectively. d is the thickness of the core. The effective refractive index n_{eff} is a proportionality coefficient between speed of light in vacuum and speed of mode propagation. The refractive index n of the core material should be higher than n_0 and n_2 to provide total internal reflection condition:

$$\theta_{tot} = arc\sin\left(\frac{n_{cladding}}{n_{core}}\right) \qquad [1.38]$$

The intensity is oscillatory inside of the core and decays monotonically in the cladding areas (**Fig. 9**). The relation of energies concentrated inside and outside of the waveguide core is defined by refractive index contrast between core and cladding.

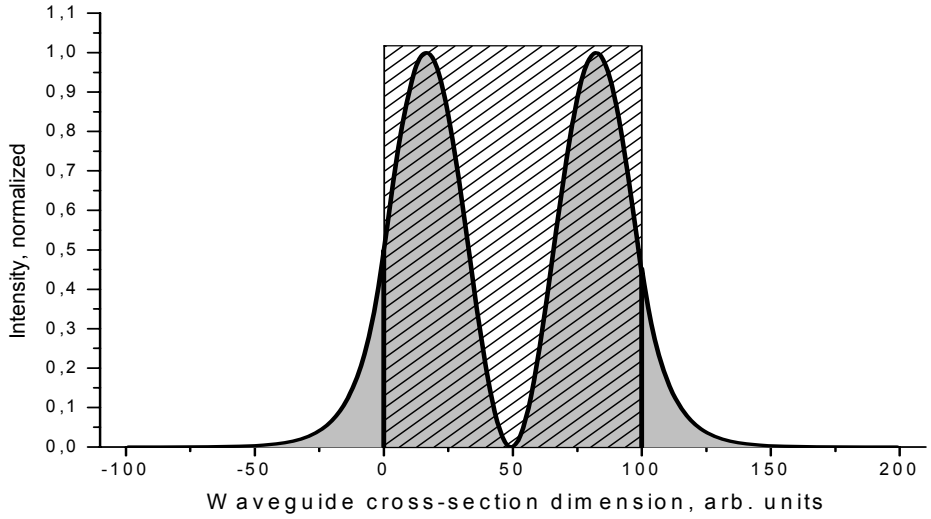

Fig. 9: Intensity distribution inside the waveguide. The rectangular marked area represents the core. An exponential penetration into both claddings can be found outside of the core. Here $n_0=n_2$ was assumed.

A typical scheme of a prism-coupling setup is shown in Fig. 10. A sharp tip presses the substrate that carries the film (core of the waveguide) directly to the prism base. The air gap between film and prism decreases in dependence to the force, which is chosen enough to allow the light to penetrate by means of its evanescence field into the film.

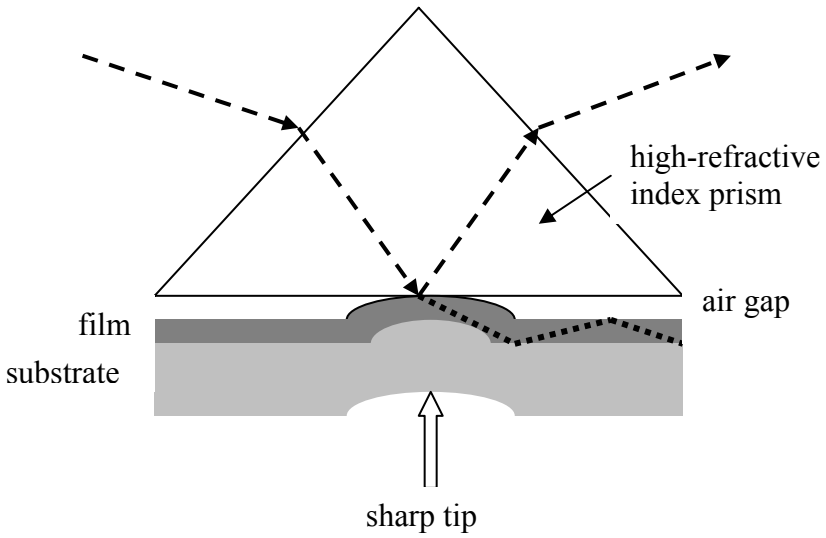

Fig. 10: Schematic presentation of the prism-coupling experiment. The thickness of the air gap between the film surface and the prism base is below 1 μm. In experiments, a prism with refractive index of 1.89 was used.

Concerning the application for characterization of linear and nonlinear waveguides, the prism coupling is a preferable technique because it is based on exciting guiding modes in the film. For instance, one can directly get the number of modes of both TE and TM polarizations. The values of effective refractive indices of every mode can be directly obtained from the experiment. Other techniques like ellipsometry provide the bulk material refractive index only after extensive calculations and the use of optical model parameters.

Optical Waveguide Light-mode Spectroscopy (OWLS)

The basic principle of the optical waveguide light-mode spectroscopy is based on coupling linearly polarized light by a diffraction grating into the waveguide layer.

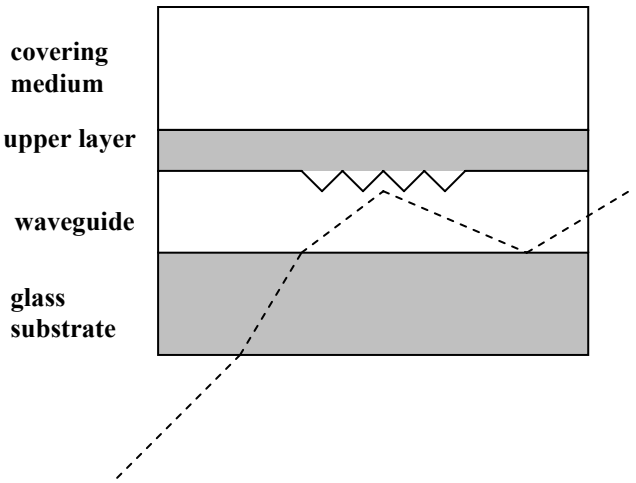

Fig. 11: Structure and scheme of laser beam propagation used in OWLS. The investigated media are the upper layer or the covering medium if the upper layer is not present.

The incoupling of light appears at a certain angle, which is defined by the period of the diffraction grating, the laser wavelength and the refractive indices of core and both of the claddings. The coupled light is guided by total internal reflection to the ends of the waveguide layer where it is detected by photodiodes. By changing the angle of incidence, the OWLS spectrum can be obtained. This assembly is mounted on a precision goniometer, which adjusts the angle of incidence of the external laser. Even small changes of refractive index of the upper cladding lead to a shift of the coupling angle. The sensitivity of the method allows us to investigate the thermal dependence of the refractive index.

The optical waveguide grating coupler sensor chips OW2400 provided by MicroVacuum Ltd. has sol-gel waveguiding materials with n=1.77. The thickness of the layer is 170-220 nm.

The precision of the method allows us to detect ultrathin layers (less than several *nm*). The commercially available device OWLS 120 (*MicroVacuum Ltd.*) includes a flow cuvette applying for investigation of gas-surface or liquid-surface interactions.

Surface quality and thickness measurements by AFM

A direct way to measure the thickness of a film uses a profilometer or a more precise technique based on the same contact principle: Atomic Force Microscopy (AFM). To get the thickness of the film one can measure the profile of the film edge. An additional advantage of direct methods is the possibility to obtain 2D presentations of the surface profile (Fig. 12). This information allows to calculate roughness of the film and to analyze morphology of the surface.

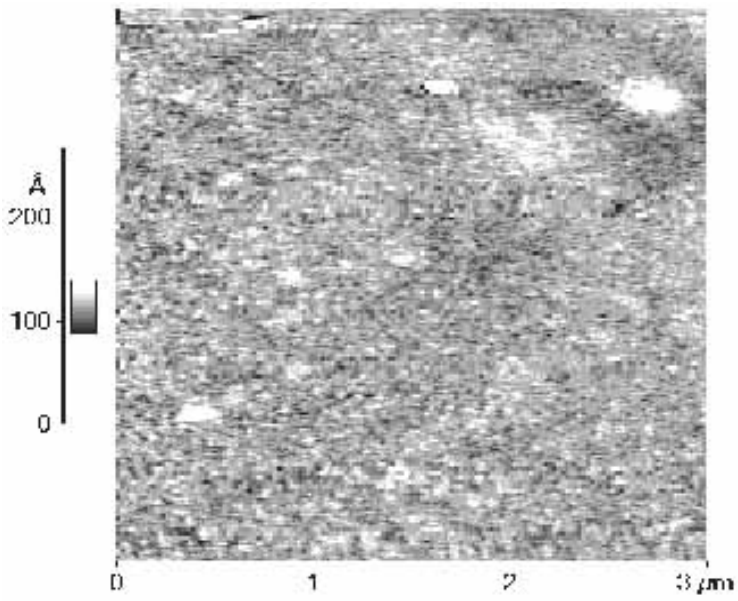

Fig. 12: AFM picture of a polyphenylquinoxaline (PPQ) based guest-host film spin-coated on glass substrate.

The RMS roughness obtained during waveguide preparation was in the order of 2-3 nm for the polymer films spin coated at various spin speeds and concentrations. From our experience, solvents with higher boiling temperature such as dichloroethane or toluene produce smother surfaces.

The linear optical techniques introduced above are used to carry out a basic optical characterisation of the materials under investigation. The obtained results are discussed in the following experimental sections.

Nonlinear optical properties, general description

General definitions

Optical nonlinearity is a phenomenon, which occurs when the dielectric polarization of a medium responds nonlinearly to the electric field of light. Applications of particular importance are nonlinear frequency conversion, phase modulation and intensity-dependent absorption. Of special interest for the present work is propagation of intense short pulses in optical waveguides or in artificial pseudo-crystals like poled polymer films.

Nonlinear wave equation

Dielectric media in an external electric field are affected by polarization effects, i.e. the electric field displaces electronic orbitals relatively to its atomic nuclei. As a result, atoms get an additional dipole moment. Typical time constants of *electron polarization* are 10^{-15}-10^{-16} s. There are also other types of polarization: *ion polarization* and *orientational polarization*. If ions are present in the materials they tend to move under the action of the field with typical time constants of the order of 10^{-11}-10^{-13} s. As a result of a relative shift between positive and negative charged ions an induced polarization appears. Rotations of dipole molecules in an electrical field occur even with lower time constants ($\geq 10^{-10}$ s) because the main mass of the molecule is much larger than the mass of an ion or an electron.

The external field includes the electrical field of the light wave. For the UV-VIS range, one must take into account only the fast electron polarization. The period of oscillations in the region (wavelength < 10 μm) is small and, therefore, allows to neglect the other polarizations.

Quantitatively, the vector of polarization characterizes the *polarization P*. In the linear optics approximation, this vector depends linearly on the applied electrical field *E*:

$$P_i = \varepsilon_a \chi_{ik} E_k \quad \text{i,k=1,2,3} \qquad [2.1]$$

where χ is the susceptibility tensor. This tensor is symmetric and can be written in diagonal form:

$$\chi_{ik} = \begin{pmatrix} \chi_{11} & 0 & 0 \\ 0 & \chi_{22} & 0 \\ 0 & 0 & \chi_{33} \end{pmatrix} \qquad [2.2]$$

Moreover,

For *isotropic media* as amorphous solids or *cubic crystals* one has $\chi_{11}=\chi_{22}=\chi_{33}=\chi$.

For *uniaxial* crystals with an optical axis along *z (3-direction)* (tetragonal, hexagonal and trigonal) the following relation exists: $\chi_{11}=\chi_{22}<>\chi_{33}$.

For *biaxial* crystals (rhombic, monoclinic and triclinic) one has $\chi_{11}<>\chi_{22}<>\chi_{33}$.

Due to the character of intermolecular forces a linear approximation can be used only for a small orbital shift (i.e. low external field, usual light sources). When the intensity of the electrical field is high (e.g. using a powerful laser beam) the linear approximation does no longer describe the polarization completely. In that case, a field depended susceptibility tensor can be used:

$$P_i = \varepsilon_a \chi_{ik}(E) E_k \quad i,k=1,2,3 \qquad [2.3]$$

where the susceptibility can be expanded into a power series of the field *E*:

$$\chi_{ik}(E) = \chi_{ik}^{(1)} + \chi_{ikj}^{(2)} E_j + \chi_{ikjm}^{(3)} E_j E_m + ... \quad [2.4]$$

where $\chi^{(1)}_{ik}$ is a linear susceptibility and $\chi^{(n)}$ are nonlinear susceptibilities of *n-th* order.

Typical values for the susceptibilities of dielectrics are:

$\chi^{(1)} \approx 1$,

$\chi^{(2)} \approx 10^{-13} - 10^{-11}$ m/V, (or 0.1 –10 pm/V)

$\chi^{(3)} \approx 10^{-23} - 10^{-21}$ [m/V]^2

One can see an extremely rapid decrease of the importance of the nonlinear terms with growing exponent *n*. Usually only second and third orders are taken into account. One can separate the linear and nonlinear response in the polarization expression:

$$P_i = P_i^{linear} + P_i^{nonlinear} = \varepsilon_a \chi_{ik}^{(1)} E_k + \varepsilon_a \left[\chi_{ikj}^{(2)} E_k E_j + \chi_{ikjm}^{(3)} E_k E_j E_m + ... \right] \quad [2.5]$$

In media with a centre of symmetry (centrosymmetric crystals, liquids, gases) even-order nonlinear susceptibilities are equal to zero. The operation of inversion of the tensor leads to a transformation of the tensor components: $x \rightarrow -x$, $y \rightarrow -y$, $z \rightarrow -z$. The operation of inversion requires that the vector of polarisation changes sign when the vector of electric field strength changes sign by going from *x* to *–x* in a medium with point symmetry: $P(E) = -P(-E)$. This equation holds for the linear and all odd-order susceptibility contributions. However, for all even-order contributions this relation is only fulfilled for vanishing susceptibility, i.e. for a quadratic susceptibility $\chi^{(2)}_{ijk} \equiv 0$.

This peculiarity allows dividing nonlinear media into quadratic-nonlinear and cubic-nonlinear media. From 32 crystalline classes, 20 classes have a centre of symmetry and, therefore, posses no quadratic susceptibility. It is worth to note that the border between two different centrosymmetric media shows a break of symmetry and generates second-order nonlinear effects. For instance, SHG from interfaces is a typical phenomenon of such type.

Electromagnetic fields in media can be described by Maxwell's equations:

$$\nabla \times \vec{E}(\vec{r},t) = -\frac{\partial \vec{B}(\vec{r},t)}{\partial t} \quad [2.6]$$

$$\nabla \times \vec{H}(\vec{r},t) = \frac{\partial \vec{D}(\vec{r},t)}{\partial t} + \vec{j}(\vec{r},t) \quad [2.7]$$

$$\nabla \cdot \vec{D}(\vec{r},t) = \rho(\vec{r},t) \quad [2.8]$$

$$\nabla \cdot \vec{B}(\vec{r},t) = 0 \quad [2.9]$$

and the constitutive equations which represent the relations between dielectric displacement $\vec{D}(\vec{r},t)$ and electric field strength $\vec{E}(\vec{r},t)$:

$$\vec{D}(\vec{r},t) = \varepsilon_a \varepsilon_r(\vec{r},t) \vec{E}(\vec{r},t) \quad [2.10]$$

with the absolute value of vacuum permittivity ε_a, the relative dielectric constant ε_r. Introducing the susceptibility χ, and the refractive index *n* we have:

$$\varepsilon_r(\vec{r},t) = 1 + \chi(\vec{r},t) = n^2(\vec{r},t) \quad [2.11]$$

These quantities are second rank tensors for anisotropic materials and scalars for isotropic materials. Inserting these quantities into the equation above one obtains:

$$\vec{D}(\vec{r},t) = \varepsilon_a \left[1 + \chi(\vec{r},t)\right] \vec{E}(\vec{r},t) \quad [2.12]$$

Similarly, for the magnetic induction $\vec{B}$ and the magnetic field strength $\vec{H}$ one has

$$\vec{B}(\vec{r},t) = \mu_a \mu_r \vec{H}(\vec{r},t) \qquad [2.13]$$

with μ_r, the relative magnetic permeability and the absolute permeability of the vacuum μ_a. Introduction of a magnetic susceptibility χ_m, provides the following relation:

$$\mu_r(\vec{r},t) = 1 + \chi_m(\vec{r},t) \qquad [2.14]$$

From that follows

$$\vec{B}(\vec{r},t) = \mu_a[1 + \chi_m(\vec{r},t)]\vec{H}(\vec{r},t) \qquad [2.15]$$

These equations allow one to introduce besides the electric polarization $\vec{P}(\vec{r},t)$, a magnetic polarization $\vec{P}_m(\vec{r},t)$ that represent the relevant material properties:

$$\vec{D}(\vec{r},t) = \varepsilon_a \vec{E}(\vec{r},t) + \vec{P}(\vec{r},t) \qquad [2.16]$$

$$\vec{B}(\vec{r},t) = \mu_a \vec{H}(\vec{r},t) + \vec{P}_m(\vec{r},t) \qquad [2.17]$$

with

$$\vec{P}(\vec{r},t) = \varepsilon_a \chi(\vec{r},t)\vec{E}(\vec{r},t) \qquad [2.18]$$

$$\vec{P}_m(\vec{r},t) = \mu_a \chi_m(\vec{r},t)\vec{H}(\vec{r},t) \qquad [2.19]$$

Separating linear and nonlinear parts of the electric polarization and taking into account that for dielectric non-magnetic media $\vec{P}_m$ can be set equal to zero, one can write:

$$\vec{P}(\vec{r},t) = \vec{P}^{linear}(\vec{r},t) + \vec{P}^{nonlinear}(\vec{r},t) \qquad [2.20]$$

$$\vec{B}(\vec{r},t) = \mu_a \vec{H}(\vec{r},t) \ (SI) \qquad [2.21]$$

Applying the curl operation to [2.6] and using [2.7] gives:

$$\nabla \times \nabla \times \vec{E}(\vec{r},t) = \left[-\frac{\partial}{\partial t}\left(\nabla \times \vec{B}(\vec{r},t)\right)\right] = -\mu_a \mu_r \frac{\partial}{\partial t}\left(\nabla \times \vec{H}(\vec{r},t)\right) \qquad [2.22]$$

Taking into account [2.9] provides:

$$\nabla \times \nabla \times \vec{E}(\vec{r},t) = -\mu_a \mu_r \frac{\partial}{\partial t}\left(\frac{\partial \vec{D}(\vec{r},t)}{\partial t} + \vec{j}(\vec{r},t)\right) \qquad [2.23]$$

According to [2.8] and assuming $\vec{j}(\vec{r},t) = 0$ one obtains:

$$\nabla \times \nabla \times \vec{E}(\vec{r},t) = -\varepsilon_a \mu_a \varepsilon_r \mu_r \frac{\partial^2}{\partial t^2}\vec{E}(\vec{r},t) \qquad [2.24]$$

Using the relation $\nabla \times \nabla \times \vec{E} = \nabla \cdot \nabla \vec{E} - \Delta \vec{E}$ and assuming for charge-free media $\nabla \vec{E} = 0$ one gets:

$$\Delta \vec{E}(\vec{r},t) = \frac{\varepsilon_r \mu_r}{c_0^2}\frac{\partial^2}{\partial t^2}\vec{E}(\vec{r},t) \qquad [2.25]$$

because for the vacuum speed of light c_0, the following relation holds: $c_0^2 = \frac{1}{\sqrt{\varepsilon_a \mu_a}}$.

In case of transparent, nonmagnetic, dielectric media one has $\mu_r = 1$. Then, from [2.11] and [2.18] follows:

$$\Delta\vec{E}(\vec{r},t) = \frac{1}{c_0^2}\frac{\partial^2}{\partial t^2}\left[\vec{E}(\vec{r},t) + \frac{1}{\varepsilon_a}\vec{P}(\vec{r},t)\right] \qquad [2.26]$$

$$\Delta\vec{E}(\vec{r},t) = \frac{1}{c_0^2}\frac{\partial^2}{\partial t^2}\left\{\vec{E}(\vec{r},t) + \frac{1}{\varepsilon_a}\left[\vec{P}^{linear}(\vec{r},t) + \vec{P}^{nonlinear}(\vec{r},t)\right]\right\} \qquad [2.27]$$

Separating linear and nonlinear parts leads to:

$$\Delta\vec{E}(\vec{r},t) - \frac{1}{c_0^2}\frac{\partial^2}{\partial t^2}\left(\vec{E}(\vec{r},t) + \frac{1}{\varepsilon_a}\vec{P}^{linear}(\vec{r},t)\right) = \frac{1}{c_0^2\varepsilon_a}\frac{\partial^2}{\partial t^2}\vec{P}^{nonlinear}(\vec{r},t) \qquad [2.28]$$

That is a wave equation for nonlinear media. Merging linear expressions on the left side leads to:

$$\Delta\vec{E}(\vec{r},t) - \frac{\varepsilon_r(\vec{r},t)}{c_0^2}\frac{\partial^2}{\partial t^2}\vec{E}(\vec{r},t) = \frac{1}{c_0^2\varepsilon_a}\frac{\partial^2}{\partial t^2}\vec{P}^{nonlinear}(\vec{r},t) \qquad [2.29]$$

This is a driven wave equation where the nonlinear polarization acts as a source term in the wave equation.

Dispersion of polarization

The reaction of electrons and nuclei under influence of an external field requires a certain time. Hence, the polarisation vector $\vec{P}$ depends on field intensity in previous moments. Thereby, equation [2.3] should be written as convolution integral:

$$P_i(t) = \varepsilon_a \sum_k \int_0^\infty \chi_{ik}^{(0)}(\tau)\, E_k(t-\tau)\, d\tau\,, \qquad [2.30]$$

where $\chi^{(0)}$ represents a time-dependent first-order susceptibility tensor.

Using Fourier transformation one can use frequency domain instead of time domain:

$$P(\omega) = \int P(t) e^{-i\omega t} dt \qquad [2.31]$$

$$E(\omega) = \int E(t) e^{-i\omega t} dt \qquad [2.32]$$

$$P_i^{linear}(\omega) = \varepsilon_a \sum_k \chi_{ik}^{(0)}(\omega)\, E_k(\omega) \qquad [2.33]$$

$$\chi_{ik}^{(0)}(\omega) = \int \chi_{ik}^{(0)}(\tau) e^{-i\omega t} dt \qquad [2.34]$$

In case of a quadratic nonlinear term of polarization, one should take into account two electrical waves:

$$P_i^{(2)}(t) = \varepsilon_a \sum_{k,j} \int_0^\infty \int_0^\infty \chi_{ikj}^{(2)}(\tau', \tau'')\, E_k(t-\tau')\, E_j(t-\tau'-\tau'')\, d\tau'\, d\tau'' \qquad [2.35]$$

in frequency domain:

$$P_i^{(2)}(\omega_1 \pm \omega_2) = \varepsilon_a \chi_{ikj}^{(2)}(\omega_1 \pm \omega_2) E_k(\omega_1) E_j(\omega_2) \quad [2.36]$$

where $$\chi_{ikj}^{(2)}(\omega_1 \pm \omega_2) = \int_0^\infty \int_0^\infty \chi_{ikj}^{(2)}(\tau', \tau'') e^{-i(\omega_1 \pm \omega_2)\tau' \mp i\omega_2 \tau''} d\tau' d\tau'' \quad [2.37]$$

Here and below $\chi^{(n)}$ denotes the nth-order susceptibility tensor in the power series development after electrical field:

$$\chi = \chi^{(0)} + \chi^{(1)}\vec{E} + \chi^{(2)}\vec{E}^2 + .. + \chi^{(n)}\vec{E}^n \quad [2.38]$$

Exchange of two interacting waves E_k and E_j gives no changes for the vector of polarization. Hence, the tensor $\chi^{(2)}$ is symmetrical with respect to permutation of the last two indices[53]:

$$\chi_{ikj}^{(2)} = \chi_{ijk}^{(2)} \quad [2.39]$$

This reduces the number of independent tensor components to 18 and it allow to use a two index system. The reduction from three to two indices is carried out as follows:

where l =1..6, ($\chi_{ijk} \Rightarrow \chi_{il}$)

jk	11	22	33	23=32	13=31	12=21
l	1	2	3	4	5	6

Moreover, for frequency ranges with weak dispersion one can apply the so-called Kleiman relations[35,53]:

$$\chi_{ikj} = \chi_{kij} = \chi_{jki} = \chi_{ijk} = \chi_{kji} = \chi_{jik} \quad [2.40]$$

The change from the time-domain to the frequency-domain for dispersion media demonstrates that the dielectric constant is a complex quantity[44]:

$$\tilde{\varepsilon} = \varepsilon' - i\varepsilon'' \quad [2.41]$$

Where the real part of the dielectric constant ε' stands for storage of field energy and the imaginary part ε'' for dissipation of field energy. In case of conductive media the imaginary part can be expressed by means of conductivity σ which is responsible for the absorption in these media (metals, semiconductors). Then one obtains:

$$\tilde{\varepsilon} = \varepsilon' - i\frac{\sigma}{\varepsilon_a \omega} \quad [2.42]$$

Commonly, nonlinear parts of the susceptibility are complex functions too:

$$\tilde{\chi}^{(n)} = \mathrm{Re}\,\chi^{(n)} - i\,\mathrm{Im}\,\tilde{\chi}^{(n)},\ n > 1 \quad [2.43]$$

In comparison to real parts, imaginary parts have usually much smaller values. The real part of the nonlinear n-th order susceptibility is responsible for the n-th harmonic generation, while the imaginary part for the n-photon absorption.

The expression for the electrical field strength can be written as:

$$\vec{E}(\vec{\mathbf{r}}, t) = \frac{1}{2}\vec{\mathbf{e}}\{A(\vec{\mathbf{r}}, t)\, e^{i(\omega t - \vec{k}\vec{\mathbf{r}})} + c.c.\} \quad [2.44]$$

where $\vec{e}$ is the polarization unit vector, $A(\vec{r},t)$ is the complex amplitude of the electrical field. The complex conjugated term provides the real character of field strength that is important in nonlinear optics, where nonlinear *E* powers like E^2, E^3 appear.

In case of one wave with frequency ω one can insert [2.44] into expression [2.36] and obtains:

$$\begin{aligned} P_i^{(2)} &= \frac{1}{4}\varepsilon_a \chi_{ijk}^{(2)} \vec{\mathbf{e}}_j \vec{\mathbf{e}}_k \{A\,\mathrm{e}^{i(\omega t - k\mathbf{r})} + c.c\}^2 = \\ &= \frac{1}{4}\varepsilon_a \chi_{ijk}^{(2)} \vec{\mathbf{e}}_j \vec{\mathbf{e}}_k \{A^2\,\mathrm{e}^{i(2\omega t - 2k\mathbf{r})} + A^{*2}\,\mathrm{e}^{-i(2\omega t - 2k\mathbf{r})} + 2AA^*\} \end{aligned} \qquad [2.45]$$

The first two members are responsible for a polarisation wave with double frequency. That can lead to Second Harmonic Generation (SHG). The condition that SHG appears is that the system must have no centrosymmetry, e.g. $LiNbO_3$ crystal or poled polymers. As we will see below, SHG can be observed also in glassy systems, where noncentrosymmetry is provided by alignment of nonlinear optical chromophores.

Second-order nonlinear processes, SHG and DFG

The electrical field of a monochromatic wave is described as:

$$E(z,t) = \frac{1}{2}Ae^{i(\omega t - kz)} + \frac{1}{2}A^* e^{-i(\omega t - kz)} \qquad [2.46]$$

where the complex conjugated part provides the real character of *E(z,t)*.

For the description of wave propagation the so-called slowly varying amplitude approximation was introduced[44]. The assumption of the slowly varying amplitude approximation means that the amplitudes A_1 (fundamental wave) and A_2 (second harmonic) are varying slowly with respect to the time *t*. That can be expressed by the following inequality:

$$\frac{\partial A_{1,2}}{\partial t}\frac{1}{\omega_{1,2}} << A_{1,2} \qquad [2.47]$$

Consequently, the functions $A_{1,2}(z,t)$ can be considered as constant on a distance range of the order of the wavelength (or during the time $t = \frac{1}{\omega}$).

The electric field in the material can be represented as Fourier series:

$$E(z,t) = \frac{1}{2}\sum_m A_m e^{i(m\omega t - k_m z)} + \frac{1}{2}\sum_m A_m^* e^{-i(m\omega t - k_m z)} \qquad [2.48]$$

where $k_m = \mathrm{Re}\left[\tilde{k}_m\right] = \mathrm{Re}\left[\frac{m\omega}{c_0}\sqrt{\varepsilon_r(m\omega)}\right]$ is the real part of the complex wave-vector $\tilde{k}_m = \mathrm{Re}(\tilde{k}_m) - i\,\mathrm{Im}(\tilde{k}_m)$.

The imaginary part of complex wave-vector $\tilde{k}_m$ describes absorption:

$$\begin{aligned} &A'_m\, e^{i(m\omega t - \tilde{k}_m z)} = A'_m\, e^{-\mathrm{Im}(\tilde{k}_m)z} e^{i(m\omega t - \mathrm{Re}(\tilde{k}_m)z)} = A_m e^{i(m\omega t - \mathrm{Re}(\tilde{k}_m)z)} \\ &\left[A_m = A'_m\, e^{-\mathrm{Im}(\tilde{k}_m)z}, \mathrm{Im}(\tilde{k}_m) < 1\right] \end{aligned} \qquad [2.49]$$

Taking into account only the first two members of each sum in [2.48] one can obtain for the intensity an expression, which is proportional to E^2:

$$m \in \{1,2\} \Rightarrow E^2(z,t) = \frac{1}{4}\left(A_1 e^{i(\omega t - k_1 z)} + A_2 e^{i(2\omega t - k_2 z)} + A_1^* e^{i(-\omega t + k_1 z)} + A_2^* e^{i(-2\omega t + k_2 z)} \right)^2 \quad [2.50]$$

that after expanding and grouping gives:

$$\begin{aligned}
A_1 \Big\{ \quad & A_1 A_1 e^{i(2\omega t - 2k_1 z)} + A_1 A_2 e^{i(3\omega t - k_2 z - k_1 z)} + A_1 A_1^* + A_1 A_2^* e^{i(-\omega t + k_2 z - k_1 z)} \\
A_2 \Big\{ \quad & A_2 A_1 e^{i(3\omega t - k_1 z - k_2 z)} + A_2 A_2 e^{i(4\omega t - 2k_2 z)} + A_2 A_1^* e^{i(\omega t + k_1 z - k_2 z)} + A_2 A_2^* \\
A_1^* \Big\{ \quad & A_1 A_1^* + A_2 A_1^* e^{i(\omega t + k_1 z - k_2 z)} + A_1^* A_1^* e^{i(-2\omega t + 2k_1 z)} + A_2^* A_1^* e^{i(-3\omega t + k_1 z + k_2 z)} \\
A_2^* \Big\{ \quad & A_1 A_2^* e^{i(-\omega t + k_2 z - k_1 z)} + A_2 A_2^* + A_1^* A_2^* e^{i(-3\omega t + k_2 z + k_1 z)} + A_2^* A_2^* e^{i(-4\omega t + 2k_2 z)}
\end{aligned} \quad [2.51]$$

Taking into account the effects related to the double frequency and thereby excluding members with $m \notin \{1,2\}$ one gets:

$$\begin{aligned}
E^2 &= A_1 A_1 e^{i(2\omega t - 2k_1 z)} + A_2 A_1^* e^{i(\omega t + k_1 z - k_2 z)} + A_2 A_1^* e^{i(\omega t + k_1 z - k_2 z)} + \\
&+ A_1^* A_1^* e^{i(-2\omega t + 2k_1 z)} + A_1 A_2^* e^{i(-\omega t + k_2 z - k_1 z)} + A_1 A_2^* e^{i(-\omega t + k_2 z - k_1 z)} = \\
&= 2 A_2 A_1^* e^{i(\omega t + (k_1 - k_2) z)} + A_1^2 e^{i(2\omega t - 2k_1 z)} + c.c.
\end{aligned} \quad [2.52]$$

This expression contains obviously one contribution which oscillates with the frequency of the fundamental and another contribution which oscillates with the doubled frequency.

General view to a system of m-th order nonlinear equations

In case of a light wave travelling along z-direction its interaction with nonlinear media can be described by the following equation:

$$\left\langle -\frac{\partial^2}{\partial z^2} + \frac{\varepsilon_r}{c_0^2}\frac{\partial^2}{\partial t^2} \right\rangle E(z,t) = \left\langle -\frac{1}{c_0^2 \varepsilon_a}\frac{\partial^2}{\partial t^2} \right\rangle P^{nonlinear}(z,t) \quad [2.53]$$

Inserting the explicit expression of the electrical field leads to the following form of the left part of eq. [2.53]:

$$\left\langle -\frac{\partial^2}{\partial z^2} + \frac{\varepsilon_r}{c_0^2}\frac{\partial^2}{\partial t^2} \right\rangle \left[A_m e^{i(m\omega t - k_m z)} + c.c. \right] \quad [2.54]$$

The first term can be rewritten as:

$$\begin{aligned}
&\frac{\partial^2}{\partial z^2}\left[A_m e^{i(m\omega t - k_m z)} + c.c. \right] = \frac{\partial}{\partial z}\left[\frac{\partial A_m}{\partial z} e^{i(m\omega t - k_m z)} - i A_m k_m e^{i(m\omega t - k_m z)} + c.c. \right] \\
&= \left[\frac{\partial^2 A_m}{\partial z^2} e^{i(m\omega t - k_m z)} - i\frac{\partial A_m}{\partial z} k_m e^{i(m\omega t - k_m z)} + c.c. \right] - i k_m \left[\frac{\partial A_m}{\partial z} e^{i(m\omega t - k_m z)} - i A_m k_m e^{i(m\omega t - k_m z)} + c.c. \right] \\
&= \frac{\partial^2 A_m}{\partial z^2} e^{i(m\omega t - k_m z)} - i 2 k_m \frac{\partial A_m}{\partial z} e^{i(m\omega t - k_m z)} - A_m k_m^2 e^{i(m\omega t - k_m z)} + c.c. \\
&\approx -i 2 k_m \frac{\partial A_m}{\partial z} e^{i(m\omega t - k_m z)} - A_m k_m^2 e^{i(m\omega t - k_m z)} + c.c.
\end{aligned} \quad [2.55]$$

because of $\frac{\partial^2 A_m}{\partial z^2} << k_m^2 A_m$

The second term of [2.56] is:

$$\frac{\varepsilon_r}{c_0^2}\frac{\partial^2}{\partial t^2}\left[A_m e^{i(m\omega t - k_m z)} + c.c.\right] = -\frac{\varepsilon_r m^2\omega^2}{c_0^2}\left[A_m e^{i(m\omega t - k_m z)} + c.c.\right] \qquad [2.57]$$

Finally, combining [2.55] and [2.57] we have:

$$\left[i\,2k_m\frac{\partial A_m}{\partial z} + k_m^2 A_m - \frac{\varepsilon_r m^2\omega^2}{c_0^2}A_m\right]e^{i(m\omega t - k_m z)} + c.c. \qquad [2.58]$$

Analysing this expression provides:

$$\left[\begin{array}{l} k_m^2 = \frac{m^2\omega^2}{c_0^2}\mathrm{Re}(\varepsilon_r(m\omega)),\quad \varepsilon_r(m\omega) = \mathrm{Re}[\varepsilon_r(m\omega)] - i\,\mathrm{Im}[\varepsilon_r(m\omega)] \\ k_m^2 - \frac{\varepsilon_r m^2\omega^2}{c_0^2} = \\ = \frac{m^2\omega^2}{c_0^2}\mathrm{Re}[\varepsilon_r(m\omega)] - \frac{m^2\omega^2}{c_0^2}\{\mathrm{Re}[\varepsilon_r(m\omega)] - i\,\mathrm{Im}[\varepsilon_r(m\omega)]\} = i\frac{m^2\omega^2}{c_0^2}\mathrm{Im}[\varepsilon_r(m\omega)] = i\frac{k_m^2}{n(m\omega)^2}\mathrm{Im}[\varepsilon_r(m\omega)] \end{array}\right]$$

Introduction of this result into [2.59] provides:

$$\left[i\,2k_m\frac{\partial A_m}{\partial z} + i\frac{k_m^2}{n(m\omega)^2}\mathrm{Im}[\varepsilon_r(m\omega)]A_m\right]e^{i(m\omega t - k_m z)} + c.c. \qquad [2.60]$$

The nonlinear polarisation can be expressed as a sum over all possible m[th]-order effects:

$$P^{nonlinear} = \sum_{m>1} P^{(m)} = \varepsilon_a \sum_{m>1} \tilde{\chi}^{(m)} \prod_{n=1}^{m} A_n e^{i(\omega_n t - k_n z)} + c.c.$$

In a simplified notation we have:

$$P^{nonlinear} = \varepsilon_a \chi^{(2)} \sum \left(C e^{i(m\omega t + \sum kz)} + c.c.\right)$$

Using this notation the right part of [2.53] can be, in case of second-order effects, directly modified to:

$$\begin{aligned} \left\langle -\frac{1}{c_0^2\varepsilon_a}\frac{\partial^2}{\partial t^2}\right\rangle P^{nonlinear} &= \left\langle -\frac{1}{c_0^2\varepsilon_a}\frac{\partial^2}{\partial t^2}\right\rangle \varepsilon_a \chi^{(2)} \sum \left(C e^{i(m\omega t + \sum kz)} + c.c.\right) \\ &= \frac{m^2\omega^2}{c_0^2\varepsilon_a}\varepsilon_a \chi^{(2)} \sum \left(C e^{i(m\omega t + \sum kz)} + c.c.\right) \end{aligned} \qquad [2.61]$$

where $\sum k$ denotes the sum of wave-vectors depending on the type of the process, for example [2.52], $(k_1 - k_2)$ relates to difference frequency generation (DFG) and $2k_1 = (k_1 + k_1)$ relates to the SHG processes respectively. Combining the final forms of left [2.60] and right-hand side [2.61] one can derive:

$$\left[i2k_m\frac{\partial A_m}{\partial z} + i\frac{\varepsilon_a k_m^2}{n(m\omega)^2}\mathrm{Im}[\varepsilon_r(m\omega)]A_m\right]e^{i(m\omega t - k_m z)} = \frac{m^2\omega^2}{c_0^2}\chi^{(2)}\sum\left(C e^{i(m\omega t + \sum kz)} + c.c.\right),$$

Dividing by $i2k_m$ provides for the right side:

$$\left[\begin{aligned}\frac{m^2\omega^2}{c_0^2}/2ik_m &= -i\frac{m^2\omega^2}{2c_0^2k_m} = -i\frac{m^2\omega^2}{2c_0^2}\frac{c_0}{m\omega n(m\omega)} = -i\frac{m\omega}{2c_0 n(m\omega)} = -i\frac{m\omega n(m\omega)}{c_0}\frac{1}{2n(m\omega)^2}\\ &= -ik_m\frac{1}{2n(m\omega)^2}\end{aligned}\right],$$

and for the left side:

$$\left[\frac{\partial A_m}{\partial z}+\frac{\varepsilon_a k_m}{2n(m\omega)^2}\mathrm{Im}\left[\varepsilon_r(m\omega)\right]A_m\right]e^{i(m\omega t-k_m z)}+c.c. = -ik_m\frac{1}{2n(m\omega)^2}\chi^{(2)}\sum\left(Ce^{i(m\omega t+\sum kz)}+c.c.\right)$$

Dividing by the exponential function one obtains:

$$\frac{\partial A_m}{\partial z}+\frac{\varepsilon_a k_m}{2n(m\omega)^2}\mathrm{Im}(\varepsilon(m\omega))A_m = -ik_m\frac{1}{2n(m\omega)^2}\chi^{(2)}\sum\left\{Ce^{i\left[\left(\sum k\right)+k_m\right]z}+c.c.\right\}$$

This equation can be rewritten as:

$$\frac{\partial A_m}{\partial z}+\delta_m A_m = -i\sigma_m\sum\left\{Ce^{i\left[\left(\sum k\right)+k_m\right]z}+c.c.\right\} \qquad [2.62]$$

Here a damping coefficient δ_m and a nonlinear coupling coefficient σ_m are introduced, defined as:

$$\delta_m = \varepsilon_a k_m\frac{\mathrm{Im}(\varepsilon(m\omega))}{2n(m\omega)^2} \qquad [2.63]$$

$$\sigma_m = k_m\frac{\chi^{(2)}}{2n(m\omega)^2} \qquad [2.64]$$

where $k_m = \dfrac{m\omega}{c_0}n(m\omega)$.

In every particular case, the right part of equations [2.62] is defined by the type of nonlinear interaction. For instance, the process of second harmonic generation includes two frequencies: ω and 2ω. This means that the right part of [2.62] contains members with $m\in\{1,2\}$ as shown below.

$$\begin{cases}\dfrac{\partial A_1}{\partial z}+\delta_1 A_1 = -i2\sigma_1 A_2 A_1^* e^{-i(2k_1-k_2)z}\\ \dfrac{\partial A_2}{\partial z}+\delta_2 A_2 = -i\sigma_2 A_1^2 e^{i(2k_1-k_2)z}\end{cases} \qquad [2.65]$$

Extended second-order nonlinear equations system for beams with finite aperture

Introducing complex amplitudes depending on the three coordinates (*x,y,z*), one can obtain the following equations which describe the spatial dependences of the amplitudes of the two involved waves

$$\begin{cases}\dfrac{\partial A_1}{\partial z}-\dfrac{1}{2ik_1}\left(\dfrac{\partial^2 A_1}{\partial x^2}+\dfrac{\partial^2 A_1}{\partial y^2}+\dfrac{\partial^2 A_1}{\partial z^2}\right)+\delta_1 A_1 = -i2\sigma_1 A_2 A_1^* e^{-i(2k_1-k_2)z}\\ \dfrac{\partial A_2}{\partial z}-\dfrac{1}{4ik_2}\left(\dfrac{\partial^2 A_2}{\partial x^2}+\dfrac{\partial^2 A_2}{\partial y^2}+\dfrac{\partial^2 A_2}{\partial z^2}\right)+\delta_2 A_2 = -i\sigma_2 A_1^2 e^{i(2k_1-k_2)z}\end{cases} \qquad [2.66]$$

From the slowly varying amplitude approximation follows the next relation:

$$\frac{\partial A}{\partial z} > \lambda \frac{\partial^2 A}{\partial z^2} \ . \qquad [2.67]$$

Eq. [2.66] is reduced to:

$$\begin{cases} \dfrac{\partial A_1}{\partial z} - \dfrac{1}{2ik_1}\left(\dfrac{\partial^2 A_1}{\partial x^2} + \dfrac{\partial^2 A_1}{\partial y^2}\right) + \delta_1 A_1 = -i2\sigma_1 A_2 A_1^* e^{-i(2k_1 - k_2)z} \\ \dfrac{\partial A_2}{\partial z} - \dfrac{1}{4ik_2}\left(\dfrac{\partial^2 A_2}{\partial x^2} + \dfrac{\partial^2 A_2}{\partial y^2}\right) + \delta_2 A_2 = -i\sigma_2 A_1^2 e^{i(2k_1 - k_2)z} \end{cases} \qquad [2.68]$$

Nevertheless the terms $\frac{\partial^2 A_1}{\partial x^2}$ and $\frac{\partial^2 A_1}{\partial y^2}$ cannot be neglected in eq. [2.66] since

$$\frac{\partial^2 A}{\partial x^2} \approx \frac{\partial^2 A}{\partial y^2} > \frac{\partial^2 A}{\partial z^2} \qquad [2.69]$$

Actually, these terms describe diffraction.

Maker fringe technique

Maker fringe analysis is the main technique of examination of the SHG intensity that oscillates as a function of pump angle[54,55]. The reason for these oscillations lies in the periodicity of energy exchange between pump wave with frequency ω and second harmonic wave with frequency 2ω. Varying the optical path by rotation of the sample, information about the nonlinear process within the sample can be obtained. This technique is strongly connected to different propagation of fundamental and SHG fields in dispersive materials.

Phase matching

Nonlinear processes like second harmonic generation or difference frequency generation require phase matching to be efficient. This means that a proper phase relationship between the interacting waves must be fulfilled along the propagation direction. More precisely, the phase mismatch has to be close to zero. For frequency doubling with collinear beams the phase mismatch is given by:

$$\Delta k = k_2 - 2k_1 \qquad [2.70]$$

where k_1 and k_2 are the wavenumbers of the fundamental and second-harmonic beam, respectively. Due to chromatic dispersion, one usually has $k_2 \neq 2k_1$, so that a phase mismatch occurs. The usual technique for achieving phase matching in nonlinear crystals is birefringent phase matching, where one exploits birefringence to cancel the phase mismatch.

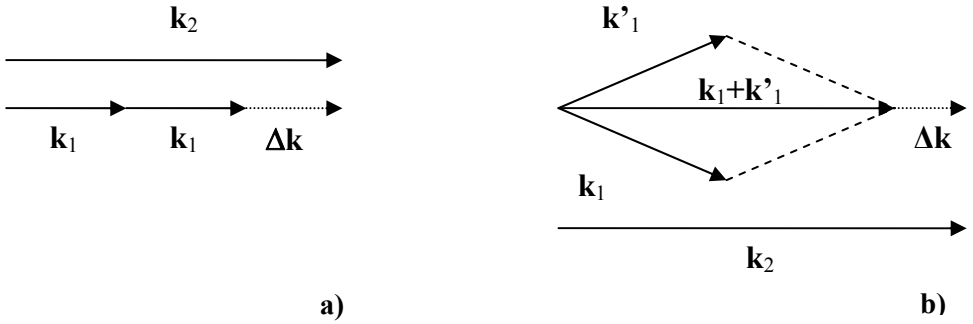

Fig. 13: Phase mismatch for second-harmonic generation. Due to chromatic dispersion, the wavenumber of the second harmonic is more than twice as large as that for the fundamental wave. This can be avoided by choosing a different polarization in a birefringent crystal (a) or by changing the angle between two fundamental beams in case of the noncollinear scheme of SHG (b)

There are two types of phase matching using birefringent films: *Type I,* where two incident photons of one polarization are converted into a single photon of the other polarization at the second harmonic. *Type II* phase matching occurs when the input beam consists of both polarization states and the second harmonic is polarized either ordinary or extraordinary depending on positive or negative birefringence, respectively[56].

In case of aligned thin polymeric films, usually only one linear polarized beam of fundamental frequency is used. This corresponds to type I phase matching. Although the two-beam SHG has some advantages especially in case of measurement of all nonzero components of susceptibility tensor[57,58] but it is more difficult to realize.

Matrix description of experiments

For a quantitative characterization of second-order nonlinear properties of poled films the Maker fringe technique is often used as reference. Usually the sample is a transparent spin-coated or vacuum-deposited film on a transparent substrate. Measurements of intensity and polarization of the second harmonic signal as a function of the angle of incidence of the fundamental beam with respect to the normal vector of film surface (Fig. 14) allows the evaluation of the components of the $\chi^{(2)}$-susceptibility tensor.

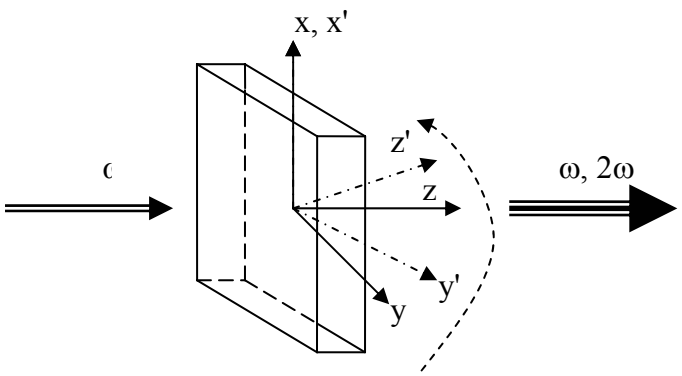

Fig. 14: Scheme of the SHG experiment. By rotating the sample around the x-axis and by change of the polarization angle one can involve in SHG different components of the nonlinear susceptibility tensor.

Sample rotation around the **x**-axis can be described by a *rotation matrix* applied to the susceptibility tensor:

$$R^{(x,\varphi)} = \begin{bmatrix} 1 & 0 & 0 \\ 0 & \cos(\varphi) & \sin(\varphi) \\ 0 & -\sin(\varphi) & \cos(\varphi) \end{bmatrix} \qquad [2.71]$$

Alternatively, $R_{i,i'}$ is a transformation operator between laboratory coordinates system *O* and coordinate system *O'* of the film principal axes. The tensor χ in O' can be written as:

$$\chi_{i'j'k'} = R_{i'i}^{(x,\varphi)} R_{j'j}^{(x,\varphi)} R_{k'k}^{(x,\varphi)} \chi_{ijk} \qquad [2.72]$$

The nonlinear polarization connected to SHG is described as:

$$P_i^{(2\omega)} = \varepsilon_a \chi_{ijk}^{(2)} E_j^{(\omega)} E_k^{(\omega)}, \qquad [2.73]$$

where $E_j^{(\omega)}$ and $E_k^{(\omega)}$ are the electrical vectors of two fundamental waves. For collinear SHG the fundamental wave can be presented as a mixture of two equivalent waves.

The first index in $\chi_{ijk}^{(2)}$ corresponds to the harmonic component while the second and third are indices of the fundamental waves.

The third-rank tensor $\chi_{ijk}^{(2)}$ in most of the cases can be replaced by a second-rank tensor d_{ij} that simplifies the description of susceptibility. Introducing the contracted notation as for $\chi_{ijk}^{(2)}$ in case of SHG (when $\omega_1=\omega_2$) one can write:

$$d_{ijk} = \frac{1}{2} \chi_{ijk} \qquad [2.74]$$

Since for SHG tensor d_{ijk} is symmetric in its last two symbols one can write it in the form of a 3x6 matrix:

$$d_{il} = \begin{bmatrix} d_{11} & d_{12} & d_{13} & d_{14} & d_{15} & d_{16} \\ d_{21} & d_{22} & d_{23} & d_{24} & d_{25} & d_{26} \\ d_{31} & d_{32} & d_{33} & d_{34} & d_{35} & d_{36} \end{bmatrix} \qquad [2.75]$$

Most of the components vanish or are equal due to symmetry. For materials with $C_{\infty v}$ symmetry (poled polymer film) and taking Kleinman's relations into account, the tensor d_{ij} in [2.75] reduces to a matrix containing only two non-zero components: d_{33} and d_{31}[53]. Therefore, the matrix **d** is:

$$\mathbf{d} = \begin{bmatrix} 0 & 0 & 0 & 0 & d_{31} & 0 \\ 0 & 0 & 0 & d_{31} & 0 & 0 \\ d_{31} & d_{31} & d_{33} & 0 & 0 & 0 \end{bmatrix} \qquad [2.76]$$

Now the polarization components are given by:

$$\begin{aligned} P_1 &= 2d_{31}E_3E_1 \\ P_2 &= 2d_{31}E_2E_3 \\ P_3 &= d_{31}\left(E_1^2 + E_2^2\right) + d_{33}E_3^2 \end{aligned} \qquad [2.77]$$

p- and s-polarization of electric field of the fundamental light can be described by the following electrical vectors:

p-polarization:

$$\mathbf{E} = \begin{bmatrix} 0 \\ E_p \\ 0 \end{bmatrix} \qquad [2.78]$$

where E_p is the y-component of the field.

s-polarization:

$$\mathbf{E} = \begin{bmatrix} E_s \\ 0 \\ 0 \end{bmatrix} \qquad [2.79]$$

where E_s is the *x*-component of the field.

d_{eff} can be defined as a scalar coefficient as follows:

$$P = \varepsilon_a d_{eff} E^2 \qquad [2.80]$$

where *P* and *E* are polarization and field amplitudes, respectively, for a certain sample position.

Performing measurements at different combinations of polarizations of fundamental and SH waves, the tensor elements of *d* can be obtained. In experiments with fixed polarization of the incident fundamental wave (s- or p-polarization) and fixed polarization of the detection system for the SH wave (s- or p-) one has p-p, p-s, s-p and s-s combinations. In the particular case of a poled polymer film the d_{eff} coefficient is:

pp-polarization:

$$d_{eff}^{p-p} = 2\,d_{31}\cos(\psi)\cos(\varphi)\sin(\varphi) + \left[d_{31}\cos^2(\varphi) + d_{33}\sin^2(\varphi)\right] * \sin(\psi) \qquad [2.81]$$

ps-polarization:

$$d_{eff}^{p-s} = 0 \qquad [2.82]$$

sp-polraization:

$$d_{eff}^{s-p} = \sin(\psi) * d_{31} \qquad [2.83]$$

ss-polarization:

$$d_{eff}^{s-s} = 0 \qquad [2.84]$$

where the angles φ and ψ are related to the fundamental and harmonic waves, respectively.

Fresnel reflection plays a significant role in that kind of configuration. Therefore, one should carefully take into account reflection rules including dispersion of refractive index at ω and 2ω.

Reflection/transmission in thin films during SHG

Passing through a thin or ultra thin layer the light of both frequencies ω and 2ω performs reflections at the air/film interface. Fig. 15 shows the propagation of both harmonic and fundamental waves. Due to dispersion of the material, the refraction angles are different for fundamental and SH beams. A special shift, also known as *walk-off effect* occurs. However, in our case the walk-off effect is negligible when the film thickness is much smaller than the beam diameter.

In addition, the nonlinearity of dyes used for guest-host systems is often of resonance or near-resonance nature. The polymers with embedded chromophores of such type have strong absorption in the UV-visible range. Together with Fresnel reflections at the air-film, film-substrate and substrate-air interface, the absorption creates significant losses especially at angles far away from normal incidence.

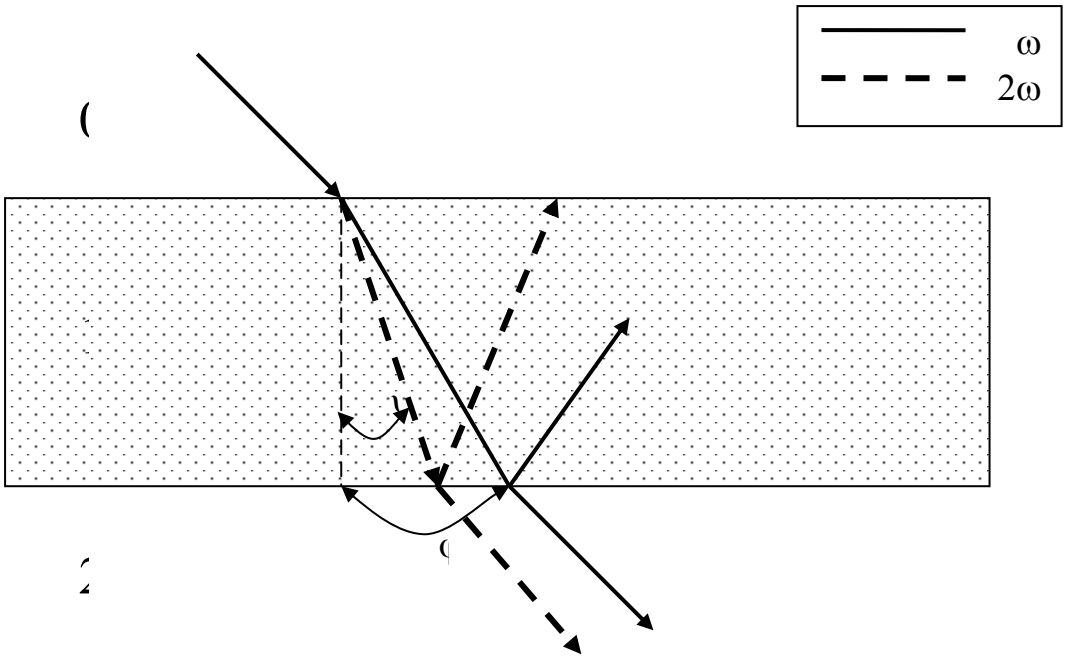

Fig. 15: Second harmonic generation by passing through a thin film. Multiple reflection for both frequencies must be included in transmission calculation.

Light transmission through a thin layer of a nonlinear material is describe by the transmission factor $T_{fh} = (t_{01}^{f} t_{12}^{f})^2$

where

$$t_{ij}^{p} = \frac{2n_i^p \cos\theta_i^p}{n_j^p \cos\theta_i^p + n_i^p \cos\theta_{ji}^p} \qquad [2.85]$$

$$t_{ij}^{s} = \frac{2n_i^s \cos\theta_i^s}{n_j^s \cos\theta_i^s + n_i^s \cos\theta_{ji}^s} \qquad [2.86]$$

are the Fresnel transmission coefficients for the field amplitudes, where *s* and *p* denote s- and p- polarizations, *h* and *f* stand for 'fundamental' and 'harmonic', respectively. The light is coming from medium *i* to medium *j*.

The typical procedure of the Maker-fringes experiment includes the measurement of the SHG signal generated by a thin quartz plate with known nonlinearity and refractive indices as a reference. The quartz plate must have known orientation so, that all Fresnel and nonlinear coefficients can be calculated. The relation between sample thickness and coherence length defines the shape of fringes. If the thickness of the sample is smaller than the coherence length, then no fringes are observed (

Fig. 17). The quartz plate is usually relatively thick, and hence, oscillations are observed as shown in Fig. 16.

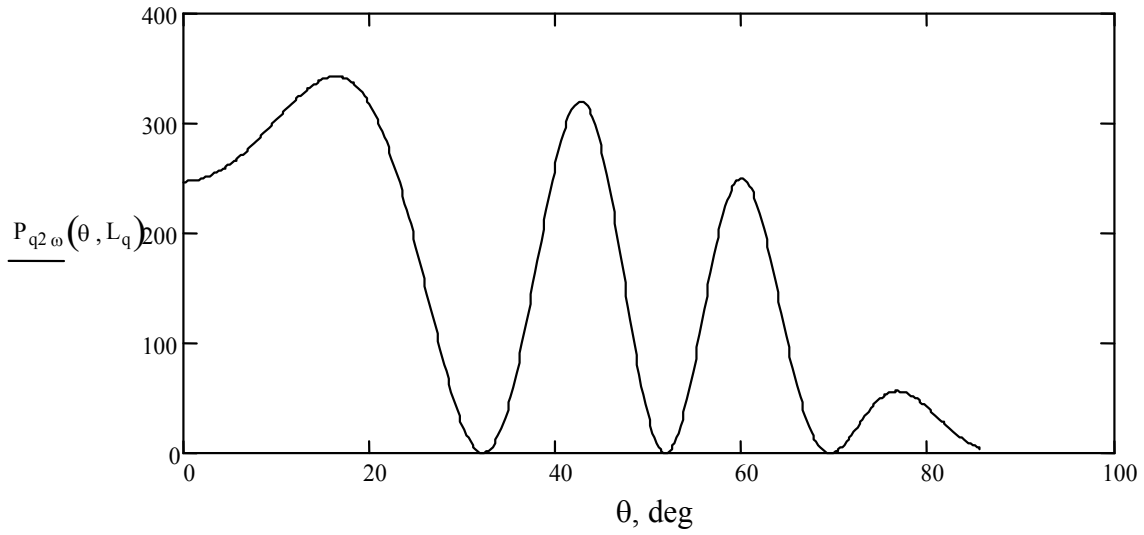

Fig. 16: Nonlinear polarization versus rotation angle calculated for a 0.47 mm thick quartz crystal. These data are used as a reference for quantitative calculation of d_{eff}

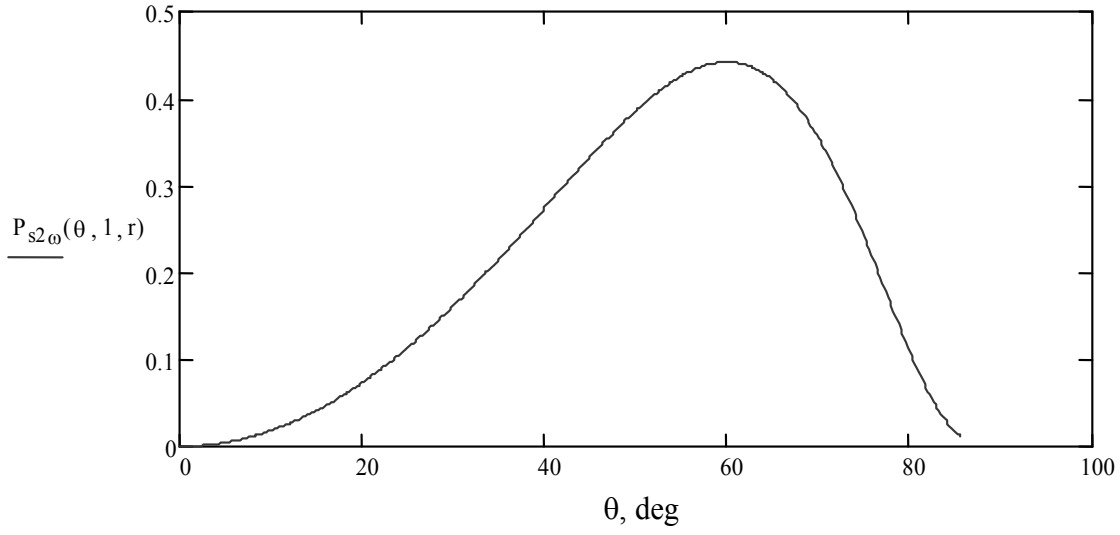

Fig. 17: The calculated nonlinear polarization of an oriented thin polymeric film. The curve shape is defined by the superposition of two effects: average orientation of dipoles normal to the surface and Fresnel reflection at higher angles.

The thickness of the quartz sample (0.47 mm) is large enough to produce fringes (Fig. 16) while a spin-coated polymeric film is thinner than the coherence length of the film material and oscillations do not exist (Fig. 17). Then the shape of the graph is mainly defined by Fresnel reflection from all surfaces and the average orientation of active molecules towards the normal of the polymer film. Assuming that the molecular dipoles are oriented along their long molecular axis, the nonlinear response at normal incidence is minimal.

Spatial pulse shape distortion during propagation in strongly nonlinear media.

The second-order nonlinear application in waveguides requires high concentration of optical energy in the waveguide core. Oriented doped polymers can have a $\chi^{(2)}$ value 1-2 orders higher than most of popular inorganic materials and crystals (LBO, KDP). The waveguide based device concept includes the assumption of high nonlinearity together with high intensity. A significant part of the fundamental beam can be converted into the second harmonic. In this case, the widely used approximation $A_\omega >> A_{2\omega}$ cannot be applied.

Analytical solution of a system of second-order nonlinear equations

The system of equations [2.66] describes the interaction between fundamental wave and second harmonic. Due to coupling between these waves, an energy exchange occurs. Since the right parts of equations [2.62] contain the amplitudes of the included waves, the propagation of both waves depends on its intensities (as usual in nonlinear optics). This problem can be solved by means of appropriate methods. In frequency conversion processes, such as SHG or DFG, two or more waves interact with each other while propagating through the nonlinear medium. In the case of type I phase matching, using the slow varying envelop approximation and assuming that there is no thermal distortion due to absorption of light, a system of two equations can be used to describe the interaction[35]:

$$\begin{cases} \dfrac{\partial A_1}{\partial z} = -i2\sigma_1 A_2 A_1^* e^{-i\Delta kz} \\ \dfrac{\partial A_2}{\partial z} = -i\sigma_2 A_1^2 e^{i\Delta kz} \end{cases} \qquad [2.87]$$

where $\Delta k = k_2 - 2k_1$ is the phase mismatch expressed by the difference between the wave vectors of the waves with circular frequency ω and 2ω, respectively, $\sigma_1 = k_1 \dfrac{\chi_{eff}^{(2)}(\omega)}{2n(\omega)^2}$ and $\sigma_2 = k_2 \dfrac{\chi_{eff}^{(2)}(2\omega)}{2n(2\omega)^2}$ are nonlinear coupling coefficients containing the effective second-order susceptibility $\chi_{eff}^{(2)}$ and refractive index n at frequencies ω and 2ω, respectively.

The functions $A_{1,2}(z,t)$ can be considered as constant at a distance range in the order of a wavelength or during a time ω^{-1} equal to the inverse circular frequency of the light wave.

Now, from complex amplitudes view, one can transform [2.87] into a system where amplitudes are real numbers. For that the phase shift between two propagating waves must be introduced. The substitution of

$$\begin{aligned} A_1(z) &= |A_1(z)|\exp[i\varphi_1(z)] = a_1 \exp[i\varphi_1] \\ 2A_2(z) &= |2A_2(z)|\exp[i\varphi_2(z)] = a_2 \exp[i\varphi_2] \\ \Psi &\equiv 2\varphi_1 - \varphi_2 + \Delta k \cdot z \end{aligned} \qquad [2.88]$$

in [2.87] gives a system of three equations[59]:

$$\begin{cases} \dfrac{da_1}{dz} + \sigma_1 a_1 a_2 \sin\Psi = 0 \\ \dfrac{da_2}{dz} - \sigma_2 a_1^2 \sin\Psi = 0 \\ \dfrac{d\Psi}{dz} - \Delta k + (\sigma_1 a_2 - \sigma_2 \dfrac{a_1^2}{a_2})\cos\Psi = 0 \end{cases} \qquad [2.89]$$

with the absolute amplitude values $a_{1,2}$ of the interacting waves, and a phase function Ψ which depends on the phase difference of the two waves, the phase mismatch factor Δk and the spatial coordinate z along the propagation direction of the travelling waves.

The invariant of the system of Eq. [2.89] is:

$$\frac{\sigma_2}{\sigma_1} a_1^2(z) + a_2^2(z) = \frac{\sigma_2}{\sigma_1} a_1^2(0) + a_2^2(0) = U^2 \qquad [2.90]$$

or, when there is no second harmonic signal at the input of the nonlinear medium we have:

$$U = \sqrt{\frac{\sigma_2}{\sigma_1}} a_1(0) \qquad [2.91]$$

The quantity U is the normalized amplitude of the fundamental wave at input. Taking into account equation [2.91], the set of equations [2.89] transforms into:

$$\begin{cases} \dfrac{da_2}{dz} = \sigma_1 (U^2 - a_2^2)\sin\Psi, \\ \dfrac{d\Psi}{dz} = \Delta k + \dfrac{\sigma_1}{a_2}(U^2 - 3a_2^2)\cos\Psi \end{cases} \qquad [2.92]$$

From the system of equations [2.92] the following differential equation can be obtained:

$$-\frac{d(\cos\psi)}{da_2} = \frac{(U^2 - 3a_2^2)\cos\psi + a_2 \Delta k / \sigma_1}{a_2 (U^2 - a_2^2)} \qquad [2.93]$$

that leads to an expression for the phase Ψ:

$$\cos\Psi = \frac{C - (a_2^2 \Delta k / \sigma_1)}{a_2 (U^2 - a_2^2)} \qquad [2.94]$$

The integration constant C is defined by border conditions $a_2(0)=a_{20}$ and $\psi(0)=\psi_0$.

Introducing *the reduced mismatch:*

$$\Xi = \frac{\Delta k}{\sigma_1 U} \qquad [2.95]$$

and the dimensionless amplitudes:

$$v_{1,2} = \frac{a_{1,2}}{U} \qquad [2.96]$$

the system [2.92] can be rewritten after transformation as[59]:

$$\begin{cases} \dfrac{dv_2}{dz} = (1 - v_2^2)\sin\Psi, \\ \dfrac{d\Psi}{dz} = 2\Xi + \dfrac{1 - 3v_2^2}{v_2}\cos\Psi \end{cases} \qquad [2.97]$$

where the dimensionless amplitude v_1 of the fundamental wave has been eliminated.

Using the following substitution: $C' = \dfrac{C}{U^3}$, one obtains

$$\cos\Psi = \frac{C' - \Xi v_2^2(z)}{v_2(z)\left[1 - v_2^2(z)\right]} \qquad [2.98]$$

and
$$C' = v_2(0)\left[1 - v_2^2(0)\right]\cos\Psi(0) + \Xi v_2^2(0) \qquad [2.99]$$

Now one can directly write down two integrals of the system [2.92]:

$$\begin{aligned} &\frac{\sigma_2 v_1^2}{2}(z) + \sigma_1 v_2^2(z) \equiv 1 \\ &v_2(z)\left[1 - v_2^2(z)\right]\cos\Psi(z) + \Xi v_2^2(z) \equiv Const \end{aligned} \qquad [2.100]$$

When there is no second harmonic at the input, i.e. $v_2(0) = 0$, we have $\cos\Psi = -\dfrac{\Xi v_2}{1 - v_2^2}$.
Substituting this result into the first equation of [2.97] we get for the evolution of the dimensionless amplitude v_2 of the harmonic wave along propagation direction z the following ordinary differential equations:

$$\frac{dv_2}{dz} = \pm\sigma_1 U\sqrt{1 - (2 + \Xi^2)v_2^2 + v_2^4} \qquad [2.101]$$

After squaring one obtains

$$\left(\frac{dv_2}{dz}\right)^2 = \sigma_1^2 U^2\left[1 - (2 + \Xi^2)v_2^2 + v_2^4\right]$$

Introducing the harmonic amplitude related to the reduced mismatch, we have

$$V_2(\rho) = \frac{v_2(z)}{\sqrt{\vartheta}} \qquad [2.102]$$

where ϑ is a normalization function which depends only on the reduced mismatch:

$$\vartheta = 1 + \Xi\left(\frac{\Xi}{2} - \sqrt{1 + \left(\frac{\Xi}{2}\right)^2}\right) \qquad [2.103]$$

and the square root of ϑ:

$$\sqrt{\vartheta} = \sqrt{1 + \left(\frac{\Xi}{2}\right)^2} - \frac{\Xi}{2}. \qquad [2.104]$$

Introducing a reduced distance $\rho = z\sigma_1 \frac{U}{\sqrt{\vartheta}}$ [2.105]

we have: $\left(\frac{d}{d\rho} V_2(\rho)\right)^2 = \left[1 - V_2^2(\rho)\right] \cdot \left[1 - \vartheta^2 V_2^2(\rho)\right]$. [2.106]

This is the equation for the Jacobi elliptic sinus $sn[\rho(z);\vartheta]$:

$$V_2(z) = \sqrt{\vartheta} sn\left[\rho(z);\vartheta\right] \qquad [2.107]$$

The Jacobi elliptic sinus $sn[\rho(z);\vartheta]$ is a periodic function of the reduced distance $\rho(z)$ and a parameter dependent period $T(\vartheta)$ which is connected to the parameter ϑ via the following equation (see Appendix for more details):

$$T(\vartheta) = 4\int_0^1 \frac{dy}{\sqrt{(1-y^2)(1-\vartheta^2 y^2)}} \qquad [2.108]$$

The coherence length (quarter distance of a period of function) is:

$$l_k = \frac{\sqrt{\vartheta}}{\sigma_1 U} \frac{T(\vartheta)}{4} \qquad [2.109]$$

It is a matter of initial conditions whether we have a purely second-harmonic generation case $a_2(0) = 0$ or a purely down-conversion case $a_1(0) = 0$. According to [2.87] in the pure down-conversion the classical description does not allow the generation of a signal at fundamental frequency from zero initial value. Quantum fluctuations are necessary to obtain such a signal[60].

$$4 \cdot \int_0^1 \frac{1}{\sqrt{(1-x^2)\cdot(1-\theta^2\cdot x^2)}}\, dx$$

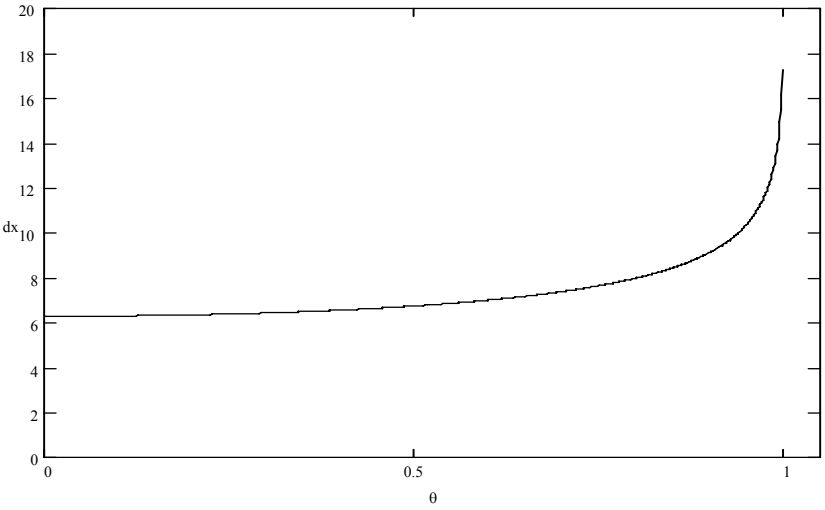

Fig. 18: The solution of the equation [2.106] for SHG is a periodic function with a parameter-dependent period. The parameter θ is defined by the phase-matching condition. For most of cases one has $\theta \approx 0$ and a corresponding period $T(\theta) \approx 2\pi$. Here the influence of the parameter ϑ on the period $T(\theta) = 4\int_0^1 \frac{1}{\sqrt{\left(1-x^2\right)\left(1-\theta^2 x^2\right)}} dx$ is shown.

According to Eq. [2.107] the harmonic field distribution within nonlinear media is described by a trigonometric periodic function in case of $|\Delta k| >> 0$ and actually achieves a constant value at $\rho > 4$ in the case when $\Delta k \to 0$ is valid (Fig. 19).

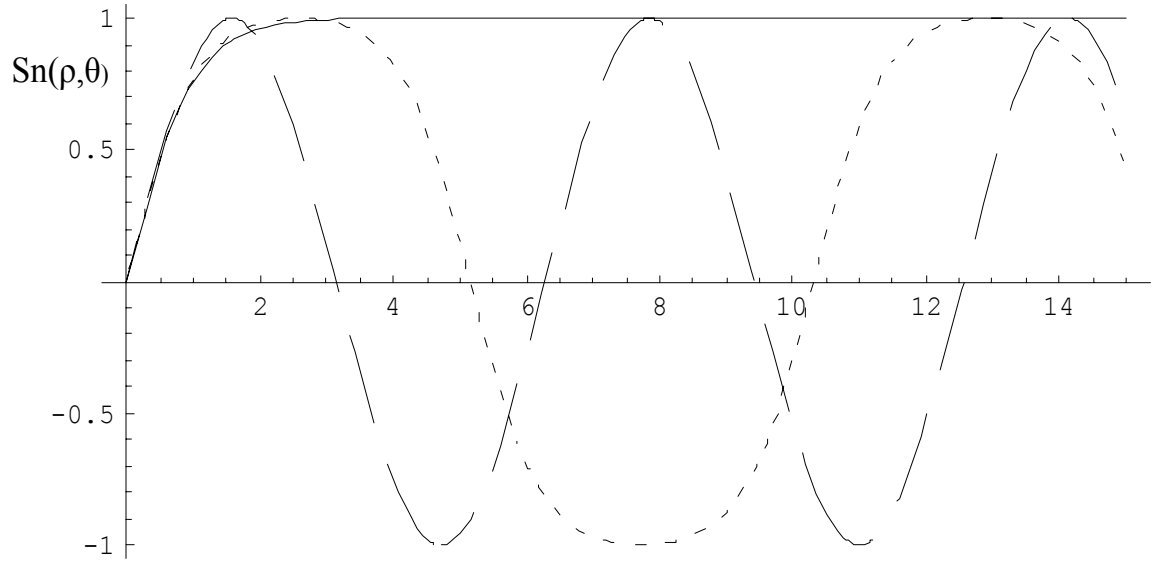

Fig. 19: Plot of the Jacobi elliptical sinus $sn(\rho;\vartheta)$ for fixed values of the parameter ϑ. (dashed) $\vartheta = 0$, sn(x;0)=sin(x); (solid) $\vartheta = 1$, sn(x,1) = tanh(x) and (short dashed) $\vartheta = 0.9$, sn(x;0.9)

When $\Xi >> 1$ $(\Delta k >> 2\sigma_1 U)$ the parameter $\sqrt{\vartheta}$ can be approximated according to $\sqrt{\vartheta} \approx \frac{\Xi}{2}\left(1+\frac{2}{\Xi^2}\right) - \frac{\Xi}{2} = \frac{1}{\Xi}$ as can be seen in Fig. 20. Hence, equation [2.107] can be replaced by:

$$v_2(z) = \frac{1}{\Xi}\sin z\sigma_1 U\Xi = \sigma_1 Uz\,\mathrm{sinc}\frac{\Delta kz}{2} \qquad [2.110]$$

where $\mathrm{sinc}\, x = \frac{\sin x}{x}$.

The coherence length l_k becomes constant: $l_k = \frac{\pi}{\Delta k}$.

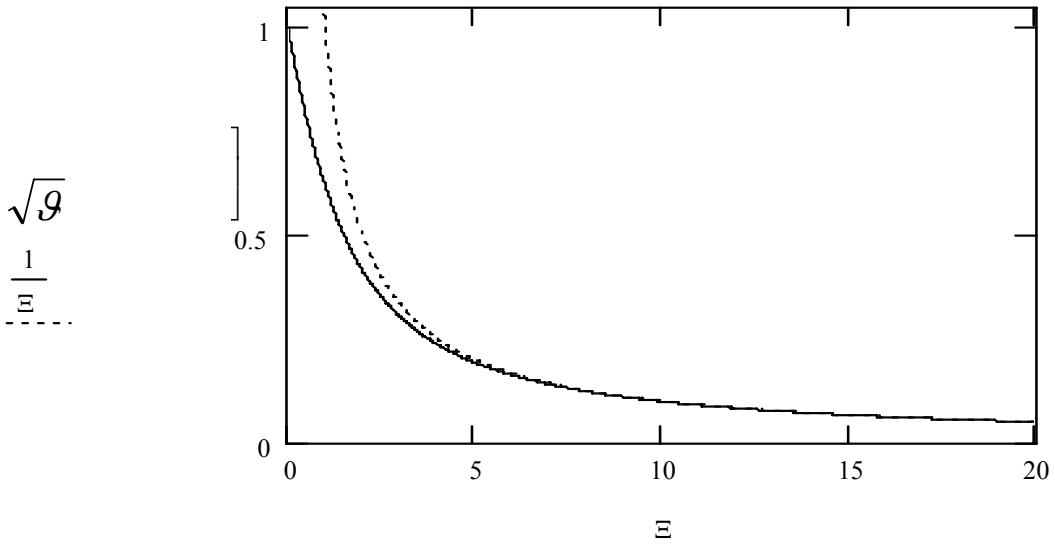

Fig. 20: Square root of the parameter $\sqrt{\vartheta} = \sqrt{1+\left(\frac{\Xi}{2}\right)^2} - \frac{\Xi}{2}$ (solid line) as functions of the reduced mismatch Ξ in comparison to the reciprocal $\frac{1}{\Xi}$ of the reduced mismatch (dashed line).

As can be seen in Fig. 20 in the limit $\Xi \to 0$ small deviations in Ξ can lead to significant changes of the parameter ϑ. This means that the period of the second harmonic amplitude distribution depends on the intensity of the fundamental wave.

The reduced mismatch $\Xi = \frac{\Delta k}{a_1(0)\sqrt{\sigma_1\sigma_2}}$ determines the character of interaction between fundamental and harmonic beams in the medium. The interaction length can be described by the dimensionless *reduced distance*:

$$\rho = z\sigma_1 \frac{U}{\sqrt{\vartheta}} = z \frac{a_1(0)\sqrt{\sigma_1\sigma_2}}{\sqrt{1+\left(\frac{\Xi}{2}\right)^2} - \frac{\Xi}{2}} \qquad [2.111]$$

A reduced distance in the range for $\Xi >> 1$ can be simplified as:

$$\rho = z\sigma_1 \frac{U}{\sqrt{\vartheta}} = z \frac{a_1(0)\sqrt{\sigma_1\sigma_2}}{1/\Xi} = z\Delta k \qquad [2.112]$$

Values of $\Xi \in 0..10$ occur either for $\Delta k \to 0$ or for large $a_1(0)\sqrt{\sigma_1\sigma_2}$ values (i.e. high fundamental field amplitude and high nonlinearity of the medium). The case $\Delta k \to 0$ is known as phase matching (PM). Other case, the process of SHG becomes sensitive to the fundamental wave amplitude distribution.

The NLO strength κ (in cm^{-1}) is defined as[61]:

$$\kappa = \sqrt{\eta P} = \frac{4\omega\chi^{(2)}}{\sqrt{2n_2 n_1^2 c^3 \varepsilon_a}}\sqrt{P} = \frac{\sqrt{2\varepsilon_a}}{\pi\sqrt{\sigma_2\sigma_2}}a_1$$
$$\eta = \left(\frac{4\omega\chi^{(2)}}{\sqrt{2n_2 n_1^2 c^3 \varepsilon_a}}\right)^2 \qquad [2.113]$$

where η is the usual NLO figure of merit (in $cm^2\ W^{-1}$), P is the power of the fundamental beam (in W). In the present case κ can be rewritten as:

$$\kappa = \frac{\sqrt{2\varepsilon_a}}{\pi}\frac{\Xi}{\Delta k}a_1^2 = \frac{\sqrt{2\varepsilon_a}}{\pi}\frac{\Xi}{\Delta k}I_1 \qquad [2.114]$$

This means the nonlinear strength is proportional to the intensity of the fundamental and proportional to the ratio of the reduced phase mismatch to the standard value of phase mismatch.

SHG in absorptive media

Fulfilment of linear properties to necessary requirements is a first step of selection of materials for photonic applications. This chapter describes these requirements and clarifies essential fabrication conditions.

Since nonlinear phenomena often contain waves with several wavelengths, the film transparency at the working wavelengths is required. For instance, when a light wave is converted into another light wave during SHG then two wavelengths are involved, the fundamental (F) and second harmonic (SH). The wavelength of the SH wave is two times shorter than the wavelength of the fundamental. During propagation within nonlinear media the energy of the fundamental is converted into the SH (Fig. 21a, where the fundamental has a wavelength λ = 1064 nm and the SH has λ = 532 nm). Even a small value of imaginary part $\kappa = 10^{-4}$ of refractive index $\tilde{n}=n-i\kappa$ at fundamental frequency is enough for a significant reduction of conversion efficiency of SHG (Fig. 21b).

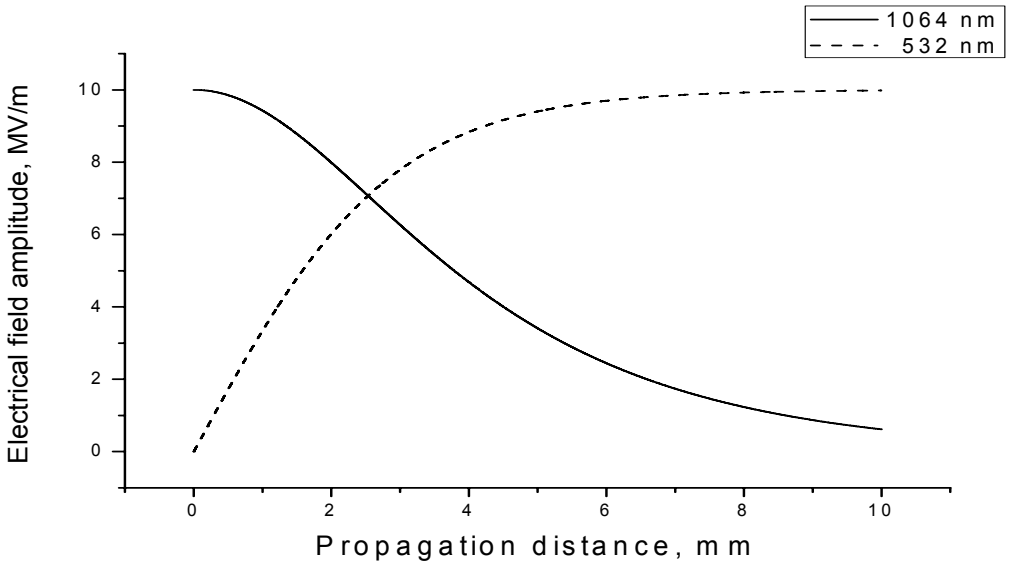

a) $\kappa_{1064}=0$, $\kappa_{532}=0$

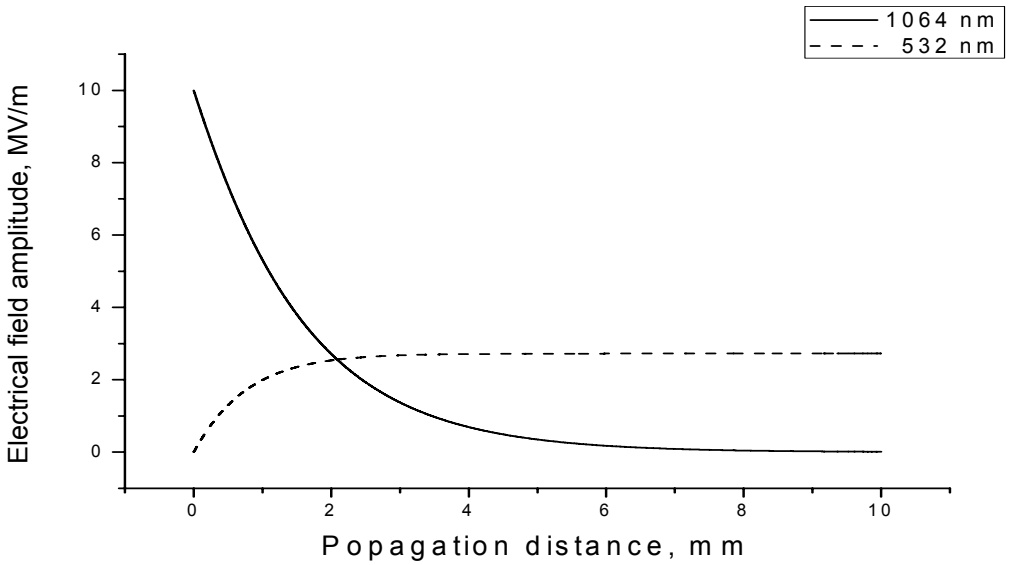

b) $\kappa_{1064}=10^{-4}$, $\kappa_{532}=0$

Fig. 21: SHG process in presence of a small absorption. The efficiency is reduced 5 times when the imaginary part (κ) of refractive index at fundamental frequency is equal to 10^{-4}.

In absence of optical losses ($\kappa = 0$) a strong decrease of fundamental intensity with increasing propagation length can be seen. Simultaneously, the intensity of the SH wave is increasing due to complete energy transfer from the fundamental to the SH wave. In contradiction to that, we find even for small optical losses at fundamental wavelength a complete different situation. The fundamental intensity decreases strongly with increasing propagation length but the SH intensity increases only slightly although no absorption of SH intensity was assumed. The reason for the observed behaviour is that already at small losses a significant portion of fundamental intensity is dissipated so that only a certain fraction can be converted into the SH wave. However, a more common situation includes that the second harmonic is absorbed while the fundamental is not (Fig. 22a). This is connected to the fact that the SH wave has a shorter wavelength than the fundamental, and is influenced by electronic transitions laying in the UV and visible range which cause optical losses. The fundamental wave typically lies in the infrared range where those mechanisms do not play a significant role. The conversion into the SH wave is less efficient than in the lossless case and shows a maximum versus propagation length.

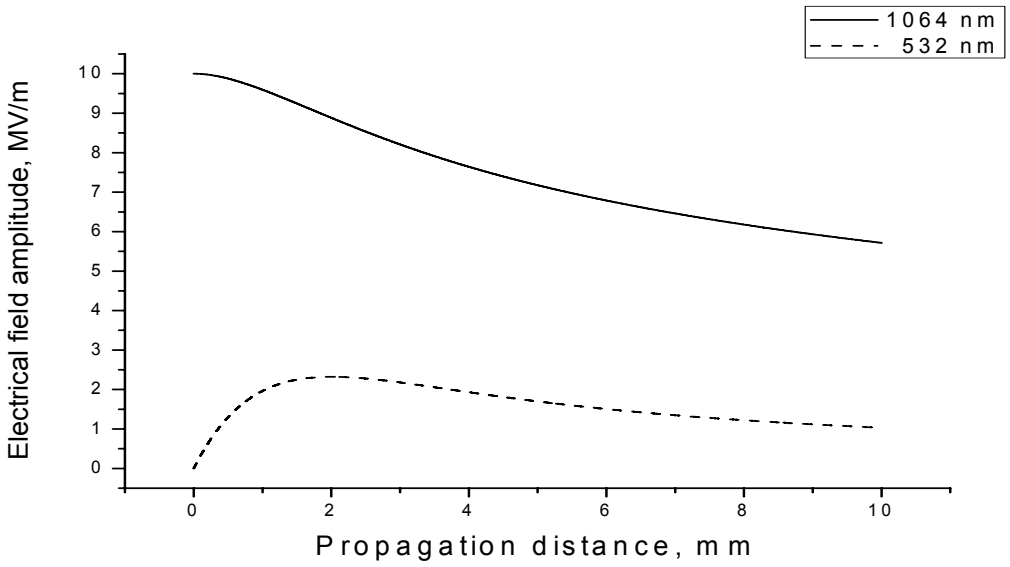

a) $\kappa_{1024}=0$, $\kappa_{532}=10^{-4}$

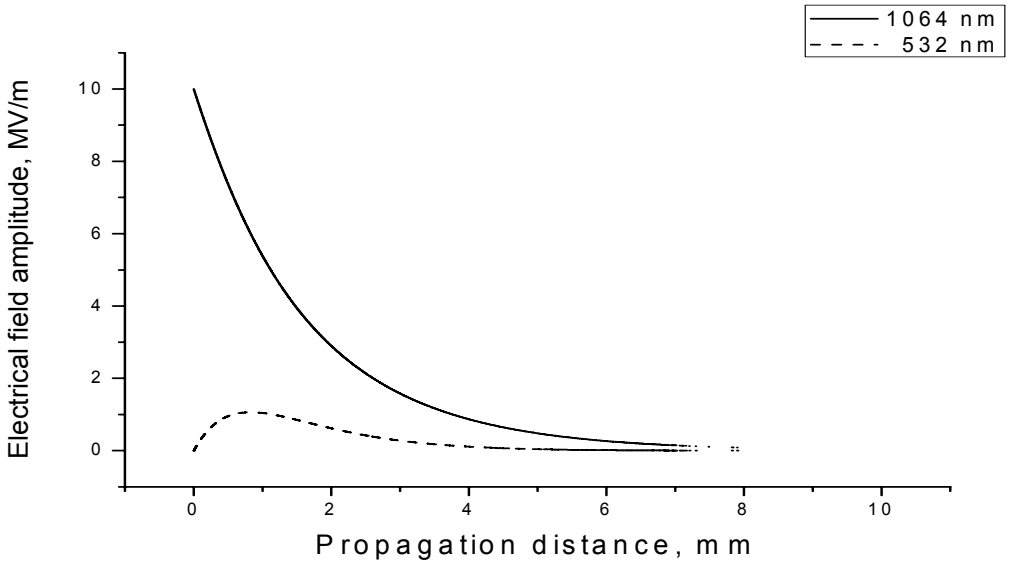

b) $\kappa_{1024}=10^{-4}$, $\kappa_{532}=10^{-4}$

Fig. 22: Electric field amplitude for fundamental and SH wave versus propagation length at presence of optical losses for the SH wave which reduce efficiency of conversion over a long distance. The SH wave reaches a maximum value which defines a most favourable length for the process.

However, in case of vibrational (infrared) losses the fundamental can show attenuation too which leads to a further reduction of conversion efficiency (Fig. 22b). Also in that case a maximum of SH intensity versus propagation length is found so that an optimum conversion length can be defined (cf. Figs. 22a and 22b).

Propagation of the beam with Gaussian profile

In the following the behaviour of a Gaussian pulse shape in nonlinear media is analyzed. In most cases, the intensity distribution of a laser beam along a direction *r*, which is normal to the propagation direction, can be described by a Gaussian distribution by the following equation:

$$a_1(r) = a_{\max} \exp\left(-\frac{r^2}{2w^2}\right) \qquad [2.115]$$

where *w* is the characteristic width, and *r* is the distance from the beam centre taken to be perpendicular to the propagation direction.

A Gaussian beam has a maximum intensity value in the centre and decays towards zero at the periphery. Therefore, different parts of the pulse have different values of the parameter $\sqrt{\vartheta}$ in eq. [2.107]. This leads to differences in the corresponding periods defined in eq. [2.108] and the coherence lengths defined in eq. [2.109]. Consequently, long nonlinear interaction distances as in waveguides lead to a perturbation in the planes of equal phase.

Both the parameters of the travelling waves and the properties of the material have influence on the behaviour of the pulse shape in space and time. One can highlight the different possible situations as follows:

1.) The situation for the reduced mismatch characterized by $\Xi >> 1$ (see Fig. 23) is described by a sinusoidal law [2.110] for the dimensionless amplitude ν_2, a weak field of the fundamental wave together with low nonlinearity of the medium, and leads to a vanishing pulse shape distortion. The SH signal achieves a maximum at a quarter of the coherence length $l_k = \frac{\pi}{\Delta k}$. This corresponds to the situation used in the quasi phase-matching (QPM) technique.

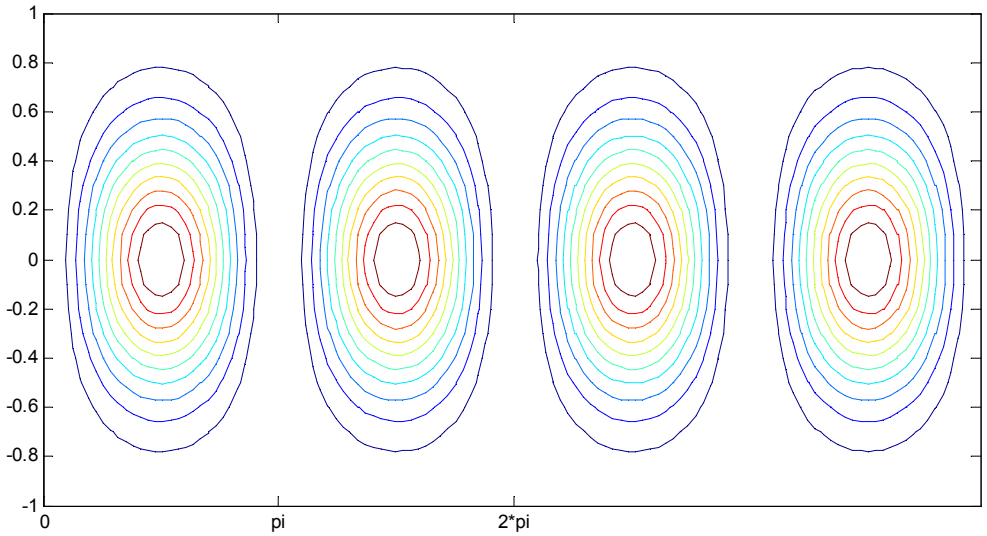

(a)

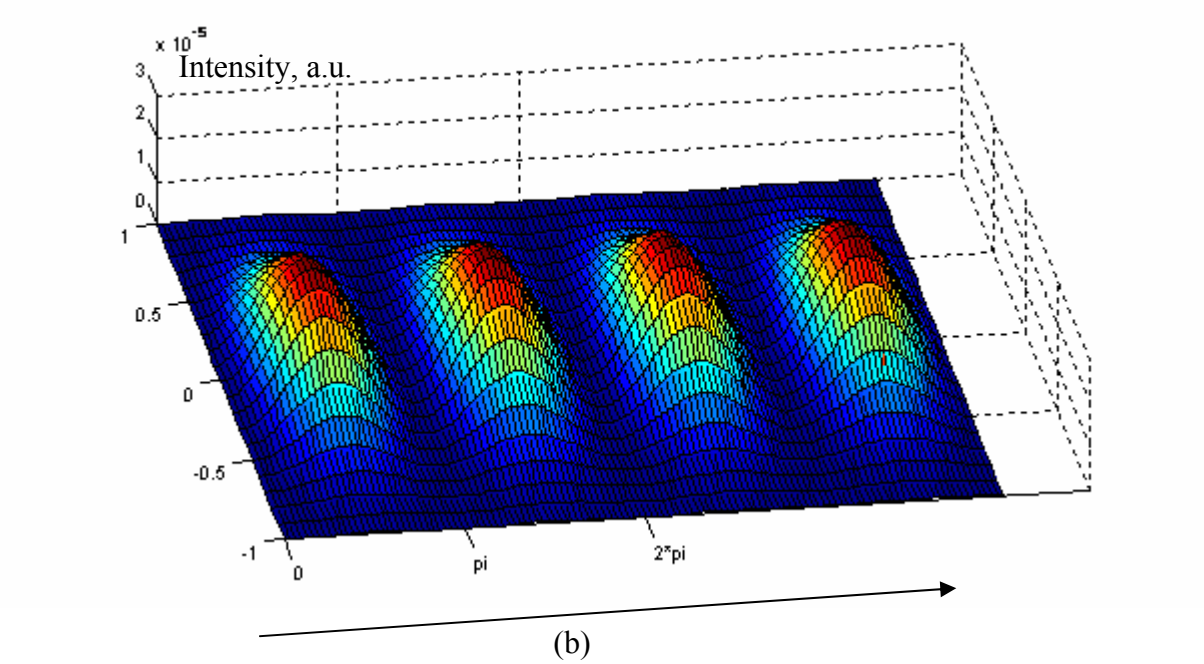

(b)

Fig. 23: Normalised SH intensity generated by a Gaussian beam along the normalized propagation direction p: (a) projection to the *y*-*p*-plane, (b) 3-d contour plot.

2.) In the case, where the reduced mismatch is in the range $\Xi \in 1..10$ (Fig. 24), a situation is described by the medium with a high optical nonlinearity together with a strong field of the fundamental wave or interaction distance is long. This causes a clear pulse deformation.

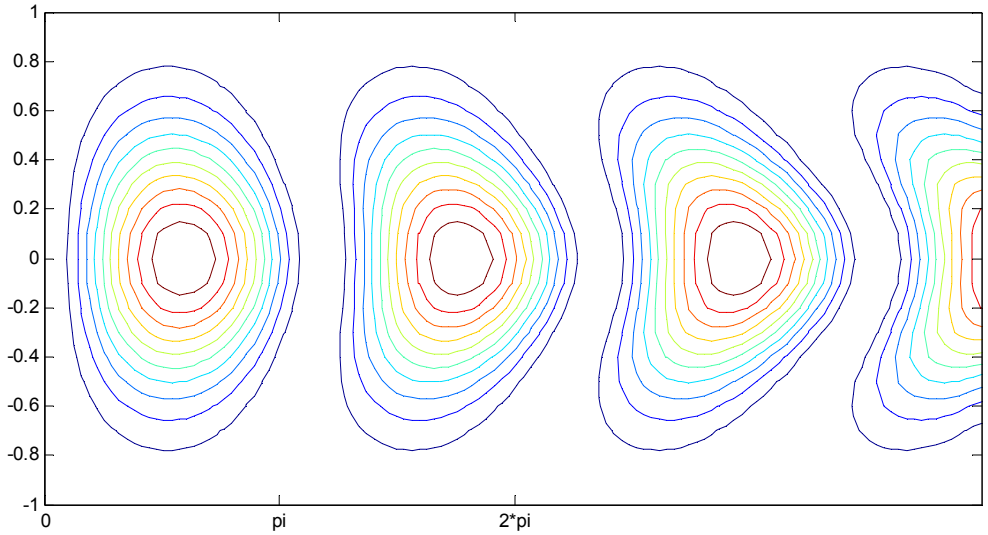

(a)

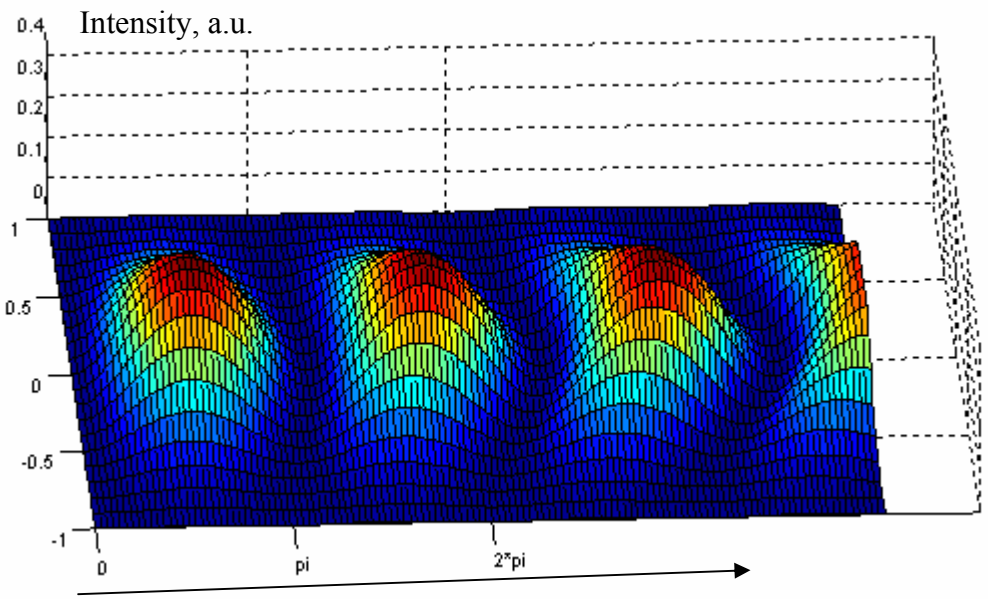

(b)

Fig. 24: Projection and contour plots of SH intensity versus reduced distance generated by a Gaussian beam propagating in a medium where $\Xi = 1.5$, first 3 periods (a,b).

The original pulse is deformed in the course of the first few periods (Fig. 24 a,b), divides subsequently into two pulses and into more pulses with further propagation. The efficiency of pulse splitting becomes higher as Ξ approaches 1. It is necessary to take into account that a considerable deformation can be achieved only in the case of a long sample, i.e. if the distance travelled is sufficiently long (Fig. 25). However, a long distance can be coupled to further distortion effects such as diffraction.

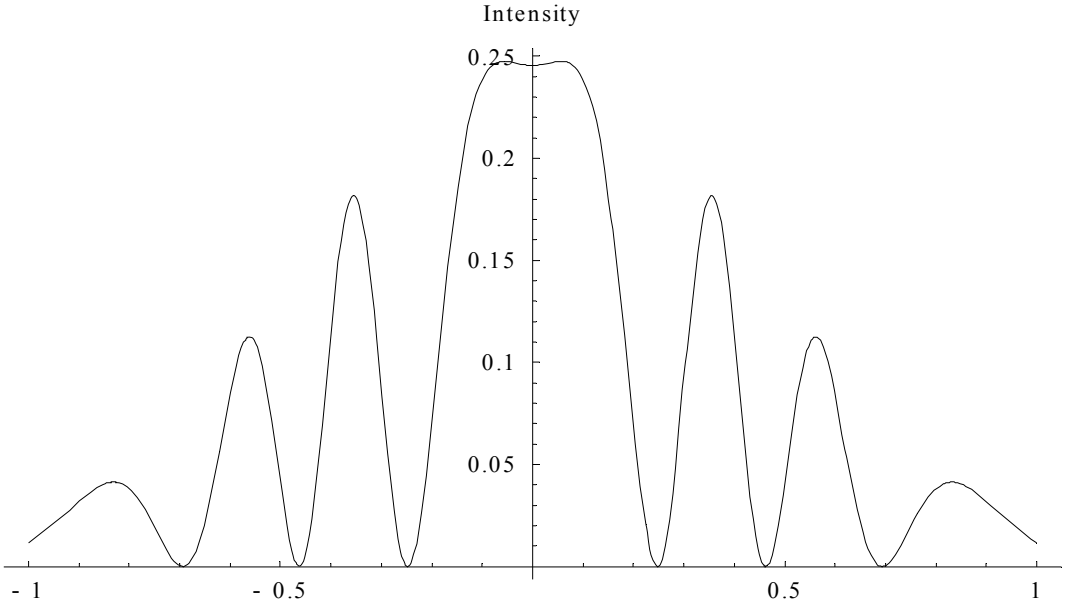

Fig. 25: Cross-section through a SH pulse at long distance perpendicular to the propagation direction. The reduced distance is 52π.

3.) The situation where the reduced mismatch is in the range $\Xi < 1$ includes a high nonlinearity ($\chi^{(2)} \sim 10^{-10} \div 10^{-11} \frac{m}{V}$), a strong fundamental field ($\geq 10^{8} \frac{V}{m}$) and small values of phase mismatch ($\Delta k < 10^{6} m^{-1}$), all of which leads to a situation where the centre of the pulse propagates practically according to a hyperbolic tangent dependence, while the pulse wings still follow an almost sinusoidal dependence. This reduces the pulse half-width and divides it into 2-3 pulses during the first few periods (Fig. 25).

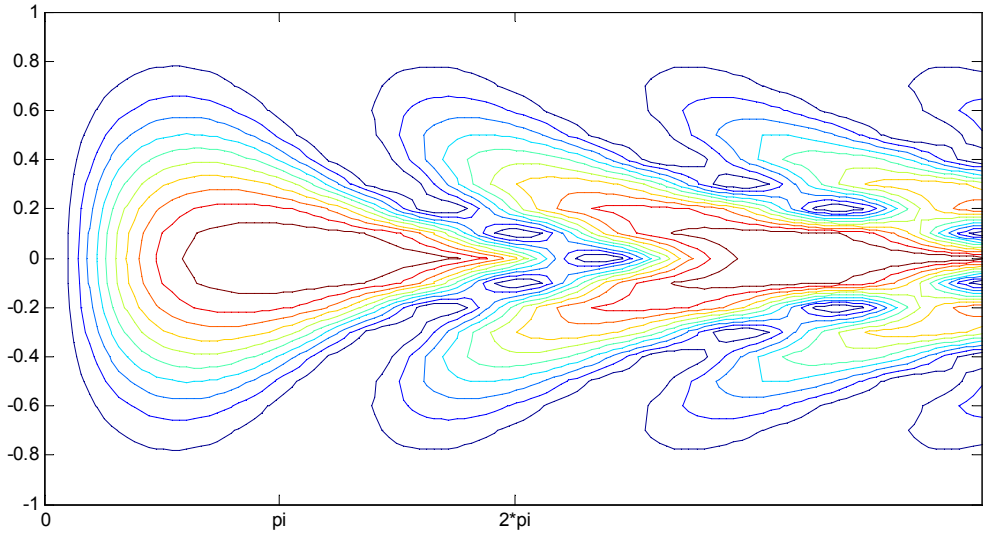

(a)

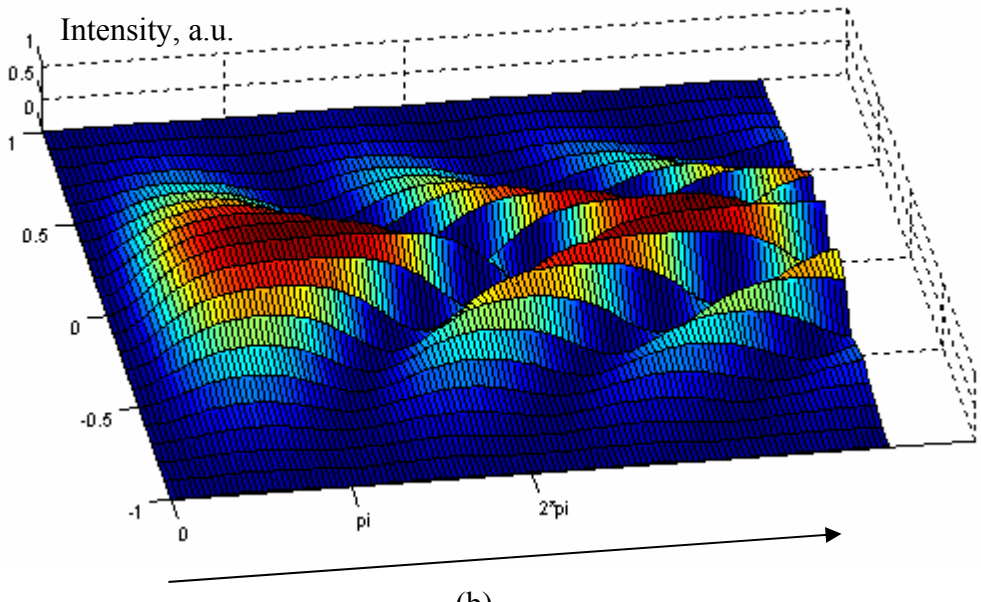

(b)

Fig. 26: SH Gaussian beam propagation in media when $\Xi = 0.1$, for the first 3 periods (a) 2-d contour plot, (b) 3-d plot.

The situation when the central part of the SH pulse overlaps with the wings of the peak of the next period can be interpreted as splitting of the SH beam (Fig. 27).

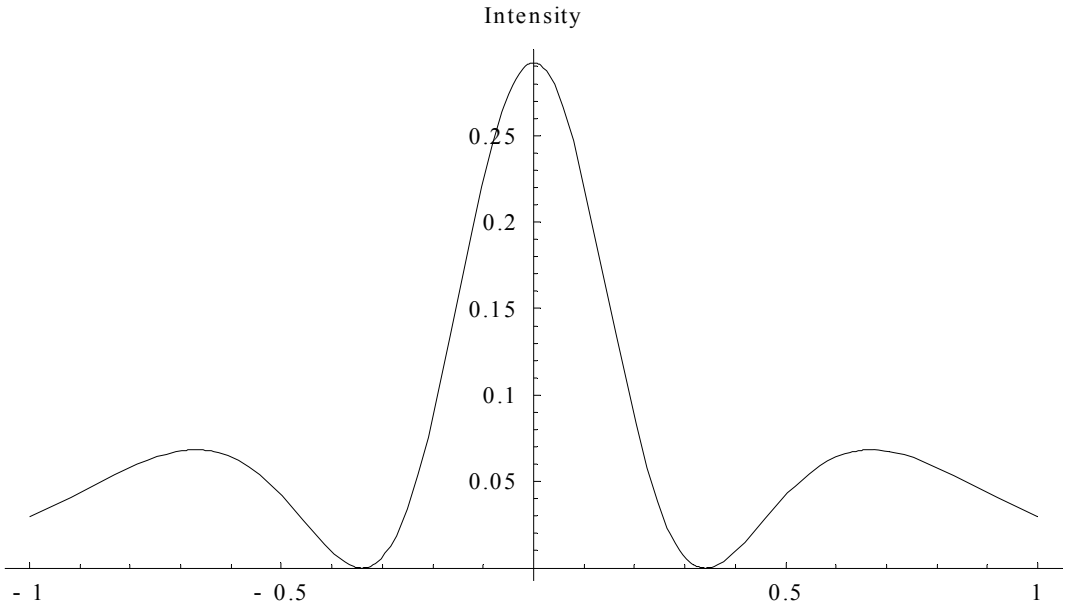

(a)

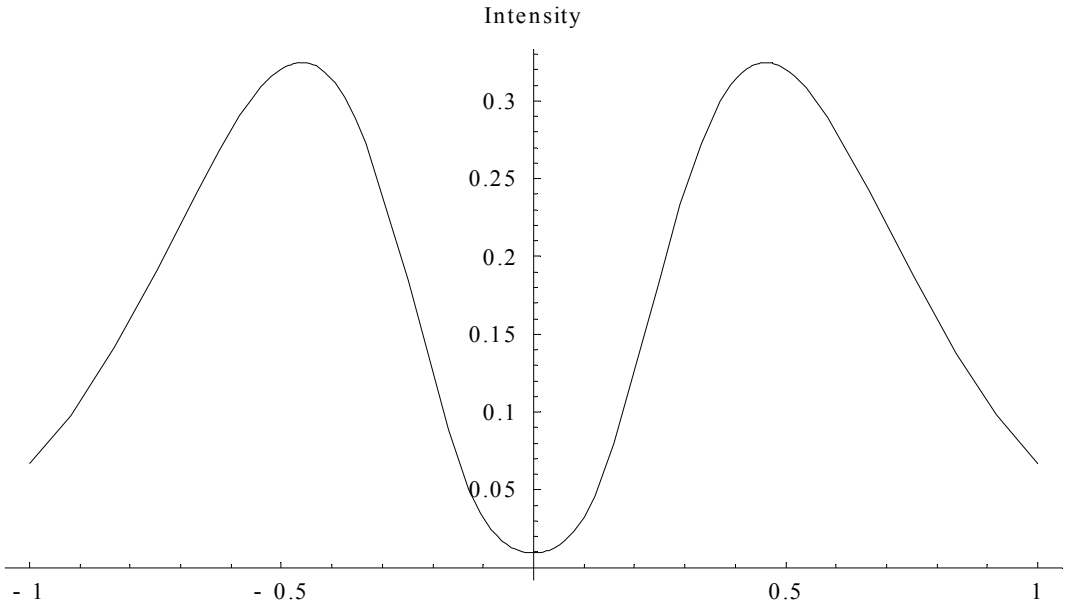

(b)

Fig. 27: Spatial cross-sections through a pulse propagating with a parameter value $\Xi = 0.2$ at (a) z=1.25π and (b) z=1.5π. Two satellites appear and later the pulse divides into two pulses as described by Flueraru et al.[61]

As an example a laser system is considered which generates pulses of $\tau = 30\,ps$ duration with an energy per pulse of $\mathrm{E}_p = 1\,mJ$ which is focused onto an area $w = 1\,mm^2$. This system induces an electrical field having field strength around 10^7-10^8 V/m (the exact value depends on the pulse temporal profile). The power per unit area P is in that case $P = \frac{\mathrm{E}_p}{\tau \cdot w^2} = 3.33\frac{GW}{cm^2}$. The damage threshold for a lithium triborate LiB_3O_5 (LBO) crystal is $45\frac{GW}{cm^2}$ at 1.064 μm[62]. Since the nonlinear properties of the LBO crystal have low values in

comparison with most organic nonlinear materials, pulse distortion can barely be observed. So the type I SHG in LBO at 1064 nm has a non-linear coefficient of $d_{eff} = 0.96\frac{pm}{V}$. The reduced mismatch under such conditions, reaches a value of $\Xi = 53.4$, which does not allow a clear observation of the pulse distortion effect.

Coupling equations for QPM

A.Armstrong and N.Blombergen with co-workers have offered at once three ways of realisation of phase synchronism[16], three experimental arrangements to provide phase correction, if the phase velocities of the fundamental and second harmonic are not matched:

(a) After a distance $\frac{\pi}{\Delta k}$ the crystal is replaced by its inversion image. The nonlinear susceptibility $\chi^{(2)}$ changes sign. The linear optical properties remain the same.

(b) Both fundamental and second harmonic undergo multiple total reflections in a crystal of thickness $\frac{\pi}{\Delta k}\cos\theta_{total}$. On each reflection E_1 and E_2 undergo a π phase shift, the product E_2E_1 changes sign.

(c) The travelling wave at ω_1 pumps the interferometer cavity, which contains a nonlinear dielectric and is resonant at ω_2. The backward harmonic wave does not interact with the pump. On each forward pass it has the correct phase for amplification.

In the first way synchronism was carried out by using a set of thin plates from a NLO material, the direction of each optical axis periodically (from a plate to a plate) changes the direction of optical axis. In the second way it was suggested to use an optical waveguide from the nonlinear material, designed in such a manner that the generalised phase at full internal reflection at the waveguide walls changes by π. The third way consisted in using an interferometer, filled with a nonlinear material and adjusted to the second harmonic wave. The common approach in all these ways was that the thickness of each plate in the set of plates, or the size of a way of one pass of light between waveguide walls, or an interferometer thickness should be equal to the coherence length of SHG, on which the amplitude of the second harmonic does not decrease. The jump of the generalised phase in all these cases allows a wave of the second harmonic to continue with amplitude increase in the following plate, or in the following pass between waveguide walls, or the following pass of the resonator. Phase synchronism of such discrete type has received the name Quasi Phase Matching (QPM)[63]. Furthermore, the idea of Blombergen using the set of plates was essentially added and developed, that finally has led to modern solutions of creation of highly effective crystals from regular domain structures[59].

As an example of QPM, periodically poled media can be described by a similar set of equations, given below as Eq. [2.97]. The solution can also be expressed by a Jacobi elliptical sinus given by Eq. [2.107]. Hence, the same common principles can be applied to the field distribution within the media under consideration. However, due to the inhomogeneity some additional effects should be taken into account. The procedure must include an exact solution on every domain including the boundary conditions (phase and amplitudes of both signals, i.e. fundamental and SH). This requires the application of numerical methods.

The process of SHG and the pulse propagation in periodically poled media are described by the following system of equations:

$$\begin{cases} \dfrac{dv_2}{dz} = \dfrac{2}{m\pi}(1-v_2^2)\cos\Psi, \\ \dfrac{d\Psi}{dz} = \dfrac{2}{m\pi}\left(m\pi\beta - \dfrac{1-3v_2^2}{v}\sin\Psi\right), \end{cases} \quad [2.116]$$

where β and K_m are defined via $\beta = \Xi\dfrac{\Delta k - K_m}{\Delta k}, K_m = \dfrac{2\pi m}{\Lambda}$, Λ is the QPM grating period, and m is the QPM order. β is a measure for the phase mismatch in the QPM structure and K_m represents the m-th order quasi wave vector of the periodic structure.

Replacement of the variables in Eq. [2.89] by $\theta = \pi/2 - \Psi$, $\xi = 2z/m\pi$ leads to equations similar to Eqs. [2.97]:

$$\begin{cases} \dfrac{dv_2}{dz} = (1-v_2^2)\sin\theta, \\ \dfrac{d\Psi}{dz} = -m\pi\xi + \dfrac{1-3v_2^2}{v_2}\cos\Psi \end{cases} \quad [2.117]$$

If there is no SH signal at the input one can solve system [2.117] and obtain the solution v given by the following equation:

$$v_2 = \sqrt{\gamma}\,sn(u,\gamma) \quad [2.118]$$

Where $\sqrt{\gamma} = \sqrt{1+\left(\dfrac{m\pi\beta}{4}\right)^2} - \dfrac{m\pi|\beta|}{4}$, $u = \dfrac{2\xi}{m\pi\sqrt{\gamma}}$,

It should be mentioned that [2.118] is similar to [2.107] but the term $\dfrac{\Delta k - K_m}{\Delta k}$, which is part of the coefficient β is independent on intensity. However in the case of a material dependent phase mismatch $\Delta k \neq 0$, tuning of K_m can be used to compensate for the natural material dispersion and to make the parameter β to zero. This implies that the pulse shape distortion is almost negligible due to the weak intensity dependence of the conversion efficiency typical for the situation far from phase matching. This means that different parts of a propagating pulse are converted to the harmonic wave and back with the same conversion factor, i.e. the spatial pulse shape is invariant under these conditions.

Second-order nonlinear effects

Molecular nonlinear optical properties of organic materials

Molecular materials are of interest because they can show extraordinary high off-resonant optical nonlinearities. In order to estimate nonlinear optical properties one has to get information about the electronic structure of the materials of interest. Quantum chemical (QC) calculations allow one to get basic information about the electronic structure on a certain molecular level. Various QC methods of different degrees of sophistication are used to get more inside into the origin of optical nonlinearities.

Schrödinger equation

The starting point for description of the electronic structure of the nonlinear chromophores is the non-relativistic time-independent Schrödinger equation:

$$\hat{H}\Psi = E\Psi \qquad [3.1]$$

where the Hamiltonian, $\hat{H}$, in atomic units is[64] :

$$\hat{H} = -\sum_i \frac{1}{2}\nabla_i^2 - \sum_A \frac{1}{2M_A}\nabla_A^2 - \sum_{i,A} \frac{Z_A}{|\mathbf{r}_i - \mathbf{R}_A|} + \frac{1}{2}\sum_i \sum_j \frac{1}{|\mathbf{r}_i - \mathbf{r}_j|} + \frac{1}{2}\sum_i \sum_A \frac{Z_A Z_B}{|\mathbf{R}_A - \mathbf{R}_B|} \qquad [3.2]$$

where $r_{i,j}$ and $R_{A,B}$ are the position vectors for the electrons and nuclei. The first two terms are related to the kinetic energy of the electrons and the nuclei, respectively, the third term is the operator for the Coulomb attraction between the electrons and the nuclei, and the last two terms express the Coulomb repulsion between pairs of electrons and pairs of nuclei[65].

According to molecular orbital theory, each molecule has a set of molecular orbitals. Each molecular orbital wave function ψ_i may be written as a simple weighted sum of the n constituent atomic orbitals φ_j:

$$\psi_i = \sum_j C_{ij}\phi_j \qquad [3.3]$$

where C_{ij} is a matrix of coefficients.

In the ground state, electrons populate the molecular orbitals with the lowest energy first as can be seen in Fig. 28a. Linear optical excitation transfers one electron from the highest occupied molecular orbital (HOMO) to the lowest unoccupied molecular orbital (LUMO) as shown in Fig. 28b.

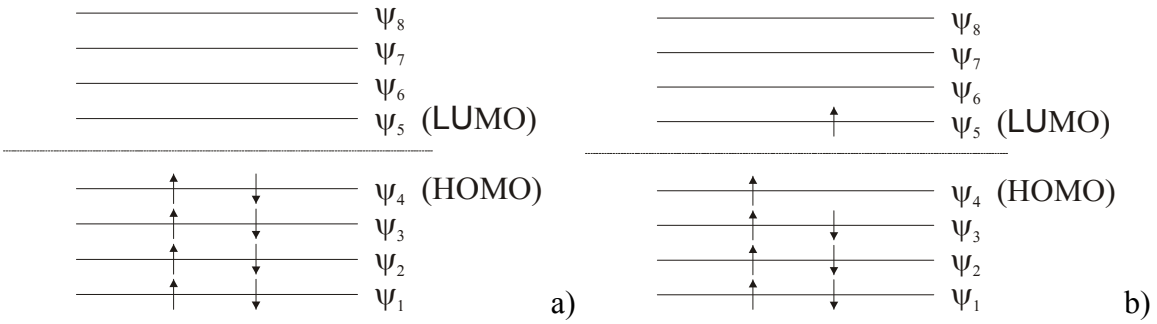

Fig. 28: Ground state and excited state of a molecular system. The arrows represent the spins of electrons. The distance between highest occupied molecular orbital (HOMO) and lowest unoccupied molecular orbital (LUMO) is the single particle optical gap E_{ge}.

Calculation of molecular orbital energies gives information about many properties that can be observed in experiment. For instance, according to Koopmans' theorem the first ionization energy of a molecule is equal to the energy of the highest occupied molecular orbital (the HOMO), and the electron affinity is the negative of the energy of the lowest unoccupied orbital (the LUMO).

Ab-initio calculations

In *ab-initio* calculations, the basis sets (linear combination of atomic orbitals) describe the molecular orbitals. Widely used orbital types are Slater Type Orbitals (STO) that are based on an *exp(-αr)* spatial dependence, and Gaussian Type Orbitals (GTO) based on an *exp(-αr²)* law. These molecular orbitals are usually associated with shells, such as an s-shell, sp-shell, etc. The basis sets determine the only parameters in ab-initio calculations. Usually, ab-initio methods use only fundamental physical constants (Planck's constant, speed of light in vacuum etc.) without introducing empirical parameters.

Semi-empirical calculations

Two approaches are usually involved in semi-empirical calculations. The first approach includes the formation of the Hamiltonian matrix using empirical data or data obtained by ab-initio methods. The second approach neglects some differential overlap terms in two-electron integrals. Since the number of two-electron integrals is sufficiently high (N^4) such approach significantly decreases calculation time.

The simplest approximation is the *complete neglect of differential overlap* (CNDO) expressed by:

$$\phi_i\phi_j = \delta_{ij}\phi_i\phi_i \quad . \qquad [3.4]$$

Another approximation is the *neglect of diatomic differential overlap* (NDDO):

$$\phi_i^A\phi_j^B = \delta_{AB}\phi_i^A\phi_j^B \qquad [3.5]$$

where *A* and *B* correspond to the numbers of atoms in the molecule. The NDDO approximation is the basis for the MNDO (Modified Neglect of Differential Overlap), MNDO/d (MNDO with *d*-functions), AM1 (Austin Model 1), and PM3 (Parameterized Model number 3) methods. In addition to the integrals used in the INDO (Intermediate Neglect of Differential Overlap) methods, they have an additional class of electron repulsion integrals. This

class includes the overlap density between two orbitals centred on the same atom interacting with the overlap density between two orbitals also centred on a single (but possibly different) atom. That allows the calculation of the effects of electron-electron interactions on different atoms[66].

Semi-empirical calculations are much faster than ab-initio methods. Therefore, using semi-empirical methods on can obtain the molecular parameters used for calculation of microscopic nonlinear properties of relatively big molecules containing tens or hundreds of atoms.

Two level model

The molecular second-order hyperpolarisability term β is described in a simple manner by the two-state quantum mechanical model, which was introduced by Oudar and Chemla[67]. This model is based on the sum over states approach. From the optimized geometry of the ground state the dipole moments for ground and first excited states together with HOMO-LUMO gap can be calculated. Then the low-frequency hyperpolarisability can be obtained according to the following formula[35,52]:

$$\beta_0 = \frac{\left(\mu_{ee} - \mu_{gg}\right)\mu_{ge}^2}{E_{ge}^2} \qquad [3.6]$$

where $\mu_{ee} - \mu_{gg}$ is the difference between excited and ground state dipole moments, μ_{ge} is the transition dipole moment and E_{ge} is the (HOMO–LUMO) gap.

Low-frequency hyperpolarisabilities at optical frequencies are connected by[68,69]:

$$\beta_\omega = \beta_0 \frac{\omega_{eg}^4}{\left(\omega_{eg}^2 - 4\omega^2\right)\left(\omega_{eg}^2 - \omega^2\right)} \qquad [3.7]$$

The commonly used figure of merit for second-order nonlinear properties is the product of the dipole moment μ and the hyperpolarsability β because they appear in equations expressing $\chi^{(2)}$. In Fig. 29 to Fig. 32 several so-called "π-conjugated" chromophores with high $\mu\beta$ are shown, which have been investigated in more detail in the present work.

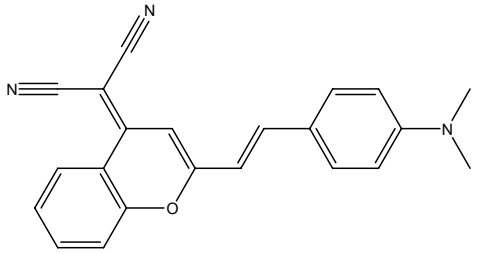

Fig. 29: The dye CH0. IUPAC name: (E)-2-(2-(4-(dimethylamino)styryl)-4H-chromen-4-ylidene)malononitrile

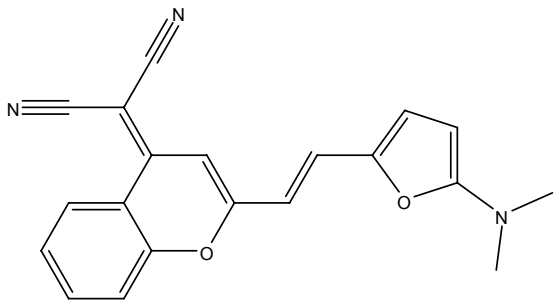

Fig. 30: The dye CH1. IUPAC name: (E)-2-(2-(2-(5-(dimethylamino)furan-2-yl)vinyl)-4H-chromen-4-ylidene)malononitrile

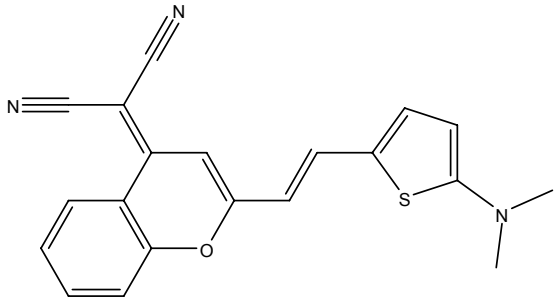

Fig. 31: The dye CH2. IUPAC name: (E)-2-(2-(2-(5-(dimethylamino)thiophen-2-yl)vinyl)-4H-chromen-4-ylidene)malononitrile

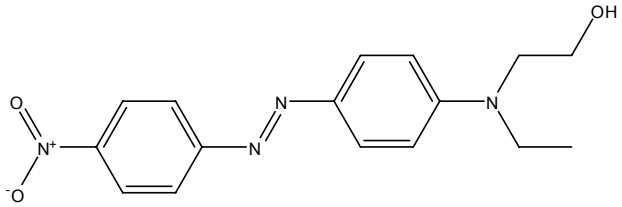

Fig. 32: Nonlinear dye Disperse Red 1 (DR1). IUPAC name: 2-(Ethyl-[4-(4-nitro-phenylazo)-phenyl]-amino)-ethanol

The name "π-conjugated" means that their structure can be shortly described as D-π-A, where D is the electron donor and A is the electron acceptor part, respectively and "-π-" stands for a bridge of delocalized π-electrons. It should be noted that the convention in NLO chromophores is to draw the donor on the left of the molecule, differently from the common presentation of absorbing dyes and pigments.

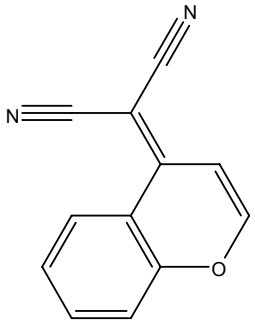

Fig. 33: Electron acceptor part of used chromophores. 2-(4H-chromen-4-ylidene)malononitrile

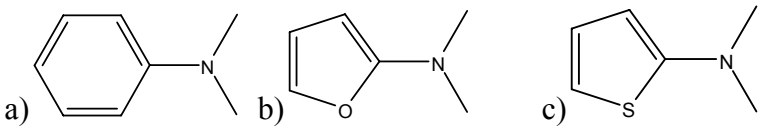

Fig. 34: Electron donor parts of used chromophores. a) N,N-dimethylaniline b) N,N-dimethylfuran-2-amine c) N,N-dimethylthiophen-2-amine

Several chromophore features can be obtained by quantum chemical calculations. Tab. 1 shows dipole moments, energies of HOMO and LUMO levels and the optical single particle gap calculated by means of *ab-initio* methods using the HF/6-31G basics set. The HOMO represents the ground state of the molecule while the LUMO stands in a first approximation for the excited state.

Dye code	Dipole, D	HOMO, eV	LUMO, eV	E_{ge}, eV
CH0	11.6	-7.37	0.70	8.07
CH1	12.1	-7.28	0.65	7.93
CH2	12.2	-7.17	0.66	7.83
DR1	10.6	-7.62	0.57	8.19

Tab. 1: Dipole moments, HOMO, LUMO and optical gaps, calculated in HF/6-31G basis for the set of dyes.

The shape of HOMO and LUMO illustrates delocalization of valence electrons (Fig. 35, Fig. 36). In case of the π-conjugated chromophore CH0 charge of the HOMO state is mainly localised at the donor part of the molecule while in the LUMO state charge is mainly localised at the acceptor part of the molecule. The double bond bridge between both parts allows charge transfer between the donor and acceptor part while going from the ground to the excited state. This charge transfer is rather typical for chromophores which show large second-order hyperpolarisability, and can be described in a first approximation by the simple two state-model introduced by Oudar and Chemla[67].

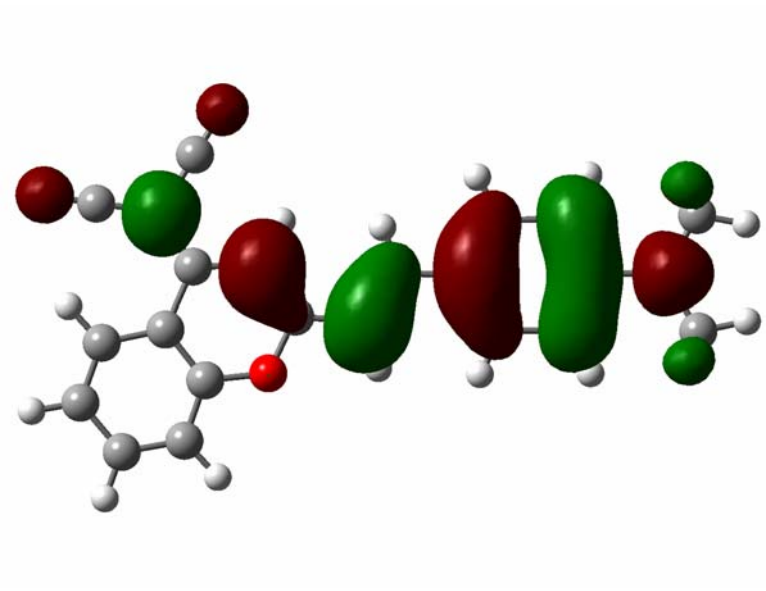

Fig. 35: Highest Occupied Molecular Orbital (HOMO) of CH0. Calculation performed by ab-initio HF/6-31G basic set

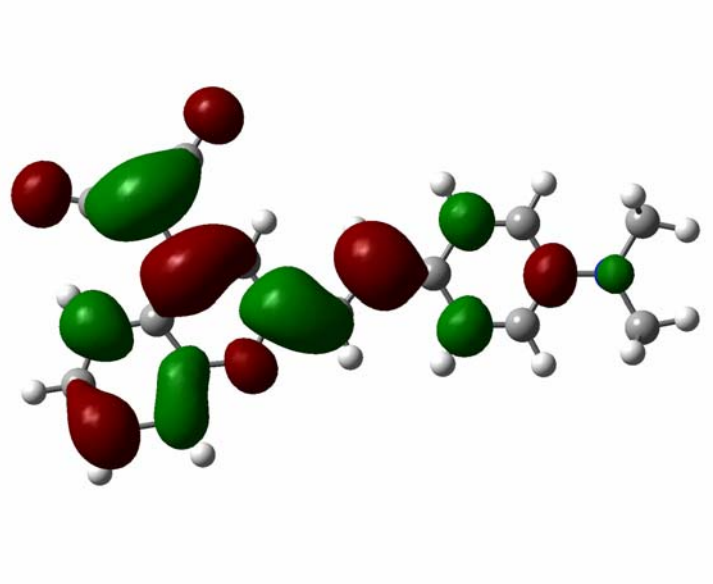

Fig. 36: Lowest Unoccupied Molecular Orbital (LUMO) of CH0. Calculation performed by ab-initio HF/6-31G basic set

However, nonlinear properties of the assembly of molecules (crystals and microcrystals) may be different from those of isolated molecules because the interaction between the chromophores may modify the overall response of the system towards higher optical nonlinearity[70].

Matrix and host materials for nonlinear interfaces

Guest-host systems

Polymers used in preparation of optical waveguides must have certain properties such as high transparency at working wavelength, homogeneity and proper refractive index (high for core material and low for the cladding). Moreover, nonlinear applications require the ability to embed different types of active molecules into a polymeric matrix. This means that suitable matrix polymers should be miscible with nonlinear optical chromophores forming optically homogeneous layers. In the special case of electro-optical applications, the materials must have insulating properties to allow to built-up of an electrical modulating field within the active layer. The following number of selected polymers used in the present work fulfils these requirements.

In order to estimate the requirements with respect to nonlinear optical properties of the guest-host materials to be used in integrated photonic devices one should remember that a typical diode laser can provide about 10 mW of optical power at 800 nm. In order to achieve 25% conversion in a 1 μm square guide of 3 mm length the nonlinear core material with a refractive index n=1.8 should have according to basic calculations a nonlinear coefficient of d_{eff}>30 pm/V[71]. Doped polymers can have even higher nonlinearities while the widely used inorganic nonlinear crystal lithium niobate has a nonlinear optical coefficient of d_{eff}=4.52 pm/V.

Polyphenylquinoxalines (PPQ)

Polyphenylquinoxalines are interesting matrix materials because they show glass transition temperatures above 200°C and can, hence, guarantee long-term orientational stability of

chromophores in these materials. They are synthesized from aromatic tetraketones and aromatic tetraamines in cresol by polycondensation reaction towards high molecular mass polymers (180,000 to 270,000 g/mol)[72-77].

All byproducts and low-molecular reaction products of synthesis are eliminated by repeated precipitation. The molecular structure and purity are verified by NMR spectroscopy, chromatography, UV/VIS spectroscopy and IR spectroscopy. Synthesis is carried out in solvents of spectroscopic purity grade.

Two different polymer structures as shown in Figs. 37 and 38 , namely PPQ2b and PPQ3, with inherent viscosities η=1.23 dl/g and η=2.3 dl/g, respectively, were used to form films from polymer solutions in 1,1,2,2-tetrachloroethane (5% by weight). The solubility of the polymers in different solvents was tested but 1,1,2,2-Tetrachloroethane was found to be the best one. The dissolved polymer was stored in solution at room temperature for about 18 hours, avoiding any kind of stirring or shaking of the solution to prevent the formation of micro bubbles in the solution. Before film preparation, the polymer solution is filtered through a 0.2-µm-pore filter. The filtered solution is deposited onto a substrate of BK7 glass (Melles Griot) precleaned in 1:3 solution mixture of hydrogenperoxide and sulphuric acid. After rinsing and drying the substrates the polymer is deposited on them by spin coating with rotation speeds in the range of (700–1200 rpm), producing a uniform thin film of thicknesses in the range of (0.8–1.85 µm) depending on the viscosity and spin speed. The thin films formed are thermally annealed at 160°C for one hour to remove any residual solvent. Thin films at low concentrations are also prepared on quartz substrates for absorption measurements to obtain the imaginary part of the refractive index.

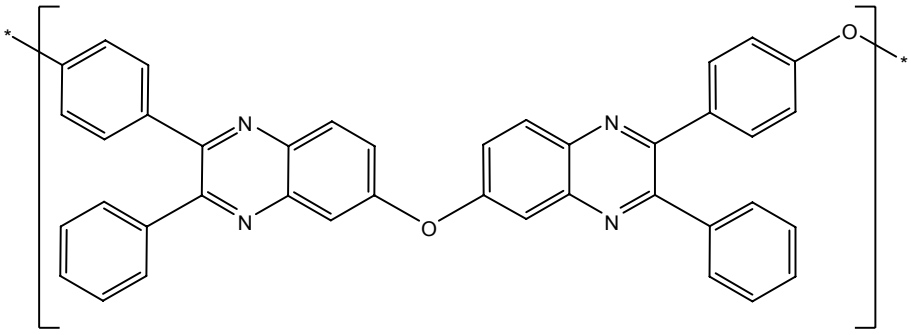

Fig. 39: Chemical structure of PPQ2b. IUPAC name of single unit: 7,7'-oxybis(2,3-diphenylquinoxaline)

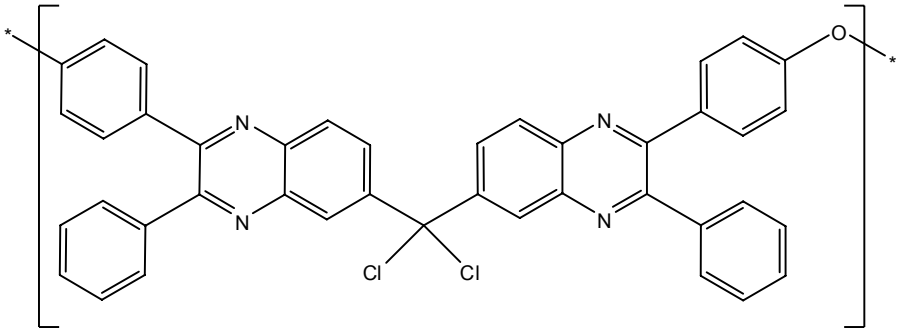

Fig. 40: Chemical structure of PPQ3. IUPAC name of single unit: dichlorobis(2,3-diphenylquinoxalin-6-yl)methane

Hydrodynamic forces appearing during spin coating induce birefringence in the obtained films. Tab. 2 reports the values obtained by prism-coupling measurements It is well known

that this effect is observed in polymers with relatively long, stiff polymer units while in case of more flexible chains formed from short monomeric units (polycarbonate, PMMA) no significant difference in refractive index for TE and TM modes at 1-2 μm thick films is observed. Birefringence due to the orienting influence of the substrate is particularly evident in ultra thin films (where the average monomer length is larger than the film thickness).

Material	Laser wavelength			
	532 nm (Green)	632.8 nm (Red)	980 nm (IR)	1064 nm (IR)
PPQ2b TE	1.778	1.741	1.700	1.697
PPQ2b TM	1.719	1.688	1.655	1.652
PPQ3 TE	1.773	1.737	1.697	1.693
PPQ3 TM	1.731	1.700	1.666	1.662

Tab. 2: Refractive indices of two types of PPQ measured at different wavelengths by the prism-coupling method.

PPQ was identified by O'Brien *et.al.*[78] as being a potential electron transport material for use in electroluminescence devices due to the presence of electron deficient nitrogen containing quinoxaline moieties in the polymer chains. This characteristic rules out the possibility to use this material for electro-optical applications.

Because the refractive index of PPQ is higher than the refractive index of most types of glasses this polymer can easily be used as core material for preparation as planar and channel waveguides on glass substrates.

Polycarbonate (PC)

Polycarbonate, or specifically polycarbonate of *bisphenol A*, is a clear plastic widely used in electric and optics applications. The chemical formula of polycarbonate is shown on Fig. 41. The refractive index of pure polycarbonate lies in the range between 1.584 - 1.586. Polycarbonate is transparent in the range from 400 nm to 1560 nm.

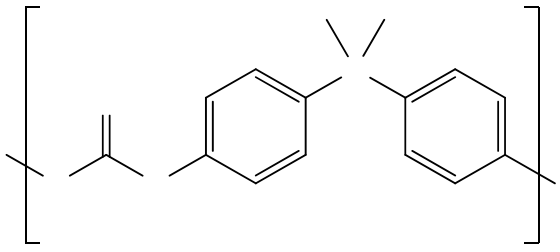

Fig. 41: Structural formula of polycarbonate.

Polycarbonate is excellent for poling applications, because of its high dielectric strength and high volume resistivity. The electrical breakdown strength has values of 15-67 kV/mm depending on molar mass and purity. The surface resistivity is 10^{15} Ω/m^2, volume resistivity 10^{12}-10^{14} Ω·m. The glass transition temperature is 150°C partially limiting the use of this polymer for practical devices.

Polymethylmethacrylate (PMMA)

PMMA is a polymer with optical transparency similar to polycarbonate. However, the glass transition temperature T_g=105 °C limits the area of application. Nevertheless, PMMA is transparent in the IR up to 2800 nm and in UV >300 nm. The material is very stable against UV that makes it promising as a matrix for UV-pumping devices. PMMA is highly transparent in the visible range and can be used as material for polymeric fibres (POF).

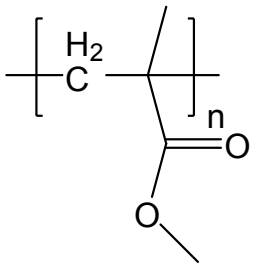

Fig. 42: Structural formula of Poly(methyl methacrylate).

The decomposition of PMMA starts at temperatures above 200°C so that processing above these temperatures, e.g. during fibre drawing, is only possible for a short time.

Polytetrafluoroethylene (PTFE)

Poly(tetrafluoroethylene) [$(CF_2)_n$; PTFE] is one of the polymers, which has been widely used for chemical, medical, and electronic applications due to its excellent chemical stability, low surface energy, electrical insulation, thermal stability, physiological compatibility and further advantageous properties. Due to the steric hindrance among the fluorine atoms, the PTFE chain adopts helical conformation under usual conditions (Fig. 43b).

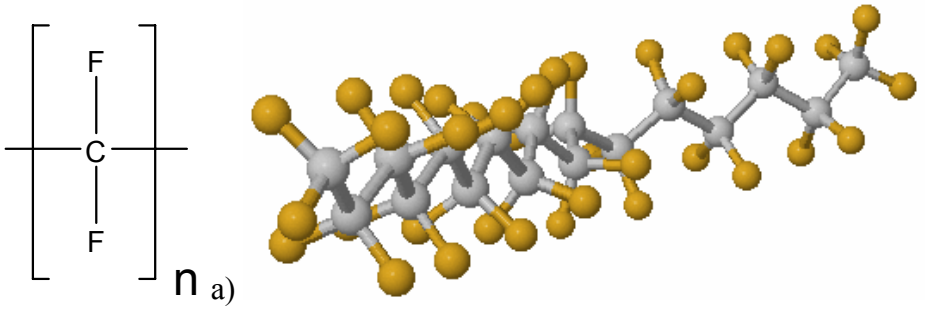

Fig. 43: Structural formula (a) and helical conformation (b) of Poly(tetrafluoroethylene). The bond between carbon and fluorine is very strong, and the fluorine atoms shield the vulnerable carbon chain. This unusual structure gives Teflon its unique properties. In addition to its extreme slipperiness, it is inert to almost every known chemical.

The chemical and physical properties of PTFE are related to its valence electronic structures, and its elucidation is important from the viewpoints of both basic science and practical applications[79]. PTFE has excellent dielectric properties. This is especially true at high radio frequencies, making it suitable for use as an insulator in cables and connector assemblies and as a material for printed circuit boards used at microwave frequencies. Combined with its high melting temperature, this makes it the material of choice as a high-performance substitute for the weaker and lower melting point polyethylene that is commonly used in low-cost applications. Its extremely high bulk resistivity makes it an ideal material for fabricating long life electrets, useful devices that are the electrostatic analogues of magnets.

Electrical field poling of thin films

In order to obtain second-order materials from an amorphous matrix, which contains polar nonlinear chromophores, an alignment procedure is necessary. An electrical field can align the chromophore molecules in one direction, but intermolecular forces and entropic effects in the polymer matrix act against the alignment.

One of the methods of the alignment consists in heating up the polymer matrix above glass transition temperature T_g and holding the sample under the influence of electrical field while cooling down. That procedure allows freezing in the dipoles in the oriented position. Such thermoelectric treatment generates a so-called "electret", the electrostatic analogue of a magnet. The electrical field applied at temperatures around the glass transition temperature orients the dipole groups preferably along the direction of the applied field causing a noncentrosymmetric orientation with $C_{\infty V}$ symmetry. Cooling below T_g decreases molecular mobility and noncentrosymmetry can be "frozen-in". The final orientation will never be perfect because of thermal randomization.

One possibility to apply an electrical field to polymer films is the use of an electrode, directly deposited on top of the film. If the lateral dimension of the electrode is large compared to the film thickness, then the edge effects are negligible and the electric field can be regarded as homogeneous (Fig. 44).

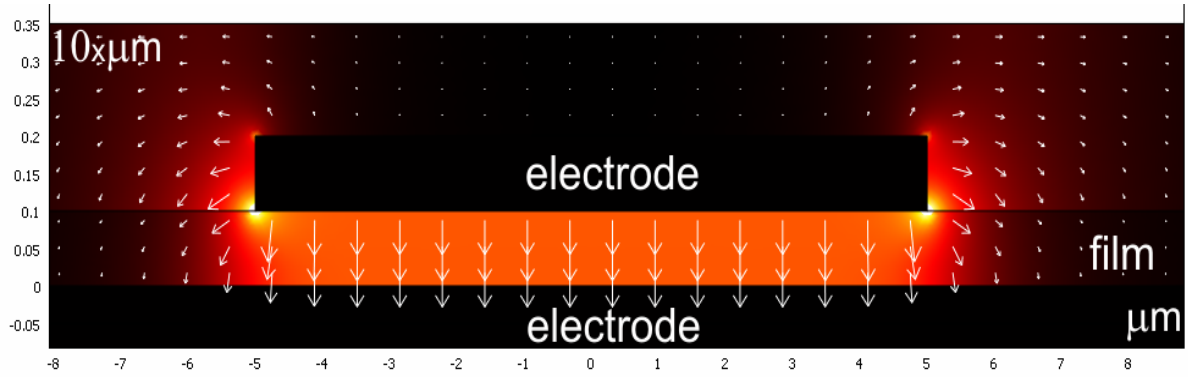

Fig. 44: Electrical field distribution in a film of 1 µm thickness and lateral dimension of 20 µm on top of the sample. Gradient fill is proportional to the field strength. Arrows show the field direction.

Problems occur when more fine electrode structures are required, for instance if the poling direction must be modulated in space. As can be seen in Fig. 45, in this case there is a transition zone on the border of poled domains. A periodically poled film with 1 µm thickness and a distance between electrodes of 2 µm has a modulation depth of about 50%. As will be shown later, that effect reduces the efficiency of periodically poled structures.

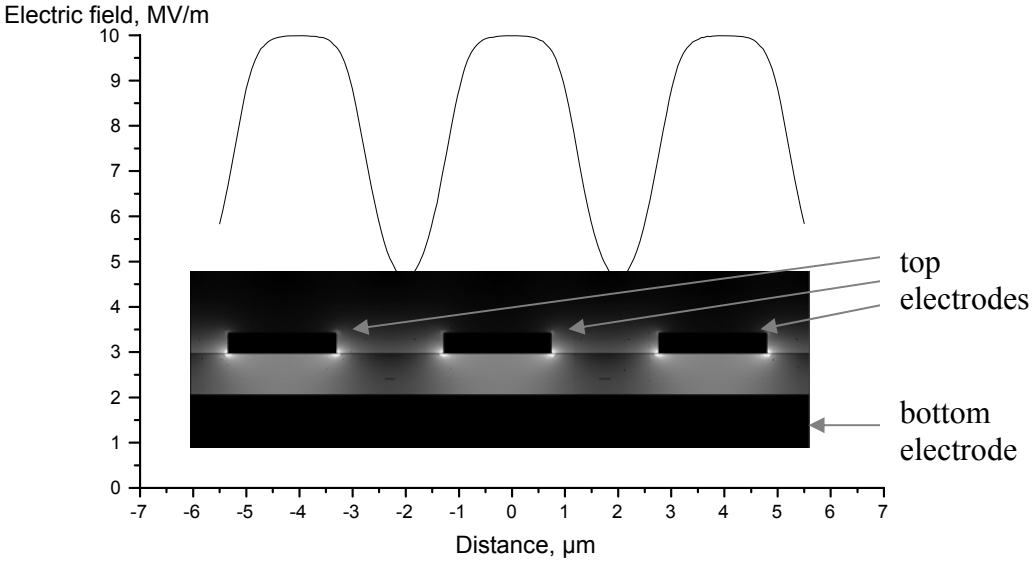

Fig. 45: Strength of electrical film calculated by means of FEA for the cross-section on the middle of the film thickness (the plane between electrodes). The inset picture shows the corresponding two-dimensional field distribution map. The bottom electrode is negatively charged. The top electrode (2 μm thick stripes on top of the film) is charged positively. The distance between electrodes (film thickness) is 0.5 μm.

More complicated in realization, but more effective for efficiency in SHG is bidirectional poling. In that case, the electrical field between next pairs of electrodes must have alternate direction as shown in Fig. 46.

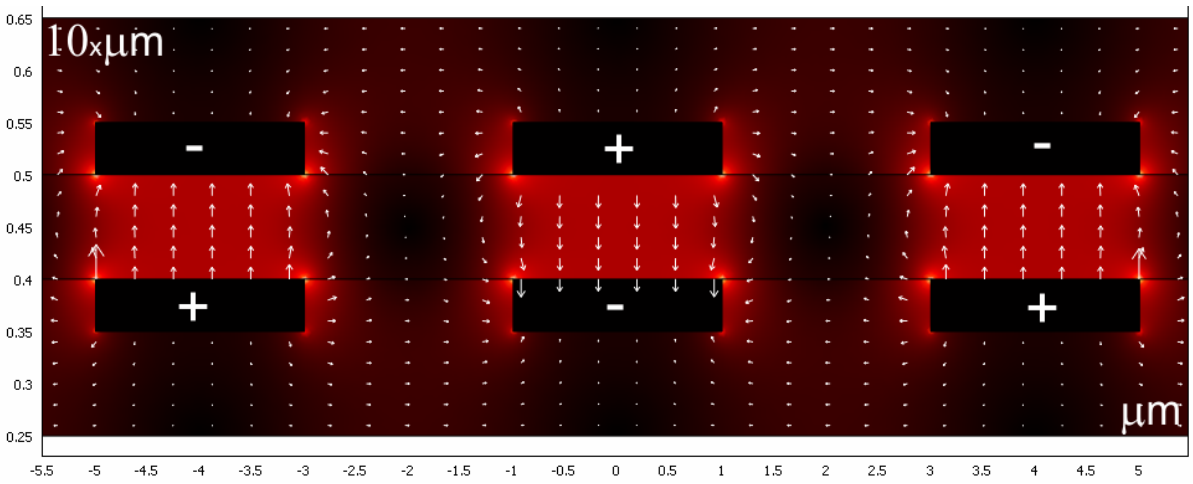

a)

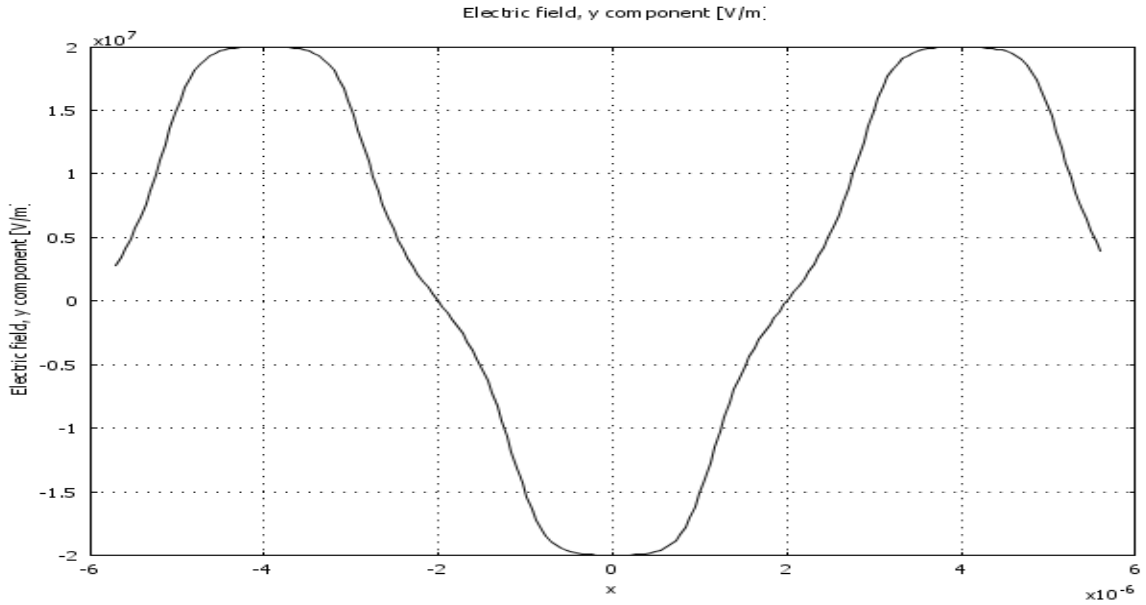

b)

Fig. 46: a) Electrical field distribution in a periodically-poled film of 1 μm thickness with electrodes of 2 μm width on top. Gradient fill is proportional to field strength. Arrows show field direction.
b) y-component of electrical field vector within the film.

The obtained average orientation depends on the strength of the poling field. Corona poling is a further important poling technique. Here the upper electrode is formed by a corona generated charged layer which covers the surface of the dielectric film. In order to obtain such a layer, a high voltage is applied on a sharp needle that ionizes the surrounding gas (air or N_2). The ions generated in the surrounding gas travel towards the polymer surface and form there the charge surface layer, which acts as a virtual electrode.

In many cases corona poling is more effective than other poling techniques because it allows reaching values of electrical field up to several MV/cm (close to the breakdown field strength) high enough to reach an ultimate degree of orientation. Another advantage of the method is that local short circuits (as result of impurity) do not influence the field at other places of the sample surface since the surface charge shorted only next to the defect site but does not discharge the whole surface layer. On the contrary, the electrode poling method is indeed sensitive to local defects so that one short circuit leads to the damage of whole structure.

Corona poling can be used for *in-situ* measurements (Fig. 47). The SHG signal depends on average dipole orientation and hence on temperature and applied field. Due to this, the poling condition can be optimized for maximum efficiency of second-order nonlinearity.

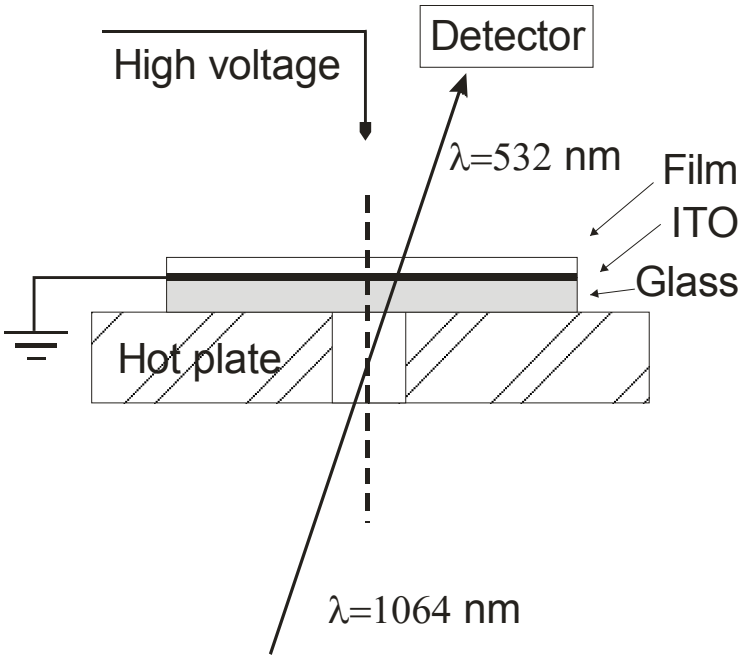

Fig. 47: Scheme of an in-situ poling setup. High voltage (5-10 kV) is applied to a sharp needle that creates an ionic flow into the direction of the grounded sample. Heating the film to the glass transition temperature causes chromophore orientation, which induces SHG. The value of the SH signal correlates with the average orientation of dipoles.

Orientational order

In Fig. 48 the orientation of a dipolar molecule is shown. Being placed in an oscillating electrical field the dipole moment does not remain constant but oscillates together with the field. If the field strength is high enough, the dipoles do not follow the harmonic law and can be presented as series:

$$\mu(E) = \mu_0 + \alpha E + \beta E^2 + \gamma E^3 + \ldots \qquad [4.1]$$

where μ_0 is the permanent dipole moment, α, β and γ are first(linear), second and third order hyperpolarisabilities. Since the dipole moment is a vector, the coefficients are first (vector), second, third and fourth-rank tensors, respectively.

For rod-like molecules with uniaxial symmetry, the principal hyperpolarisability tensor component lies along the dipole moment. In that case, the relation between microscopic nonlinearity and macroscopic nonlinearity, i.e. between second-order hyperpolarisability β and second-order susceptibility $\chi^{(2)}$, respectively, depends on the orientational angle θ between molecular principle axis and poling direction:

$$\chi^{(2)} \propto N \cdot f \cdot \beta \cdot g(\theta) \qquad [4.2]$$

where N is the number density (molecules per unit volume), f is a local field factor, $g(\theta)$ is a distribution function of average orientation and β is the averaged hyperpolarisability along the molecular principal axis. Here one assumes that the hyperpolarisability has one dominating contribution along the molecular principle axis.

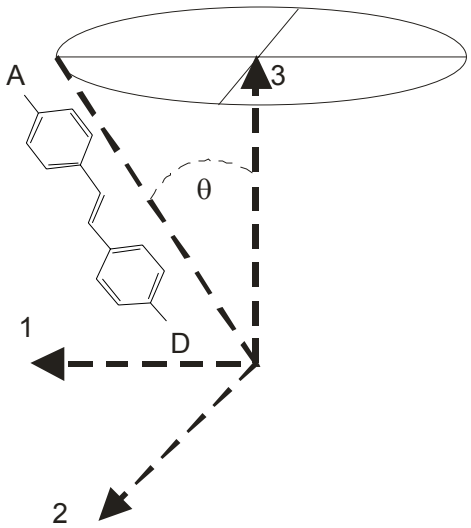

Fig. 48: A single dipolar donor(D)-acceptor(A) substituted π-conjugated molecule (D-π-A) in an external electric poling field. The poling field is applied along the Z or 3-direction

Second-order nonlinear properties of poled polymers (symmetry $C_{\infty,v}$) are mainly described by two elements of the macroscopic tensor $\chi^{(2)}$: $\chi^{(2)}_{333} \equiv \chi^{(2)}_{zzz}$ and $\chi^{(2)}_{311} \equiv \chi^{(2)}_{zxx}$. These two elements of the macroscopic susceptibility tensor can be expressed through the dominating component β_{zzz} of the hyperpolarisability tensor as:

$$\chi^{(2)}_{333} = \chi^{(2)}_{zzz} = N \bullet f \bullet \beta_{zzz} \bullet \left\langle \cos^3 \theta \right\rangle \qquad [4.3]$$

and

$$\chi^{(2)}_{311} = \chi^{(2)}_{zxx} = N \bullet f \bullet \beta_{zzz} \bullet \left\langle \frac{1}{2} \cos\theta \sin^2 \theta \right\rangle \qquad [4.4]$$

Here is assumed that the other components of the hyperpolarisability tensor can be neglected.

On the other hand, we can express the values of $\chi^{(2)}$-tensor elements, which can be reached under action of the external electric field using first- and third-order Langevin functions: $L_1(p)$ and $L_3(p)$ where the variable p is the ratio between potential energy of the dipole in the poling field and kT[53,55]:

$$p = \frac{\mu E}{kT} \qquad [4.5]$$

with μ the dipole moment, E the field strength, k is Boltzmann's constant, and T is the absolute temperature:

$$\chi^{(2)}_{zzz} = Nf\beta_{zzz}L_3(p) \qquad [4.6]$$

$$\chi^{(2)}_{zxx} = Nf\beta_{zzz}\frac{1}{2}\left[L_1(p) - L_3(p)\right] \qquad [4.7]$$

In the general case, the n-th order Langevin function is defined as:

$$L_n(p) = \frac{\int_0^{\pi} \exp(-p\cos\theta)\cos^n\theta\sin\theta\, d\theta}{\int_0^{\pi} \exp(-p\cos\theta)\sin\theta\, d\theta} \qquad [4.8]$$

The first three Langevin functions and their relationship to the thermally averaged values of the Legendre polynomials $\langle P_n(\cos\theta)\rangle$ are[80,81]:

$$L_1(p) = \coth p - \frac{1}{p} = \langle P_1(\cos\theta)\rangle \qquad [4.9]$$

$$L_2(p) = 1 + \frac{2}{p^2} - \frac{2}{p}\coth p = \frac{1}{3}\left(2\langle P_2(\cos\theta)\rangle + 1\right) \qquad [4.10]$$

$$L_3(p) = \left(1 + \frac{6}{p^2}\right)\coth p - \frac{3}{p}\left(1 + \frac{3}{p^2}\right) = \frac{1}{5}\left(2\langle P_3(\cos\theta)\rangle + 3\langle P_1(\cos\theta)\rangle\right) \qquad [4.11]$$

with,

$$\langle P_1(\cos\theta)\rangle = \langle\cos\theta\rangle \qquad [4.12]$$

$$\langle P_2(\cos\theta)\rangle = \frac{1}{2}\langle 3\cos^2\theta - 1\rangle \qquad [4.13]$$

$$\langle P_3(\cos\theta)\rangle = \frac{1}{2}\langle(5\cos^2\theta - 3\cos\theta)\rangle \qquad [4.14]$$

For small values of the parameter p, the equations [4.12] and [4.14] may be simplified by using of the replacement of Langevin functions by ratios:

$$L_1(p) \approx \frac{p}{3} \qquad [4.15]$$

$$L_3(p) \approx \frac{p}{5} \qquad [4.16]$$

Substitution into [4.6] and [4.7] provides the following simplified expressions for macroscopic nonlinearities:

$$\chi^{(2)}_{zzz} = \chi^{(2)}_{333} = NF\beta_{zzz}\frac{\mu E}{5kT} \qquad [4.17]$$

$$\chi^{(2)}_{zxx} = \chi^{(2)}_{311} = NF\beta_{zzz}\frac{\mu E}{15kT} \qquad [4.18]$$

The averaged value of the second-order Legendre polynomial $\Phi = \langle P_2(\cos\theta)\rangle$ is the order parameter of the system[53].

The order parameter can be obtained from the anisotropy of refractive index induced by poling:

$$\Phi = \frac{n_{\parallel} - n_{\perp}}{n_{\parallel} + 2n_{\perp} - 3n_0} \qquad [4.19]$$

where perpendicular (⊥) and parallel (||) directions are defined with respect to the poling direction. n_0 represents the isotropic refractive index prior to poling. One way to obtain experimentally this value is using multi-angle ellipsometry, based on an anisotropic model.

For rod-like conjugated molecules, the transition moment lies parallel to the permanent dipole. The random orientation of the transition dipole moments leads to a homogeneous absorption of the material. However, the orientation of a fraction of dipoles perpendicular to the film surface leads to a decrease of absorption for light incident at a direction parallel to the surface normal. The order parameter hence, can be calculated by measurement of chromophore absorption before and after poling[53]:

$$\Phi = \frac{\Delta A_{\perp}}{A_{\perp}} = \frac{3\left\langle \cos^2 \theta \right\rangle}{2} \qquad [4.20]$$

where $\Delta A_{\perp}$ is the decrease of the normalized absorption $A_{\perp}$ at normal incidence. Compared with the bulk polymer, the large polarisability of the chromophores induces a general increase of refractive index. After poling, a birefringence connected with chromophore orientation occurs.

However, the determination of the order parameter from dichroism can be problematic because of effects like sublimation of chromophores (especially in case of guest-host systems) or thermal destruction. These effects can lead to incorrect results in determination of the order parameter.

The local field factor corrects the external optical electric fields for contributions from the surrounding molecules. The chromophore is assumed to be embedded within a cavity inside a uniformly polarized medium. For a spherical cavity, one obtains for the local field factor[53]:

$$f_{\infty} = \frac{n_{\infty}^2 + 2}{3} \qquad [4.21]$$

where n_{∞} is the nonresonant optical refractive index of the material and equals the square root of the dielectric constant at electric field oscillation frequencies higher than rotational relaxation resonance frequencies. This is the Lorentz-Lorenz local field correction, which is valid at optical frequencies.

If correlations between chromophore molecule and its immediate neighbourhood are assumed to exist, one needs to include the fields associated with both external fields and neighbouring dipoles. In this case, the Onsager local field is appropriate. For a spherical cavity, the Onsager local field correction is[53]:

$$f_{\infty} = \varepsilon_r \frac{n_{\infty}^2 + 2}{n_{\infty}^2 + 2\varepsilon_r} \qquad [4.22]$$

where ε_r is the static dielectric constant. Equation [4.21] can be derived from [4.22] assuming $\varepsilon_r = n_{\infty}^2$.

According to equation [4.17], the tensor component χ_{zzz}, which can be achieved during the poling process, is proportional to the field strength of the poling field. After freezing in the orientation, χ_{zzz} keeps its value, during the SHG measurements.

Thermal relaxation of poled structures

After the structure is oriented by poling, the natural molecular motion driven by temperature leads to a randomization of dipole orientation and, hence, to a reduction of the order pa-

rameter. This decay of nonlinearity of the material is caused by rotational motion of chromophores, and structural relaxation of the polymer matrix. For the polyphenylquinoxaline (PPQ) polymer with high glass transition temperature (T_g≈250÷260°C) the time need for appearance of a significant loss of order at room temperature is long enough for practical use. Nevertheless, due to local mobility and intermolecular relaxation a reduction of orientational order was observed already at temperatures ~120°C below T_g (Fig. 49). Here the results for a spin-coated film of the guest-host system PPQ2b-DR1 (95 wt%-5 wt%) prepared by spin-coating on ITO covered glass substrates and oriented by subsequent corona poling. Constant heating with a rate of 2°C/min shows some internal changes of the film material at T=120°C, although the glass transition temperature of the matrix material, as determined by Differential Scanning Calorimetry (DSC) is 260°C.

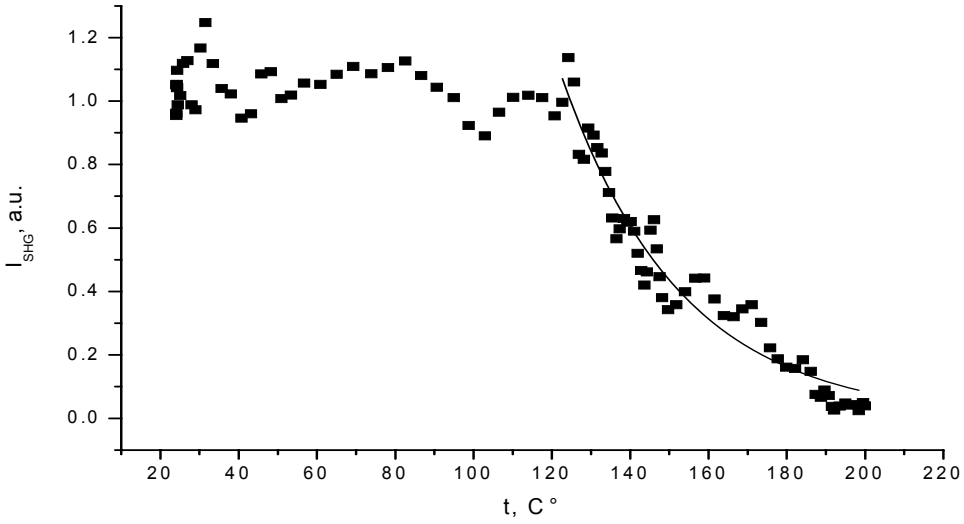

Fig. 49: In-situ SHG signal of a poled PPQ-DR1 film in dependence on temperature. Heating at constant rate of 2 C°/min.

The relaxation phenomenon was formulated by Kohlrausch and later by Williams and Watts[82,83]. They found that relaxation could be described by an exponential or a stretched exponential decay, respectively:

$$x(t) \sim \exp\left[-\left(\alpha(T)t\right)^{\beta}\right] \qquad [4.23]$$

where *x(t)* is the quantity, which characterizes the orientation. The function $\alpha(T)$ is the temperature dependent mean relaxation rate or inverse relaxation time $\alpha=1/\tau$. The exponent β is a quantity describing the dispersive nature of relaxation. Originally, β was an empirical parameter, but later some theoretical models for explanation of the stretched exponential relaxation function have been developed[84,85].

Above the glass transition temperature, the polymer is in a liquid-like equilibrium state. The relaxation time has the following form (known as Williams-Landel-Ferry law or Vogel-Fulcher-Tammann law)[86-88]

$$\tau \sim \exp\left[\frac{A}{T-T_c}\right], \qquad T > T_c \qquad [4.24]$$

where T_c is a characteristic temperature. Below T_c the system is frozen in.

Poling below T_g

A more complex analysis of results obtained for PPQ2b-DR1 (T_g=260°C) shows such complicated behaviour. To monitor the decay of the poled order at a given temperature, the film was heated to the temperature above T_g and then cooled down with applied corona field to the desired temperature. The measurement of the decay carried out when the film had reached the desired temperature and subsequently the electrical field was switched off. The decay times reported here refer to the decay of the effective second-order nonlinear optical coefficient *d*, proportional to the square root of the measured SHG intensity using *p*-polarized light at an angle of incidence of 45° to the polymer film surface.

For a poling temperature below T_g the molecular order decays. In a simplified approach, the relaxation process at 20°C can be described by a three-exponential decay with the time constants τ_1=*11 s,* τ_2=*93 s,* τ_3=*2185 s* that correspond to different mechanisms of relaxation.

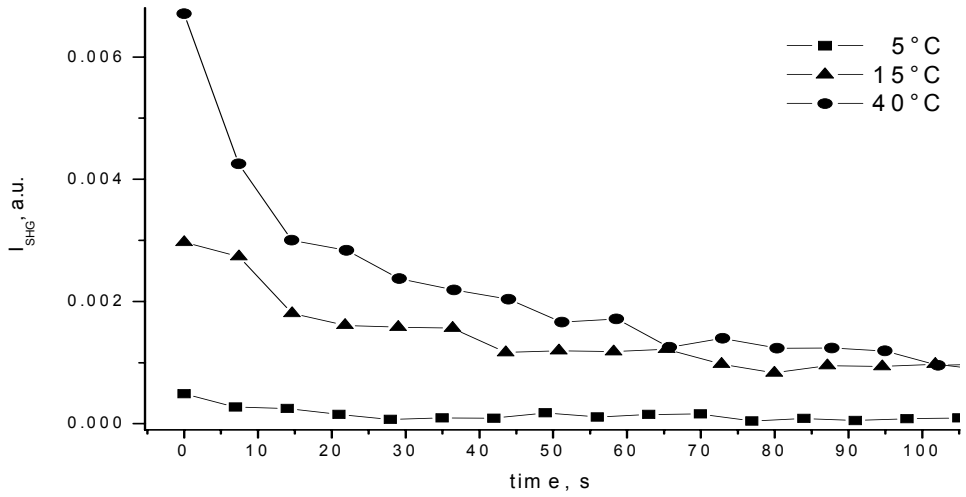

a)

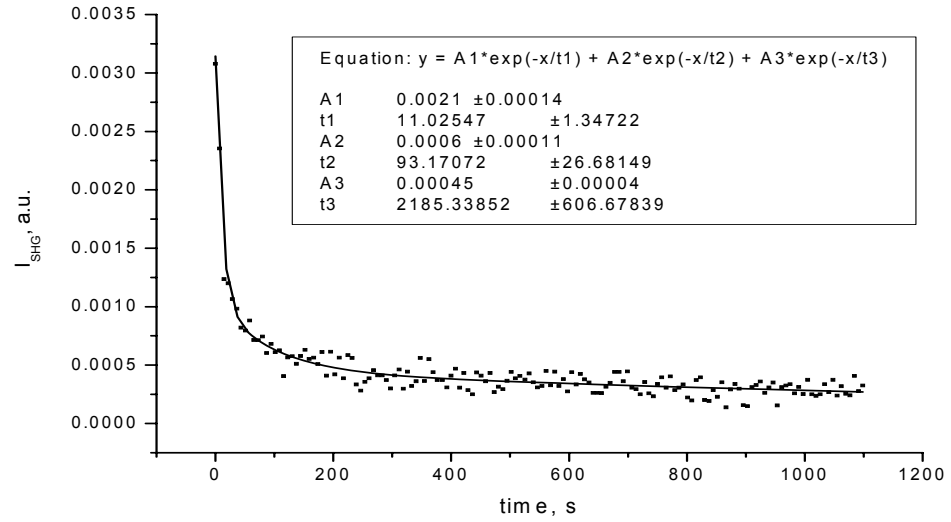

b)

Fig. 50: In-situ SHG measurements during orientational relaxation. (a) Molecular orientational relaxations take place at low temperature. (b) For example, the SHG graph of relaxation at 20°C has at least a three-exponential decay.

Low temperature depolarization is one of the factors that reduce the nonlinear efficiency of a guest-host system. The relaxation theory of guest-host polymer systems is still not completely developed. However, by proper selection of chromophore-polymer combinations one can increase the lifetime of dye orientation at room temperature.

Self-assembled crystallized systems

As was mentioned above, nonlinear media must be noncentrosymmetric to support second harmonic generation. In most cases, vacuum-deposited films are completely centrosymmetric except on surfaces. Moreover, molecules with a centre of symmetry (and therefore with zero dipole moment) cannot be ordered by poling methods.

Squarylium dyes are known as strong absorbing colorants (molar extinction $\varepsilon > 10^5$ dm^3 mol^{-1} cm^{-1}) possessing an intra-ionic structure. During the deposition process, both types of molecules show the ability to form various polymorphs as reported in the literature[89-91]. According to Ashwell et al.[92], there are in the limiting case two different structures formed by H-aggregation of the molecules in the form of a "cardpack" arrangement, and J-aggregation in the form of a "slipped stack" arrangement with an overlap of the neighbouring donor and acceptor groups. The first structure shows a sharp absorption maximum at ca. 520-530 nm, whereas the second one results in absorption near 780 nm.

Recently it was found that vacuum deposited and rubbed PTFE films also support growth of oriented dye layers[93-98]. Aligned PTFE surfaces served as excellent substrates for the growth of oriented layers for a number of materials, including inorganic crystals, small molecules, and polymers. In Fig. 51 the chemical structures of four Squarylium dyes are given, which have been studied after vacuum deposition on PTFE orientational layers.

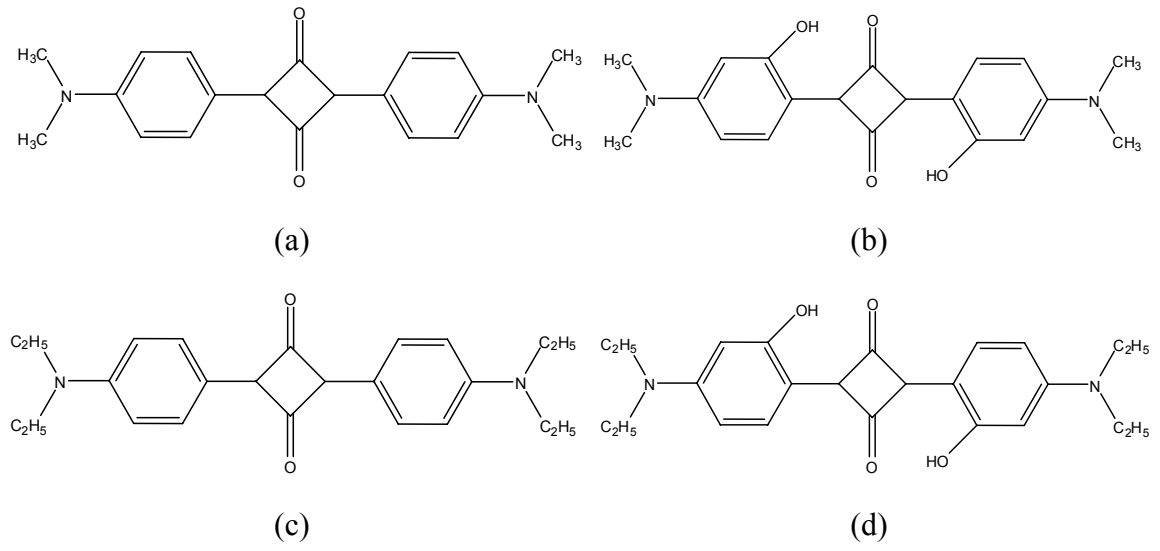

Fig. 51: Molecular structures of squarylium derivates a) Me-Sq (2,4-bis(4-(dimethylamino)phenyl) cyclobutane-1,3-dione), b) Me-SqOH (2,4-bis(4-(dimethylamino)-2-hydroxyphenyl)cyclobutane-1,3-dione), c) Eth-Sq (2,4-bis(4-(diethylamino)phenyl)cyclobutane-1,3-dione), d) Eth-SqOH (2,4-bis(4-(diethylamino)-2-hydroxyphenyl)cyclobutane-1,3-dione). The corresponding IUPAC names are presented. The SHG was observed only in PTFE films covered by Me-SqOH (b).

The samples have been prepared as ca. 50 nm thin layers on PTFE made from either of those substances. Although all four samples were prepared by the same method, only one of the four squarylium derivates, namely a Me-SqOH has shown a SHG signal. Since chromo-

phores are formally point-symmetric, one would expect no SHG signal, except the surface signal. However, Me-SqOH shows such a signal that a non-centrosymmetric structure of the electronic system must be assumed, which is formed due to the special intermolecular interaction after aggregation.

The four types of squarylium were selected based on results obtained for oriented Langmuir-Blodgett (LB) films[92,99].

Sample preparation

Chromophore films were deposited by thermal evaporation (TE) in vacuum using a tantalum boat. The pressure in the chamber was maintained at 10^{-3} Pa. The film deposition rate was controlled by a quartz crystal microbalance. The growth rate was in the range between 0.1-1 nm/s.

With the aim to align aggregates, specially prepared substrates were used. Thin films of hydroxyphenyl and aminophenyl squaraine dyes with different end groups were deposited by thermal evaporation in vacuum on uniaxially aligned poly-(tetrafluoroethylene) (PTFE) surfaces. The PTFE were prepared by vacuum deposition polymerization with subsequent rubbing of the surface using a special cloth (see Fig. 52).

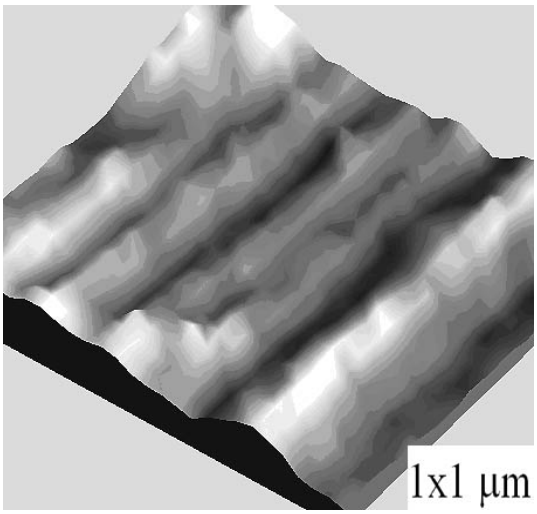

Fig. 52: Surface morphology of a PTFE film deposited at a pressure of about $2x10^{-1}$ Pa, followed by rubbing the freshly prepared layer with a special cloth.

Vacuum deposition of the squarylium dyes onto the PTFE aligned layer led to the oriented growth of nanocrystals on these layers. As can be seen on AFM pictures (Fig. 53), aggregated molecules form chains of grains aligned along the direction of rubbing.

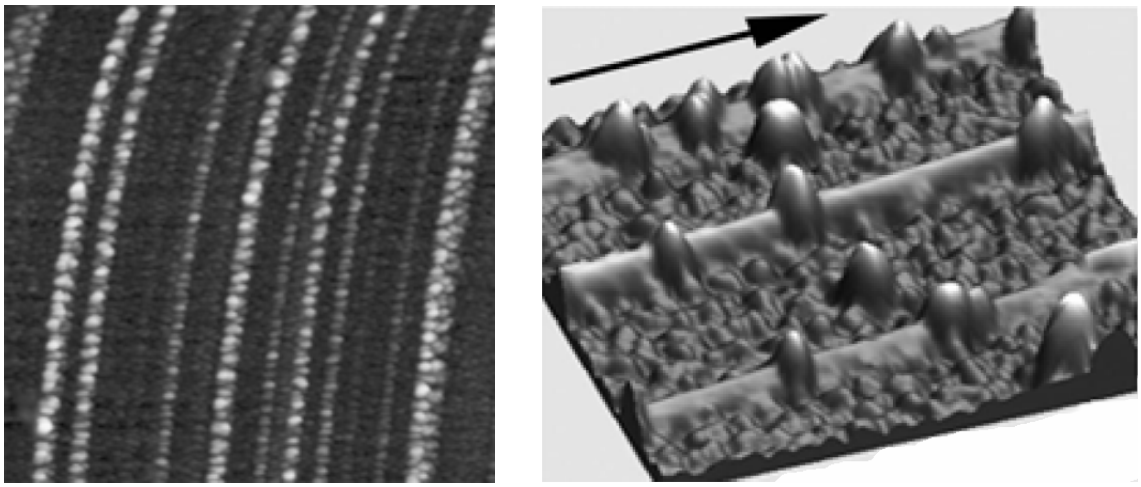

a) b)

Fig. 53: Atomic force microscopy (AFM) images of a vacuum deposited Eth-Sq film on a PTFE alignment layer. A distinct orientation of microcrystals of Eth-Sq is observed. Scale 4x4 μm (a) 1x1 μm (b), scan speed 1 nm/s.

The microcrystals formed on an oriented PTFE layer have small size in comparison to optical wavelengths in the visible range and exhibit, therefore, good transparency and homogeneity. In view of the fact that microcrystals are oriented, anisotropic optical properties of that layer are expected.

Optical measurements

In-situ measurements of transmission spectra during film growth show different mechanisms of aggregation. A set of transmission spectra each of them measured after fixed deposition time of 50 seconds (deposition rate was 0.2 nm/sec) is shown in Fig. 54.

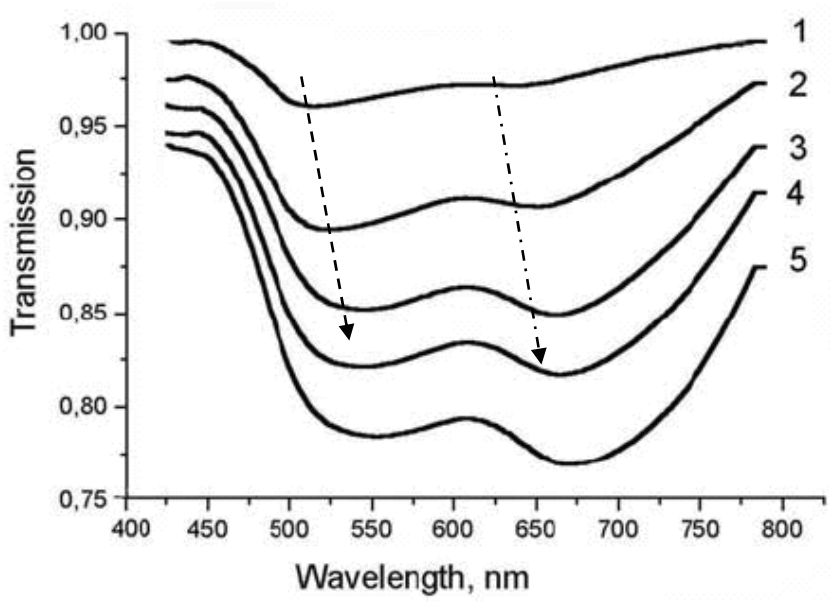

Fig. 54: Transmission spectra of Eth-Sq film growth on PTFE recorded in situ during vacuum deposition. Where curves with numbers 1,2,3,4, and 5 measured in the moment when film thickness was 10, 20, 30, 40 and 50 nm, respectively.

These spectra demonstrate a change in the aggregation mechanism during deposition. The long-wavelength peak grows faster (dash-dot arrow in Fig. 54) than the short-wavelength peak (dash arrow in Fig. 54). Assuming that each peak reflects the response of a different type of aggregate, thickness-dependent aggregate formation during film growth can be followed by this type of absorption spectroscopy.

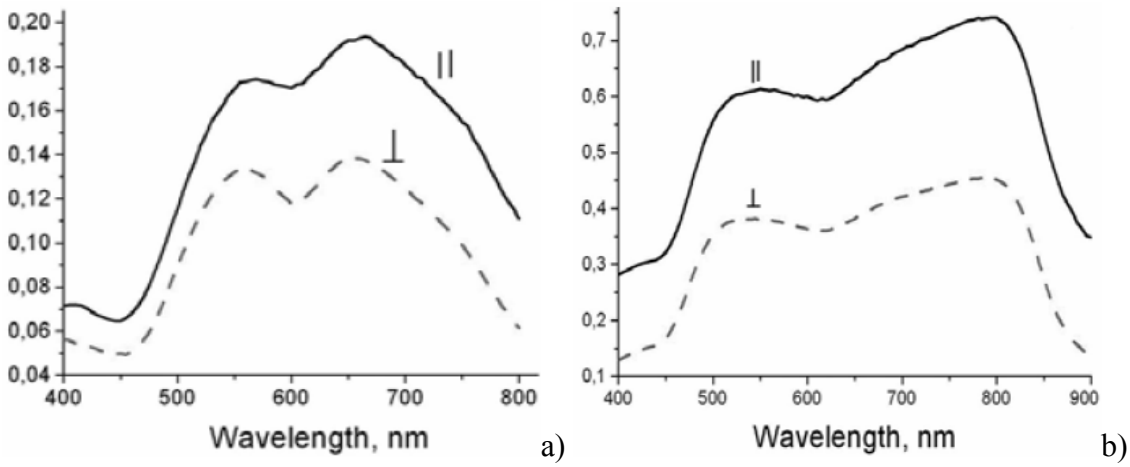

Fig. 55: Polarization dependent absorption spectra of two Sq films: (a) Me-SqOH and (b) Eth-SqOH. Parallel or perpendicular polarization means orientation of rubbing relatively to the light polarization direction (electrical field component).

Measurements in linearly polarized light show polarization-dependent absorption (Fig. 55). The dichroism reaches values in the range 1.3-2 dependend on thickness. That indicates a high order of orientation of Sq microcrystals aligned by the underlying rubbed PTFE layer.

SHG of aligned Sq films

As was shown above, oriented films of squarylium show anisotropic absorption under polarized light. With the aim to investigate nonlinear optical properties of these films, the second harmonic generation was measured. As a rule, only noncentrosymmetric structures can generate SHG signals. In case of films or crystals with centro-symmetry, the SHG signal can be produced by the border to adjacent media where symmetry is broken.

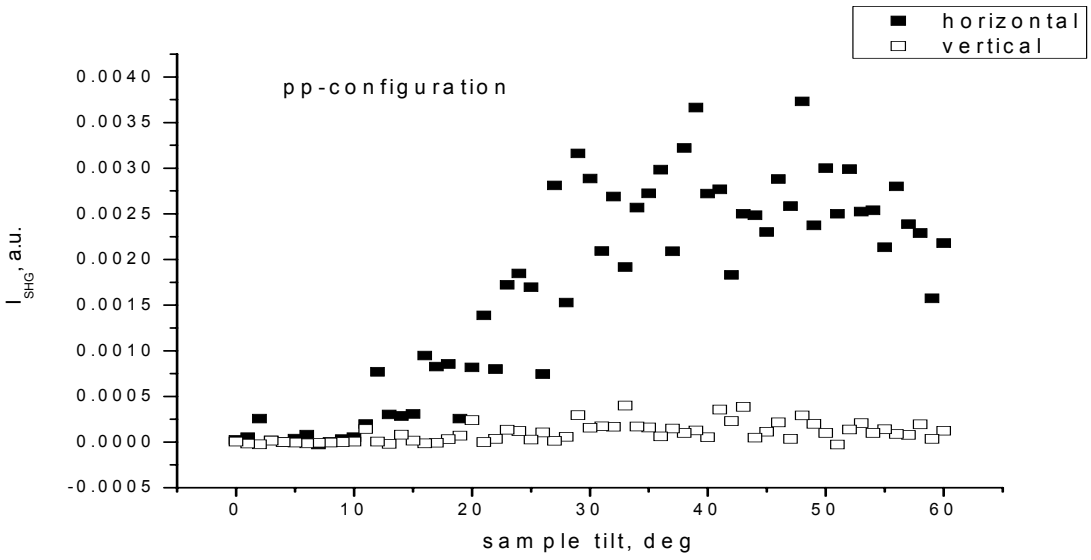

Fig. 56: Second harmonic signal from a thin Me-SqOH film (thickness is 27 nm). Horizontal sample orientation means that the p-direction is parallel to the rubbing direction. Vertical means that the p-direction is orthogonal to the rubbing direction.

As seen in Fig. 56, the oriented squarylium film shows SHG. Furthermore, this signal depends on polarization of the fundamental beam relatively to the rubbing direction. Maximum efficiency of SHG was observed in case when the direction of polarization (electrical field) is collinear to the rubbing direction.

Analysis of SHG signals obtained from a set of films with growing thickness shows that the SHG intensity is growing with the thickness (Fig. 57). That is a proof for the bulk origin of SHG in the squarylium film.

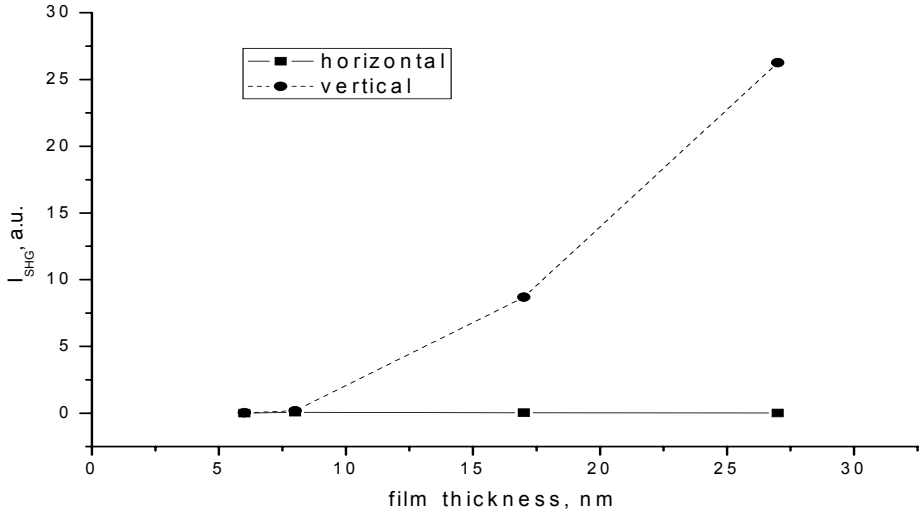

Fig. 57: Thickness-dependent intensity of SHG signal from a Me-SqOH film.

Relatively thick Me-SqOH film with 100 nm thickness also demonstrates SH at orthogonal orientation. This means that for thick films the orienting influence of the rubbed substrate is reduced.

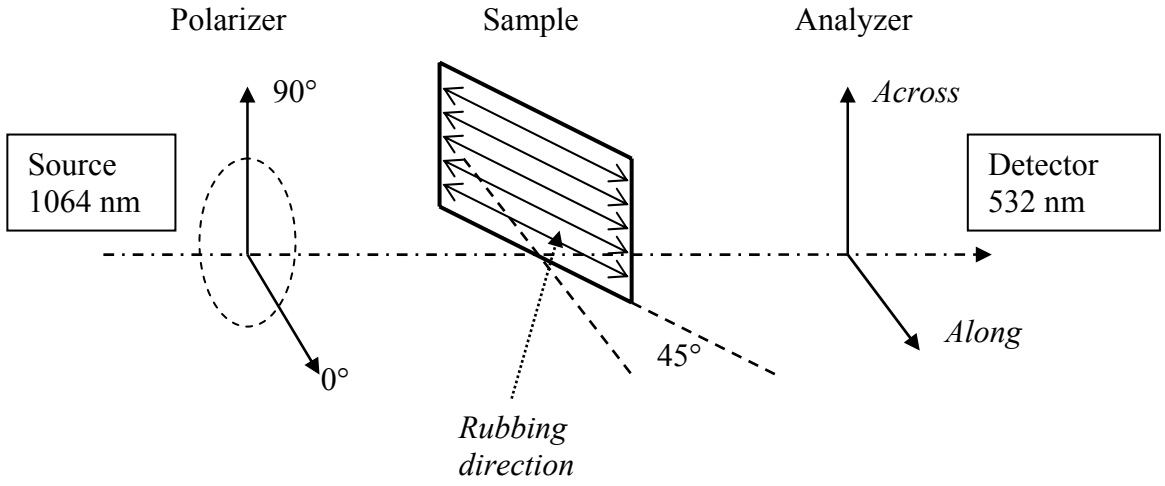

Fig. 58: Scheme of the experiment for registration of SHG from oriented squarylium layers. The polarization of the fundamental wave can be smoothly rotated with the help of a half-wavelength plate (not shown on scheme). The analyzer can be fixed in two positions: along and across the rubbing direction.

Smooth rotation of the polarization of the fundamental wave with fixed position of the analyzer (along and across the direction of rubbing) as shown in Fig. 58 shows that the value of the SHG signal achieves a maximum when both the polarizer and the analyzer are oriented along the direction of rubbing (Fig. 59).

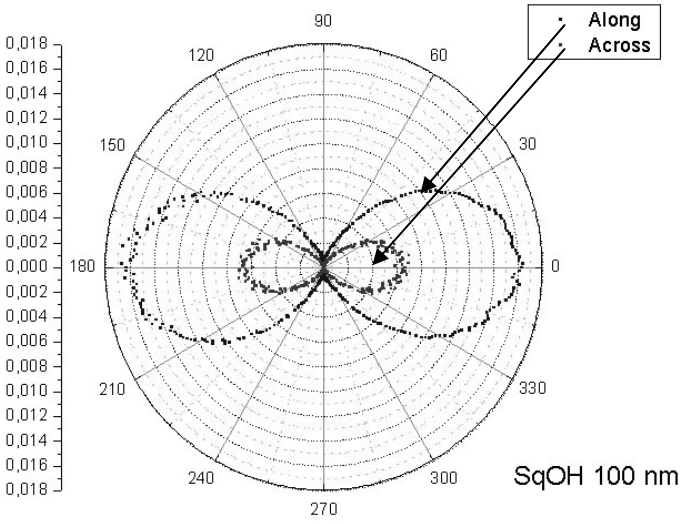

Fig. 59: SHG intensity (arbitrary units) of a 100 nm squarylium dye (Me-Sq) layer versus polarization angle of fundamental wave (zero and 90 degrees correspond p- and s- polarization, respectively). The angle between the analyzer polarization and orienting rubbing direction is denoted as across (orthogonal) and along (parallel). The sample is tilted at fixed angle of 45° against the fundamental beam.

The observed anisotropy confirms the orientational influence of the rubbed PTFE sublayer. In addition, the obtained results demonstrate the bulk origin of SHG in the investigated squarylium films which can be explained with the help of a detailed analysis of the specific type of molecular aggregation.

Single molecule properties

The molecular structure and electronic density distribution of single molecules of the squarylium-derivates MeSq (Fig. 51a,c) and Me-SqOH (Fig. 51b,d) were investigated theoretically. Both semi-empirical (PM3) and ab-initio (HF/6-31G) methods were applied. The calculations show that both molecules are centrosymmetric. This means the molecule itself cannot generate a second harmonic (excluding interface layers).

Moreover, molecular orbital energies are practically equivalent (Tab. 3). The occupied levels of Methyl-Sq are all shifted only slightly towards lower energies with respect to those of MeSqOH so that the energy gap is almost the same for both molecules. This means, according to [3.6], the nonlinearities of Sq derivates are practically equal.

	HOMO-2 eV	**HOMO-1 eV**	**HOMO eV**	**LUMO eV**	**LUMO+1 eV**	**LUMO+1 eV**	**LUMO-HOMO eV**
Me Sq	-8.91	-8.81	-6.51	0.14	3.77	3.81	6.65
Me SqOH	-8.89	-8.78	-6.47	0.16	3.78	3.82	6.63
ΔE	0.02	0.03	0.04	0.02	0.01	0.01	0.02

Tab. 3: Molecular orbital energies calculated by using a Hartree-Fock method with 6-31 basis set. Occupied levels of Methyl Sq are slightly shifted to lower energies with respect to MeSqOH so that the energy gap is slightly increased.

Furthermore, calculated dipole moments of both of the molecules have values less than 0.001 Debye. This means the probable source of nonlinear properties lies in intermolecular interactions. As known from the work of Ashwell et al.[100,101] the squarylium molecules are able to form aggregates with high second-order nonlinear activity.

Analysis of aggregation

X-ray structural analysis made by *Aschwell et. al.*[102] for the chromophore 2,4-bis(4-(N,N-dibutylamino)phenyl)squaraine which is characterized by a similar SHG activity as MeSqOH has shown that the chromophore is linear and planar and has an inversion centre. Intermolecular charge transfer between the terminal donor and central acceptor of adjacent molecules can, however, give rise to acentric "T-shaped" dimers and higher aggregates[100]. These are supposed to be the "molecular" building blocks for SHG. Since the formation of second-order active aggregates involves the central acceptor part of the molecules (-H and –OH groups) together with donor end-groups (methyl, ethyl amine) the orienting influence of the substrate plays a role by forming the initial microcrystalline layer.

At basic level mechanisms of formation can be analyzed using a model that includes interaction between two molecules. Optimization of geometry of aggregates of two molecules shows interaction between the central group (squaraine) of one molecule and the end-group (ethyl, methyl amine) of the second molecule (Fig. 60).

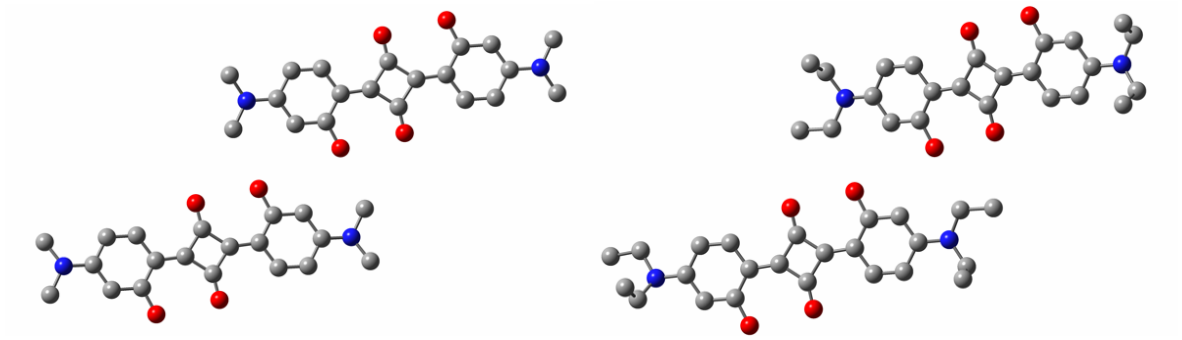

a) b)

Fig. 60: Optimized structure of a Me-SqOH (a) and Eth-SqOH (b) aggregate of two molecules. Optimization was performed by the AM1 semi-empirical method.

Although the optimized structures of two-molecule aggregates are not very distinguished, the detailed analysis of their molecular properties shows significant differences. As can be seen in Tab. 4, the aggregate of two molecules of Me-SqOH has a maximal value of charge transferred between molecules. This means the centrosymmetry of the aggregate is broken by charge redistribution between molecules.

	Dipole, D	Charge transfer, *e*
2 Me-Sq	0.1039	0.0017
2 Me-SqOH	**0.2303**	**0.0472**
2 Eth-Sq	0.2392	0.0104
2 Eth-SqOH	0.1818	0.000

Tab. 4: Calculated dipole momentums and intra-molecular charge transfer of two-molecule aggregates calculated by the B3LYP/6-311 *ab-initio* method. The value of intra-molecular charge transfer between two molecules correlates with the efficiency of SHG of oriented films.

Vacuum deposited Ethyl-SqOH films exhibit strong SHG, comparable with the intensities from films of poled guest-host systems of nonlinear dyes with donor-(π-bridge)-acceptor structure. Intermolecular charge transfer is responsible for the high second-order nonlinearities of the oriented films. The growth of SHG with film thickness provides evidence that the anomalous second-order properties are a characteristic of the film and not of the interface. The noncentrosymmetric dimers are probably responsible for fulfilling of the structural requirements for SHG.

Having the possibility to create homogeneous, nonlinear-active, and mechanically stable layers one can utilize several advanced techniques to improve weak nonlinear optical properties. Since optical nonlinearity is more effective in case of high intensity of light, the localization of electromagnetic energy of light in limited space and keeping it as long as possible, extends the area of practical exploitation of nonlinear optical effects. These requirements are fulfilled by highly transparent optical waveguides.

Frequency conversion and phase modulation in poled waveguides

Channel waveguides

Planar waveguides can be modified by various methods with the aim to optimize light propagation. Channel waveguides which confine the light to a desired volume (Fig. 61) are basic elements of integral optics. Side elements of cladding can be created by several methods. We applied excimer laser etching, photolithography and photo bleaching. Photolithography was found to be the most precise but in the same time the most expensive method for structure preparation under laboratory conditions, since most of photoresists are working only with UV radiation. The same situation was found for photobleaching. Only UV light can break chemical bonds and bleach chromophores. That requires application of quartz masks.

Computer controlled excimer UV laser is able to form structures with a resolution in the order of 1-10 μm. Depending on the value of laser energy, either etching by photoablation (with high power) or bleaching (low power) can be achieved. Etched structures can be covered by another layer for instance by spin-coating or vacuum deposition techniques.

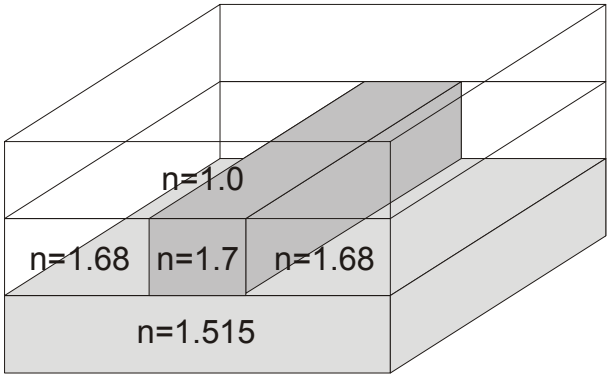

Fig. 61: Three-dimensional scheme of a channel waveguide. The substrate is BK7 glass; the channel can be obtained by combination of two different polymers or by bleaching through a mask.

The mathematical analysis even for more complicated geometries such as that given in Fig. 61 provides information about the formation of optical waveguide modes and about their propagation behaviour under the given geometrical constraints.

For carrying out this analysis, we assume a wave, which propagates into the z direction and which has for the electrical field the form:

$$\mathbf{E}(x,y,z,t) = \mathbf{E}(x,y)e^{-i(\omega t-\beta z)} + c.c. \qquad [5.1]$$

Alternatively, in case of the magnetic field we have:

$$\mathbf{H}(x,y,z,t) = \mathbf{H}(x,y)e^{-i(\omega t-\beta z)} + c.c. \qquad [5.2]$$

where ω is the angular frequency and β the propagation constant. An eigenvalue equation for the electrical field ***E*** is derived from the Helmholtz equation:

$$\nabla\times\left(\nabla\times\mathbf{E}\right) - n^2\beta_0^2\mathbf{E} = \mathbf{0} \qquad [5.3]$$

or, for the magnetic field **H**

$$\nabla \times \left(n^{-2} \nabla \times \mathbf{H} \right) - \beta_0^2 \mathbf{H} = \mathbf{0} \qquad [5.4]$$

which is solved for the eigenvalue $\lambda = -\beta^2$.

The numerical calculations of the propagation of light in channel waveguides can be performed by the finite element method (FEM) or by finite difference method (FDM)[103]. The precision of the solution in FEM depends on the generation of a proper mesh. Mostly used is the triangular type of mesh (Fig. 62).

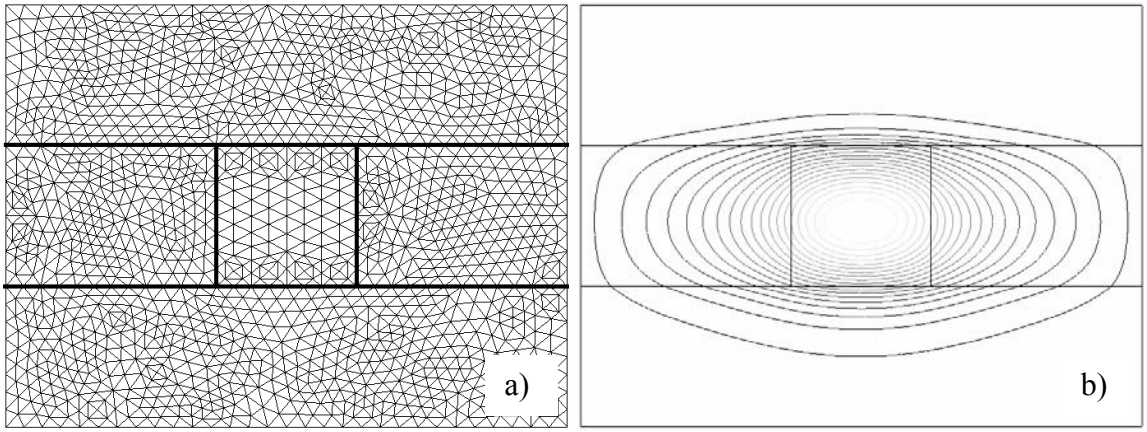

Fig. 62: (a) Triangular mesh used for numerical simulation; (b) Electrical field energy distribution (contour lines) of a TE0 mode of a channel waveguide calculated by use of a triangular mesh. Due to the waveguide asymmetry (the substrate has a higher refractive index than the superstrate), the electrical field penetrates deeper into the substrate.

The FEA calculations in this work were performed using commercial software COMSOL Multiphysics. This program also provides automatic mesh generation and post-processing of results of calculations.

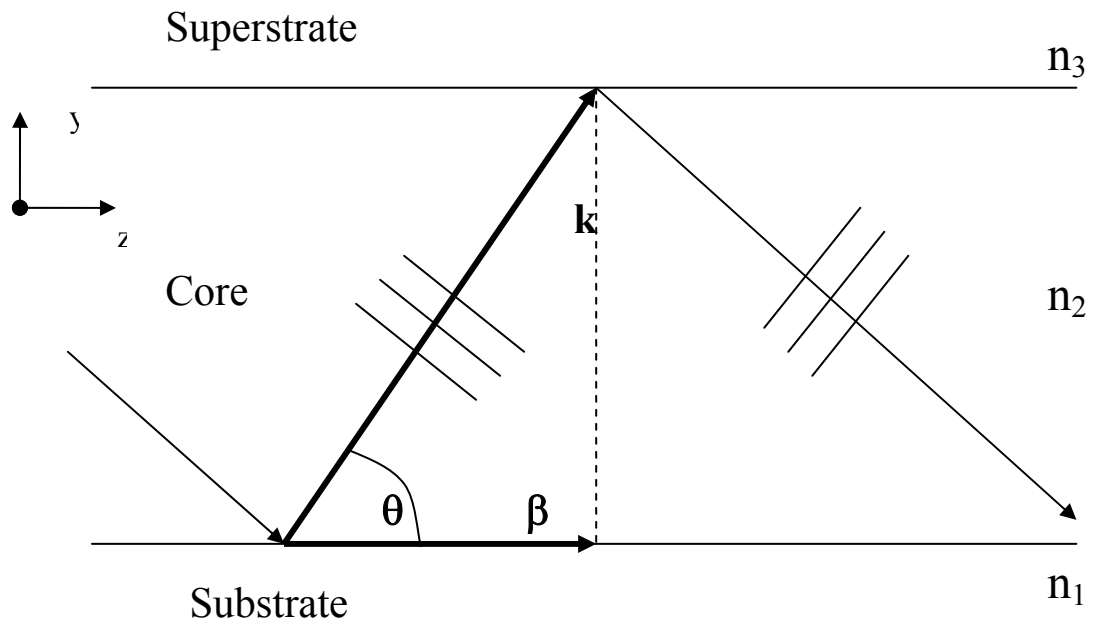

Fig. 63: Light propagation within an optical waveguide; k –propagation wector, θ - bouncing angle, n_1,n_2,n_3 – refractive indices of substrate, core, and superstrate, respectively. β - effective propagation vector.

For the situation shown in Fig. 63 the following relations are fulfilled in case of waveguiding:

$n_1, n_3 < n_2$

$n_{eff} = n_2 \cdot \cos\theta$

$k = k_0 \cdot n_2$

$\beta = n_{eff} \cdot k_0 = k \cdot \cos\theta$

Hence, one can obtain the effective modal refractive index from the formula:

$$n_{eff} = \frac{\beta}{k_0} \qquad [5.5]$$

In the general case, when n_{eff} is a complex number it includes losses as imaginary part.

As boundary condition along the outside of the cladding, the magnetic field is set to zero. Because the amplitude of the evanescence field decays rapidly with cladding thickness, this is a valid boundary condition.

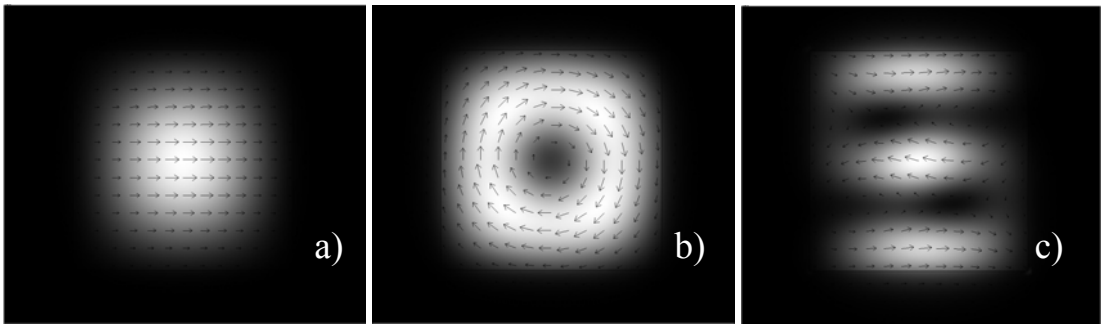

Fig. 64: (a) First, (b) second, and (c) ninth-order mode of a waveguide with a square profile (1x1 μm). The wavelength is 633 nm. The refractive index of the core is n_{core}=1.54. The cladding is air with n_{cladd}=1. The values of n_{eff} are 1.49 for (a), 1.42 for (b) and 1.29 for (c). At lower-order modes the energy (surface plot) is concentrated in the center of the waveguide. Higher-order modes have a complicated distribution of the electrical field vector (arrows).

Fig. 64 shows the electromagnetic field energy distribution (surface plot) and the distribution of the electrical field vector (arrows) for a fused silica waveguide. The dimension of the waveguide (1 μm^2) supports multi-mode propagation at a wavelength of 633 nm. As can be seen from Fig. 64 (b,c), the higher-order modes (with lower refractive indices) tend to be distributed over the whole waveguide cross-section. The TE0 mode is concentrated in the centre of the waveguide (Fig. 64a). This is an example of light confinement along a channel.

Modal dispersion

According to equations [5.5], the effective refractive index (at fixed wavelength) depends on waveguide thickness. For a selected mode n_{eff} is in between the refractive index of the substrate and the refractive index of the core polymer. For instance, a film made of PPQ2b, i.e. from a high refractive index polymer on a BK7 glass substrate reveals an effective refractive index in the range from 1.515 (n_{BK7}) at low thickness up to 1.76 (n_{PPQ2b}) in case of thicker films (Fig. 65).

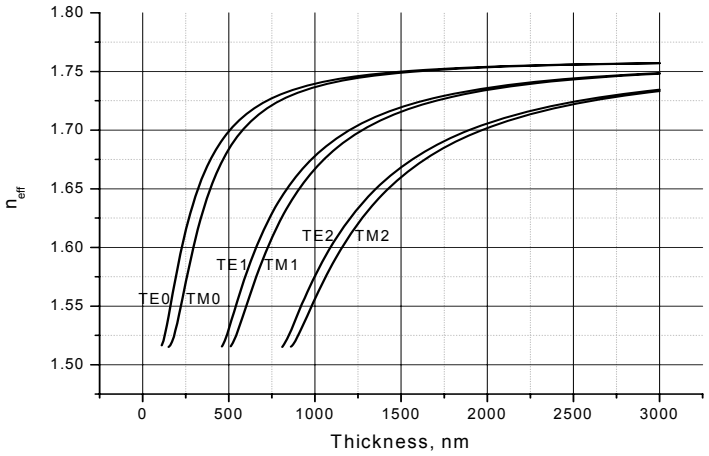

Fig. 65: Modal dispersion of different modes in PPQ2b films for a wavelength of λ = 632 nm. The effective refractive index of any mode stays in between the substrate refractive index n=1.515 (BK7 glass) and the bulk refractive index of the polymer n=1.76. Varying the film thickness allows to obtain any required effective refractive index.

This dependence defines *the modal dispersion* and plays an important role for phase matching between different modes in waveguides.

Phase matching conditions in waveguides

Waveguides can be used for fabrication of efficient nonlinear optical devices since they allow establishing high optical field strengths due to confinement. In waveguides prepared from poled polymer films the following types of second-order nonlinear interactions (nonlinear modulation of polarisation by electrical field of propagating light) are present:

$$\begin{aligned} P_i^{TM} &= \varepsilon_a \chi^2_{zzz} E^j_{TM} E^k_{TM} = 4\varepsilon_a d^2_{33} E^j_{TM} E^k_{TM} \\ P_i^{TM} &= \varepsilon_a \chi^2_{zyy} E^j_{TE} E^k_{TE} = 4\varepsilon_a d^2_{32} E^j_{TE} E^k_{TE} \\ P_i^{TE} &= \varepsilon_a \chi^2_{yyz} E^j_{TE} E^k_{TM} = 4\varepsilon_a d^2_{24} E^j_{TE} E^k_{TM} \end{aligned} \qquad [5.6]$$

where the *y-axis* corresponds to TM and the *x-axis* corresponds to TE polarizations. The *z-axis* is the propagation direction (Fig. 66).

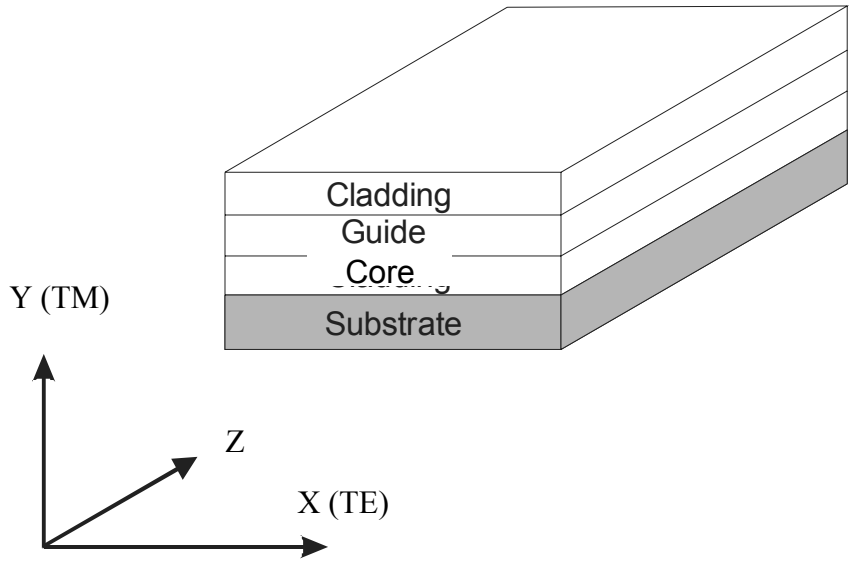

Fig. 66: Schematic presentation of a planar waveguide. Air can be the upper cladding. If the substrate is optically transparent and has a low enough refractive index, it can serve directly as lower cladding.

Although a special preparation (poling) of guiding films makes the material nonlinear active, the efficiency of SHG in waveguide configuration is mainly defined by matching between different propagating waves, e.g. the fundamental (F) and the second harmonic (SH) wave. Mismatch (and as a result destructive interference) is a reason for low-intensity of the SH (Fig. 68). Phase matching between waves involved in nonlinear interaction is one of the requirements for achieving high efficiency of the process. Naturally, dispersion of the optical materials leads to phase mismatch.

Several methods can be used for phase mismatch compensation. The main methods are listed together with their typical phase matching condition in Tab. 5:

Phase-matching method	**Condition for the wave vector difference**
Birefringent phasematching	$\Delta k = 0$
Periodic quasiphasematching	$\Delta k = \frac{2\pi m}{\Lambda}$
Fibonacci-based quasiperiodic structure	$\Delta k = \frac{2\pi(m+n\tau)}{D}; \tau = \frac{1+\sqrt{5}}{2}$

Tab. 5: The phase matching condition, required for different phase-matching techniques

1. Birefringent phase matching is realized as special direction of propagation within anisotropic nonlinear media where dispersion is compensated.
2. Periodic quasi phase matching (QPM) is based on periodically modulated nonlinearity.
3. Aperiodic QPM is an extended variant of periodic QPM that allows to support more than one nonlinear process.

For instance, true phase-matching when both interacting waves are travelling with the same speed (Fig. 67) is the optimum but difficult to realise.

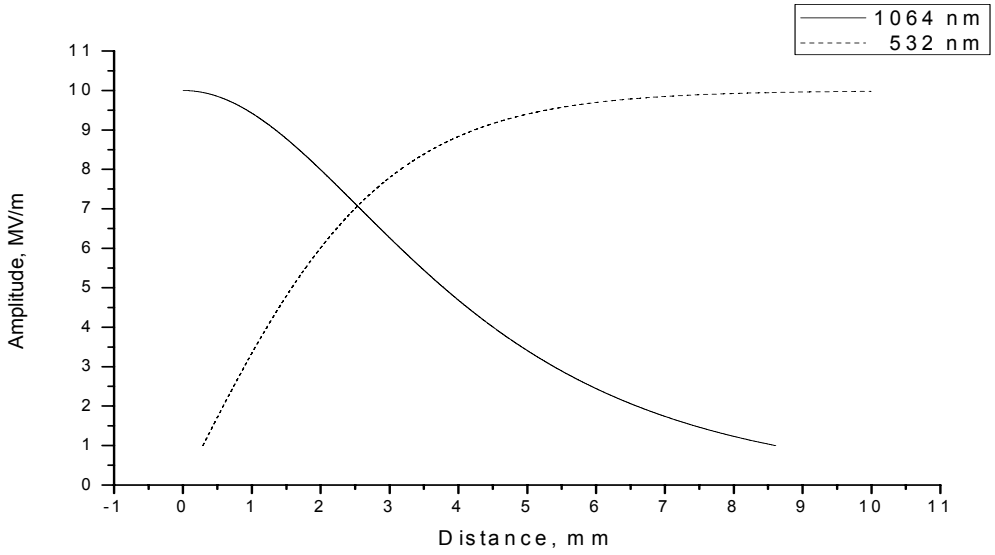

Fig. 67: Electrical field amplitudes of the fundamental (λ=1064 nm) and of the second harmonic (λ=532 nm) versus propagation distance in case of phase matching (Δk=0) for the process of SHG.

As can be seen in comparison to not matched propagation (Fig.68) almost the whole energy of the fundamental wave can be transformed into the second harmonic.

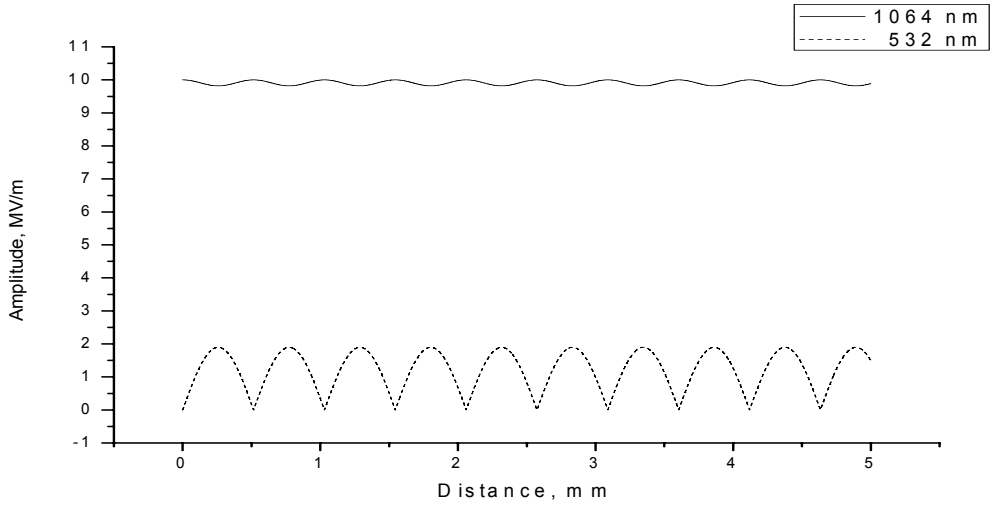

Fig. 68: Electrical field amplitudes of both F- and SH-wave versus propagation distance for a uniformly poled film. Oscillations of the SH are due to phase mismatch (n_{1064}=1.6, n_{532}=1.601). The assumed initial field strength of the F-wave is 10 MV/m (2 ns / 1 mJ / 1 mm^2), $\chi^{(2)}$=10 pm/V.

Fig. 69 presents the effective refractive index n_{eff} of waveguide modes of different order, polarisation and wavelength in dependence on the waveguide thickness.

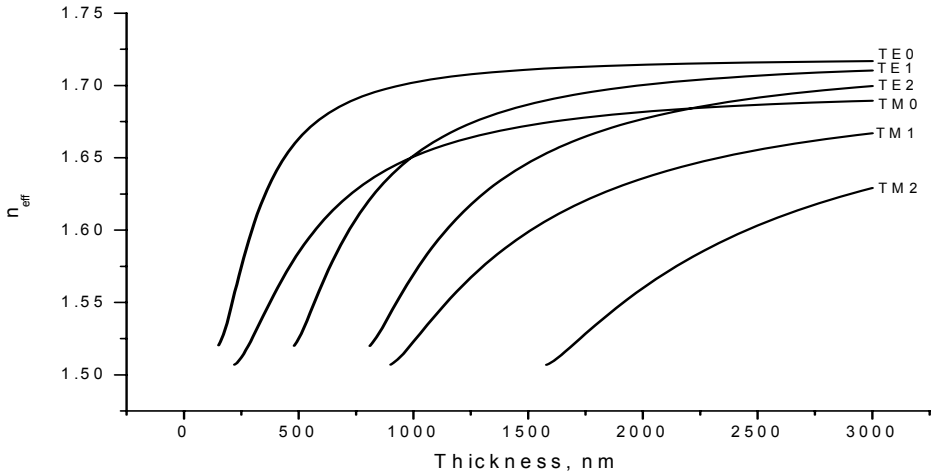

Fig. 69: Modal phase-matching in a PPQ2b plane waveguide. At thickness 989 nm the TM0 mode of the fundamental wavelength (λ=1064 nm) matches to the mode TE1 of the second harmonic (λ=532 nm). A second phase-matching appears at a the thickness of 2210 nm between TM0 (1064 nm) and TE2 (532).

As can be seen, there are certain values of waveguide thickness where different n_{eff} -traces cross each other. Therefore, different modes attain the same effective refractive index at these thickness values. At these values phase matching between different modes is reached based on modal dispersion. In order to use this type of phase matching for efficient SHG a precise control of thickness of the waveguide is necessary to keep the effective refractive index constant over the whole propagation distance. Fig. 69 presents the thickness dependence of TE modes for a wavelength of 1064 nm and for TM modes for the wavelength of 532 nm, and their phase matching points. However, phase matching points can also be found for TE or TM modes only but of different wavelength.

Indeed the dependence of effective refractive indices on film thickness (see Fig. 70) determines the thickness sensitivity of SHG efficiency.

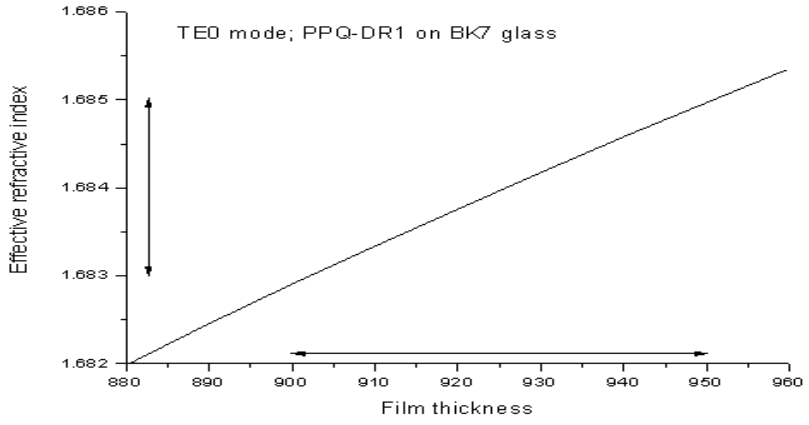

Fig. 70: Effective refractive index of the TE0 mode (λ=1064 nm) for a waveguide prepared from PPQ@10wt%DR1 on BK7 glass versus thickness of the waveguide core layer. Changes of the thickness of the core lead to changes in the effective refractive index n_{eff}. The change of $\Delta n_{eff} = 10^{-3}$ can easily be achieved by a relative thickness change of the order of 1%- 3%.

Small deviations in thickness during the deposition of the waveguide lead to a reduction or even to a complete vanishing of SHG (Fig. 71).

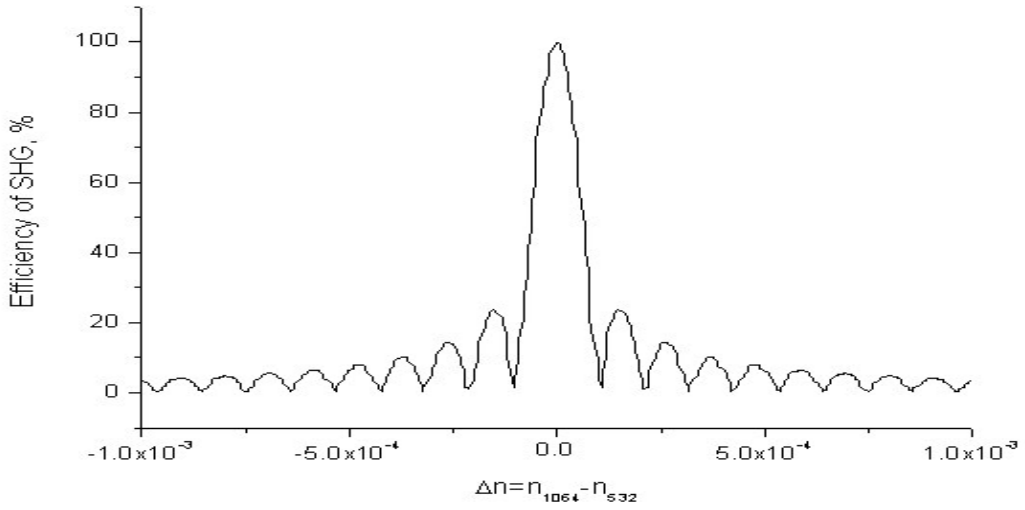

Fig. 71: Efficiency of SHG in % after a waveguide length of 5 mm versus the difference Δn between refractive indices of the fundamental n(λ=1064 nm) and of the SH wave n(λ=532 nm).

Since the effective refractive index is a function of thickness, the realization of modal phase matching in polymer films is a complicated task. Spin-coated films have the tendency to change thickness during the post deposition processing, which is necessary to stabilize the polymer layer (drying, baking or annealing).

The phase between the second harmonic wave and the wave at the fundamental frequency is intensity-dependent. The phase-matching condition is broken when intensity of fundamental or second harmonic beam is high even if it is satisfied at low intensity. The process of energy conversion from the SH wave back to the fundamental has a cyclic behaviour. Modelling of this phenomenon using two different nonlinear coefficients (coupling coefficients in the equation [2.65]) is given in following Fig. 72:

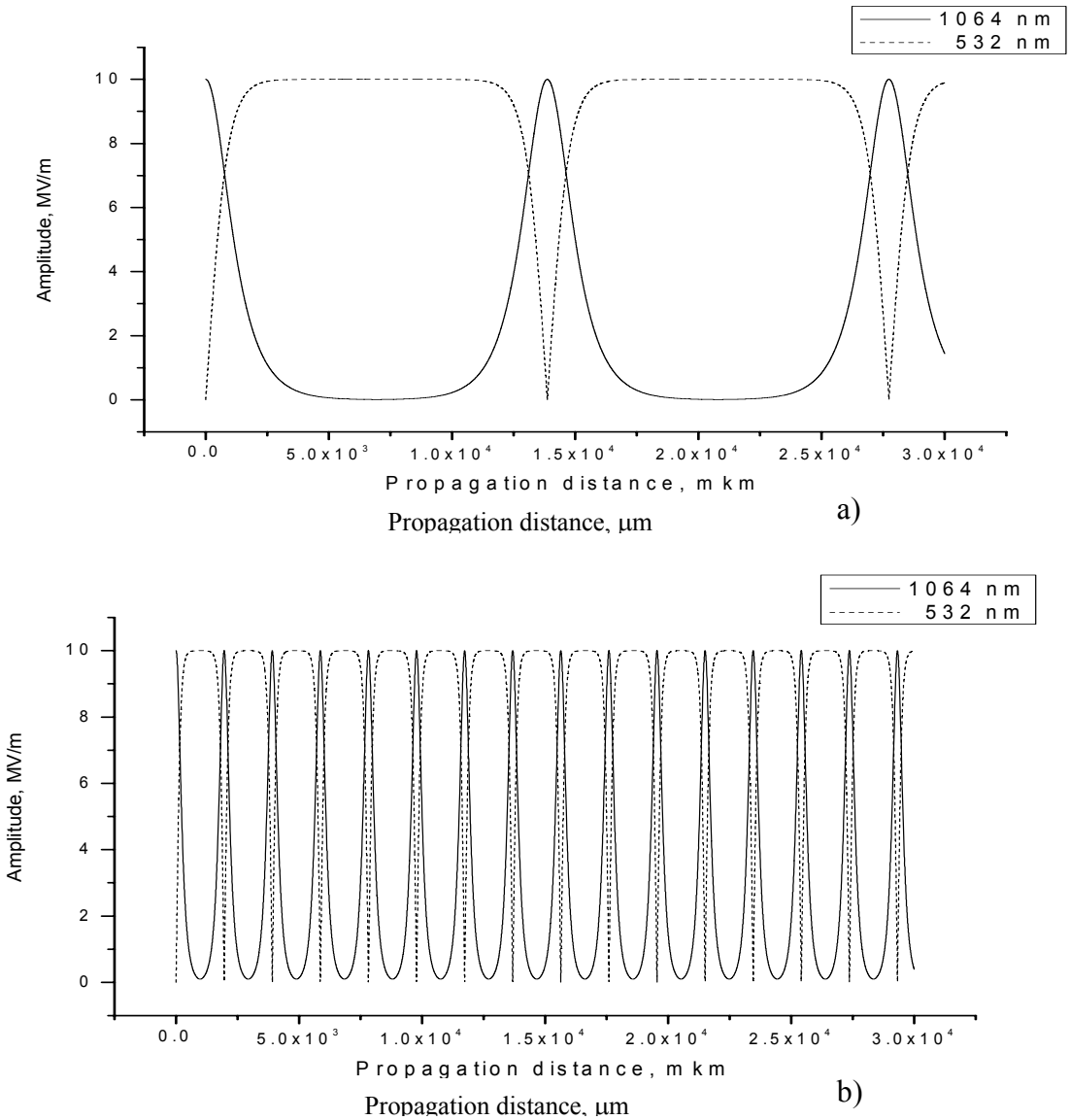

Fig. 72: Field amplitudes of fundamental and SH wave versus propagation distance. Please note the cyclic energy exchange between the fundamental and second harmonic wave. The characteristic of energy depends both on the nonlinear properties of media and on the field strength: (a) $\chi^{(2)} = 10\frac{pm}{V}$ (b) $\chi^{(2)} = 50\frac{pm}{V}$. The field strength at the waveguide input is assumed to be $A_1(0)$=10 MV/m (fundamental) and $A_2(0)$=0 MV/m (SH) in both cases.

In Fig. 72a, and Fig. 72b can be seen that the energy exchange between fundamental and SH wave reverses sign after a certain characteristic distance. This distance depends on the second order susceptibility $\chi^{(2)}$ and the field strength. Comparison of Fig. 72a with Fig. 72b shows that an increase of the $\chi^{(2)}$ value from 10 to 50 pm/V leads to a reduction of the characteristic distance for energy exchange from 14 mm to 2 mm at constant fundamental field strength at input.

When the intensity of the fundamental wave achieves a value near to zero the phase changes by +90° and the energy conversion changes direction (Fig. 73).

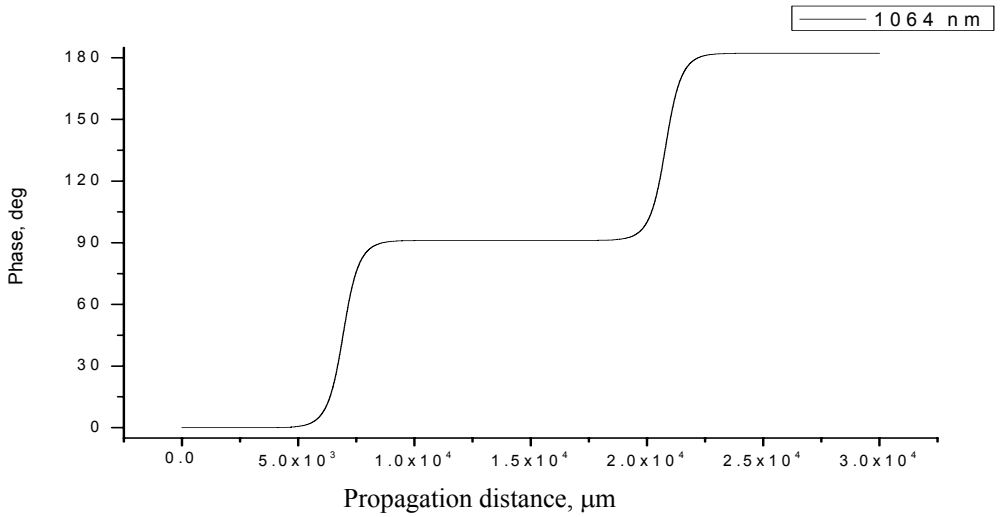

Fig. 73: Phase of the fundamental wave versus propagation distance. It can be seen that energy conversion changes direction (ω↔2ω). The phase graph corresponds to Fig. 72 (a)

The effect described above, is important for highly nonlinear systems or for systems where the interaction length is large. Modal PM is not a suitable choice in that case and other techniques of phase matching are more efficient.

Overlap integral

The waveguide geometry introduces additional requirements for an effective nonlinear interaction. The local interference (destructive or constructive) between ω and 2ω waves does not occur only along the propagation distance. The cross-section of the waveguide must also be taken into account. As mentioned above, the field distribution over the cross-section of the waveguide varies dependent on the mode order as can be seen in Fig. 74.

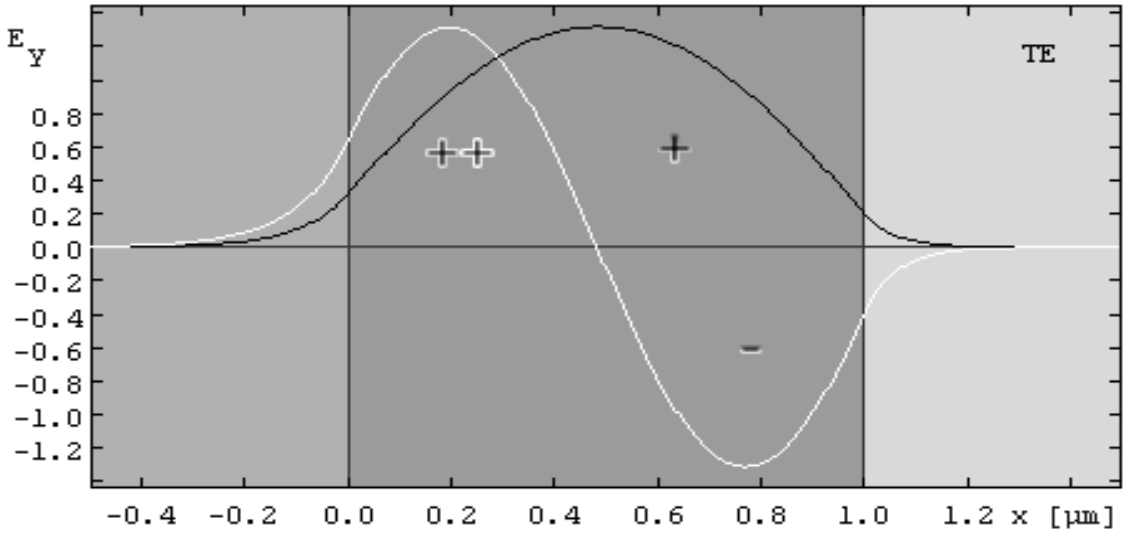

Fig. 74: Electrical field distribution of the TE0 mode (black line) and TE1 mode (white line) within a waveguide. The dark-gray region represents the core of the waveguide.

Efficient modal dispersion phase matching requires a sophisticated multilayer fabrication technique which takes the real field distribution of different waveguide modes into account in order to maximise overlap and conversion. This means that at regions of field overlap there the second-order susceptibility should have a maximum value and the right sign of nonlinearity to enable maximum conversion efficiency.

Periodic poling. Quasi phase matching.

There is a way to overcome the phase matching problems and prevent back-conversion to the fundamental frequency after some propagation distance. The waveguide media can be prepared in such a way, that the interaction processes within the guiding layer predefine their properties.

During propagation in nonlinear noncentrosymmetric media, the energy of fundamental wave is converted into the second harmonic wave in the first quarter of the coherence length. Within the second quarter the process flows into the opposite direction. The efficiency of conversion is defined by the nonlinear coupling coefficients σ_1 and σ_2. One can change the sign of the corresponding coupling coefficient at every quarter of the coherence length so that back-conversion is prevented. The sign reversal can be realized by a change of the poling direction. Finally, we will get a periodic structure where adjustable domains are poled into opposite directions. Such poling that produces the formation of domains with alternate orientation is called periodic poling. This structure provides quasi phase matching (QPM) in the material. Quasi phase matching ensures that there is positive energy flow from the fundamental frequency to the second harmonic frequency even though both frequencies are not phase locked to each other. Energy will always flow from the pump to the SH as long as the phase between the two optical waves is less than 180 degrees. Beyond 180 degrees, energy flows back from the SH to the pump frequency (Fig. 73).

Fig. 75 shows a computational result of the growth of the SH amplitude during propagation in a QPM lattice. It is very similar to true PM shown in Fig. 67.

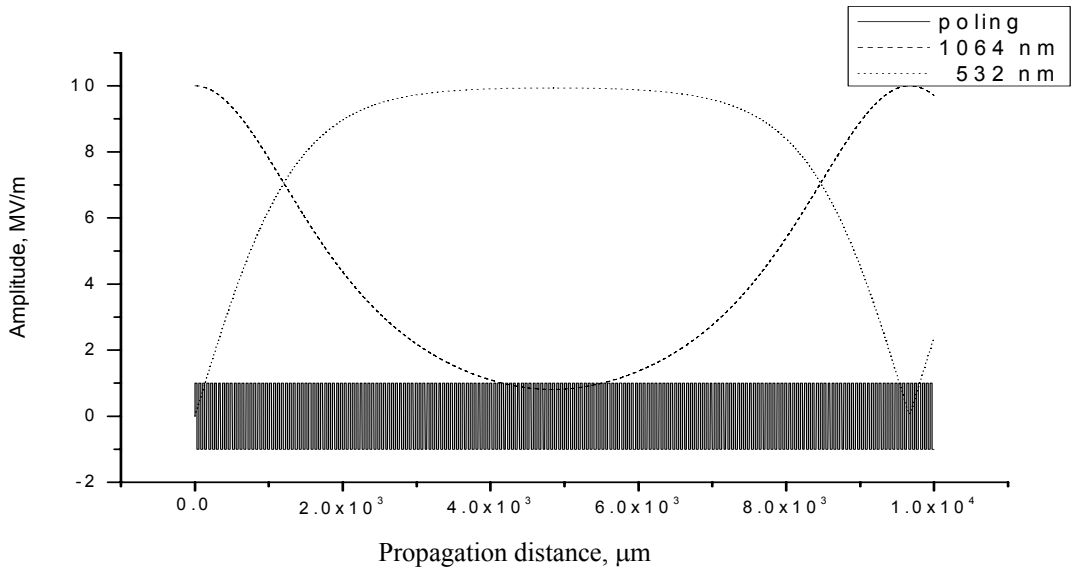

Fig. 75: Electric field amplitude of fundamental and SH wave versus propagation distance along a periodically poled waveguide. The poling period is one coherence length. A constant coherence length was assumed.

In addition, energy oscillations between interacting waves are present for long propagation distance. The domain length can be adjusted to prevent back conversion into the fundamental. To design an efficient SHG device one should take into account the intensity-dependence of the coherence length [2.109]. This can lead to efficient energy transfer from the fundamental to the SH wave as illustrated in Fig. 76.

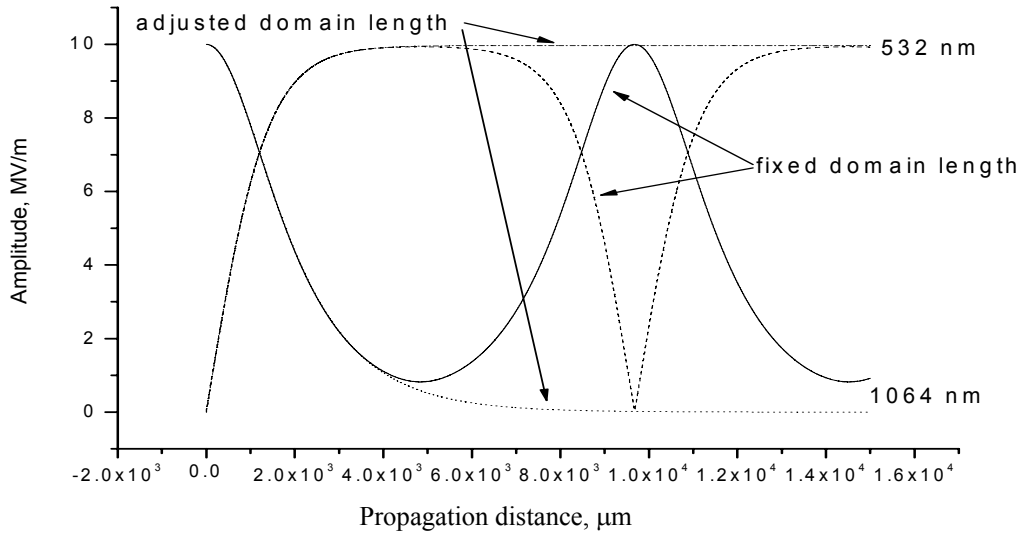

Fig. 76: Electric field amplitude of fundamental and SH wave versus propagation distance along a periodically poled structure with fixed domain size or domain size adapted to the field dependence of the coherence length.

The importance of the quasi phase matching technique can be illustrated by using the dispersion curve Fig. 70 of a polymer waveguide. As can be seen, small deviations of film thickness (less than 3%) lead to changes in effective refractive index of approximately Δn=0.001. That is enough to reduce the efficiency of second harmonic generation (SHG) by 5% (Fig. 71). Additional losses make this value even smaller. A typical tolerance in the spin-coating process is in the order of 1% over an area of approximately 1 cm^2. That means in a best-case scenario one can achieve only several percents of energy conversion.

In case of QPM, the variation of the domain lengths compensates the influence of material dispersion on conversion efficiency. Maximum efficiency of SHG in a QPM structure requires a domain size to be an odd number of coherence lengths. Fig. 78 shows that the best efficiency is achieved when the domain size is equal to the coherence length $l_k = \frac{\pi}{\Delta k}$.

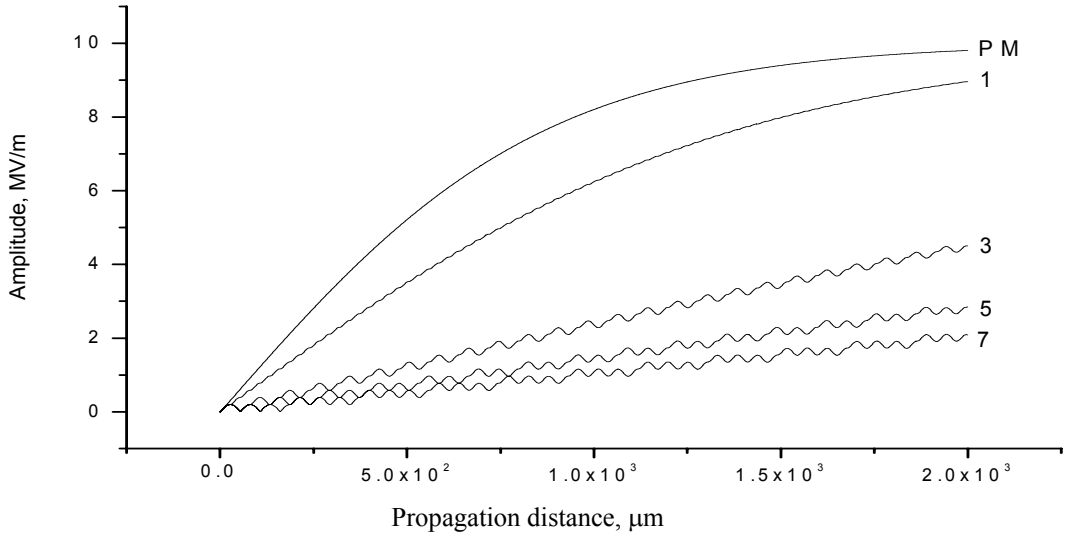

Fig. 77: Electric field amplitude of the SH wave versus propagation distance in different phase-matching systems: true PM and QPM with different domain size. The numbers (1-7) correspond to domain size expressed in coherence lengths. Most effective QPM is realized by the shortest domain size (one coherence length).

In case of high-dispersive media (as chromophore-doped polymers), this value can be a few microns. As stated before the size of electrodes (which is equal to the size of domain 1) is only two or three times the film thickness and border effects can strongly interfere. To prevent these non-desired effects a longer domain size (3,7,9.. coherence lengths) can be used.

Being optimized for a certain nonlinear process (for instance SHG from 1064 nm to 532 nm) the QPM structure demonstrates that the phase shift is equal to zero and maximum conversion efficiency is reached. By varying the pumping wavelength with the help of a tuneable laser and registering the phase difference between propagating waves, one can see that the phase difference achieves maximum and minimum values near the phase matching point (Fig. 78). That means the nonlinear phase delay, which is typically observed in third-order nonlinear effects, is induced by second-order effect. Since second-order nonlinearities have higher efficiency in comparison to third-order nonlinearities, the required intensity can have much lower values. That is important when organic materials are used as nonlinear medium.

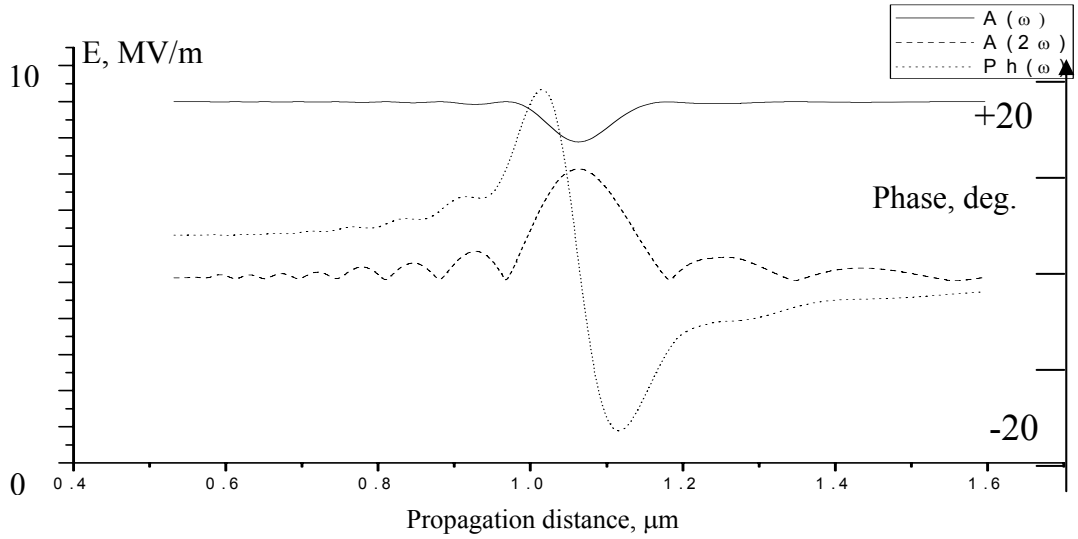

Fig. 78: Electrical field amplitudes of fundamental and SH wave, and phase of SH versus fundamental wavelength for a QPM-structure. Periodical poling was optimized for maximum efficiency of SHG at excitation with 1.064 μm.

Fig. 78 shows the calculated intensity of the fields at ω and 2ω for a given QPM waveguide (fixed domain size and waveguide dimensions) and for the Nd:YAG fundamental beam. For a wavelength different from 1.064 μm the SH intensity shows a zero phase shift of the fundamental wave at optimized wavelength and achieves minimum and maximum in the nearest area.

Consecutive poling

The most important advantage of QPM is that more than one nonlinear process can be involved simultaneously. Two second-order nonlinear processes, generation of second harmonic ($2\omega = \omega + \omega$) and sum frequency generation ($3\omega = \omega + 2\omega$), act like a third-order process like third harmonic generation ($3\omega = \omega + \omega + \omega$). However, the two involved second-order effects have a higher efficiency and appear at lower laser intensity. The requirement of low pumping intensity is important in the particular case of polymer waveguides, where damage threshold is lower than for most of the inorganic optical materials. The simultaneous action of two second-order effects, which mimic a third-order process, is called “cascading”.

Comparing PM in case of SHG realized in nondispesive media, with cascading, the latter does not show the highest efficiency of conversion into the third harmonic (Fig. 79). The reason is the concurrence between two simultaneous second-order processes: (ω+ω)↔2ω and (ω+2ω)↔3ω.

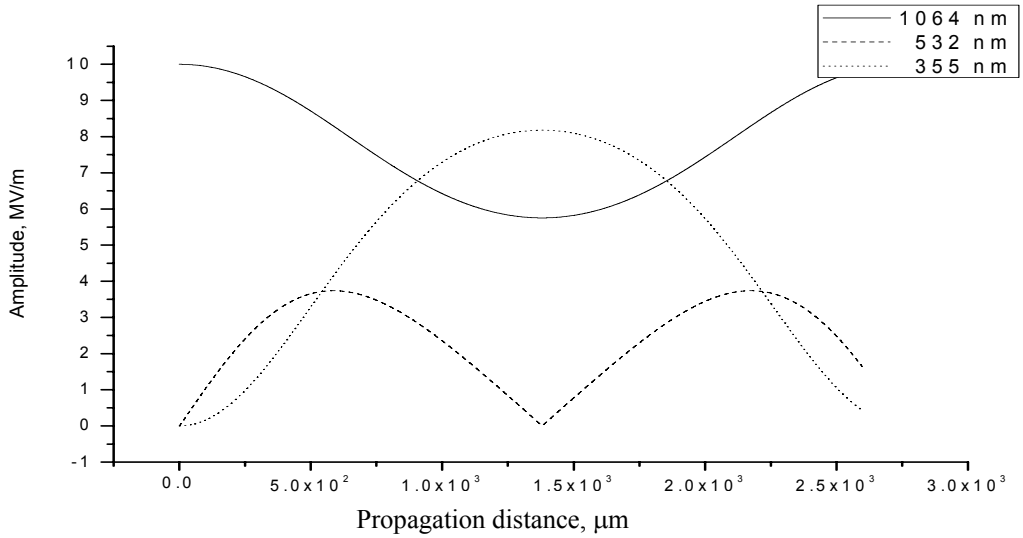

Fig. 79: Electric field amplitudes of fundamental, second and third harmonic vs. propagation distance for an ideal non-dispersive medium. The achieved conversion value is 81.8% at maximum (after ~1.4 mm of propagation). Subsequently, the back conversion into the fundamental occurs. The refractive indices of these wavelengths are assumed to be the same: $n_1=n_2=n_3=1.75$

A first (and rather direct) step to realize multi-process interaction is a sequential combination of two QPM periodic lattices into one super-lattice. Instead to create one complicated structure one can consequently combine two lattices. The combination of two QPM structures provides an efficient way to increase the outcome of two nonlinear processes. Their size is correlated to the coherence length of processes like second harmonic generation ($\omega+\omega\rightarrow2\omega$), difference frequency generation ($2\omega-\omega\rightarrow\omega$) or sum frequency generation ($2\omega+\omega\rightarrow3\omega$) to be supported by the respective lattice, and it stays constant over the whole length of the lattice. The support of two conversion processes requires two consecutive structures as shown in Fig. 80. The domain length in each part of the structure must consist of an odd number of the coherence length related the corresponding nonlinear process. If we assume a second structure which supports sum frequency generation, then the first structure must convert the fundamental frequency into a mixture of ω and 2ω waves with equivalent amplitudes as shown in Fig. 81.

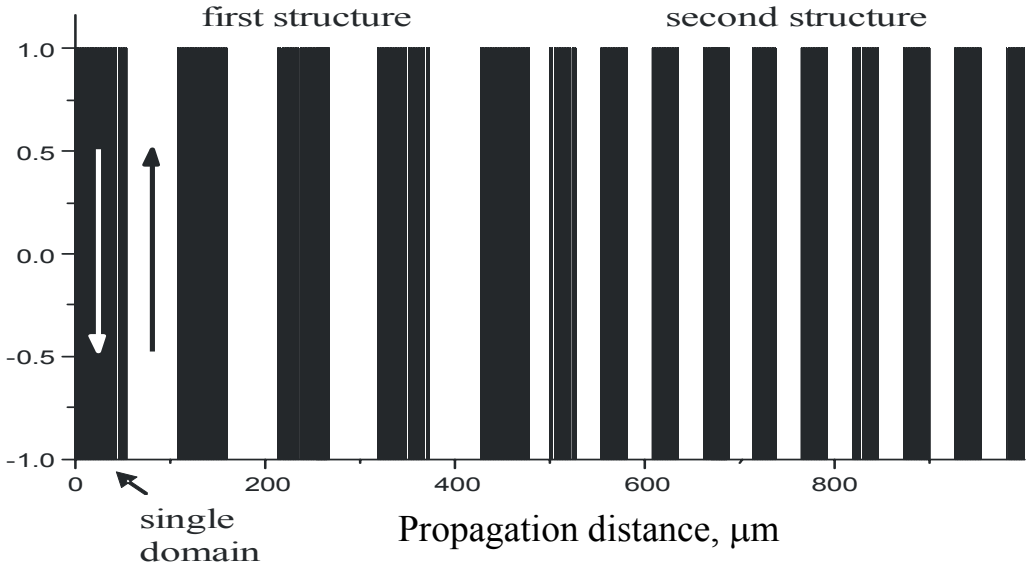

Fig. 80: Schematic presentation of a superlattice consisting of a consecutive arrangement of two different periodically poled structures. The first part is responsible for SHG. In the second part the process of SFG takes place.

A two-step conversion mechanism from the fundamental to the second harmonic followed by mixing both waves to the third harmonic (sum frequency generation) is more efficient than a pure third-order third harmonic generation (THG) because only second-order nonlinearities are involved. According to our calculations, the maximum efficiency of SFG in the second step is achieved in case of equal amplitudes of both the second harmonic and fundamental after the first conversion.

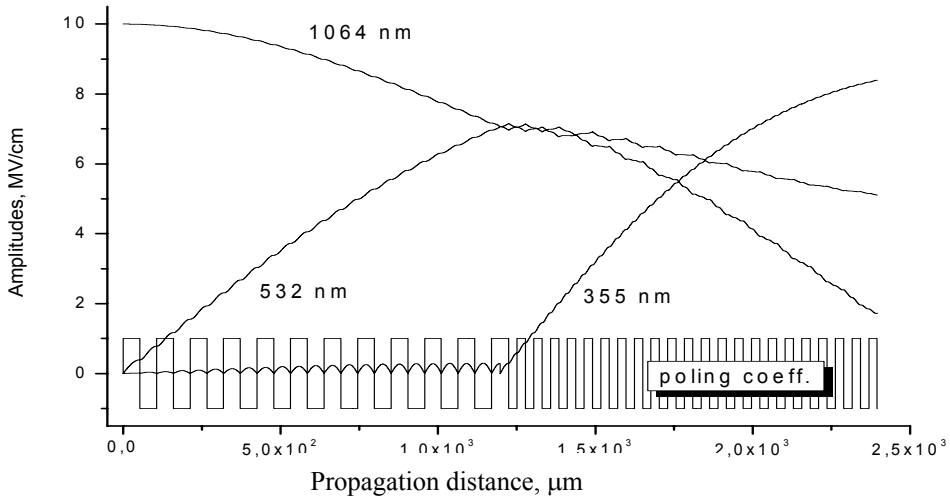

Fig. 81: Optimized QPM structure for an effective conversion via two subsequent second-order processes $\omega \to 2\omega \to 3\omega$. The structure contains two parts. The first part (0-1250 μm) provides $\omega \to 2\omega$ conversion (SHG). The second one mixes both signals, i.e. $\omega + 2\omega \to 3\omega$. The length of the first part is optimized to have equal amplitudes at input of the second part. The effective field amplitudes of the three interacting waves are plotted versus the propagation distance.

Aperiodically poled films. Fibonacci poling.

Quasiperiodic lattices (one-dimensional quasi-crystals) can be realized by a certain aperiodic poling, which supports two NLO processes simultaneously (cascading). The Fibonacci superlattice provides one interesting possibility. Such a structure is based on the Fibonacci sequence of domains ABAABABAABAAB and it is assumed that the wave vector ratio is not a rational number. Each domain A and B contains a pair of antiparallel oriented subdomains ($L_A = L_{A1} + L_{A2}$, $L_B = L_{B1} + L_{B2}$). Usually the following relations are valid for the subdomains: $L_{A1} = L_{B1} = L$ and $L_{A2} = L(1+\eta)$; $L_{B2} = L(1-\eta\tau)$, where $\tau = \left(1+\sqrt{5}\right)/2$ is the golden ratio, and η is a small number (adjusting parameter). Fig. 82 shows an example of a Fibonacci lattice optimized for the simultaneous support of two second-order NLO processes (SHG and SFG towards THG).

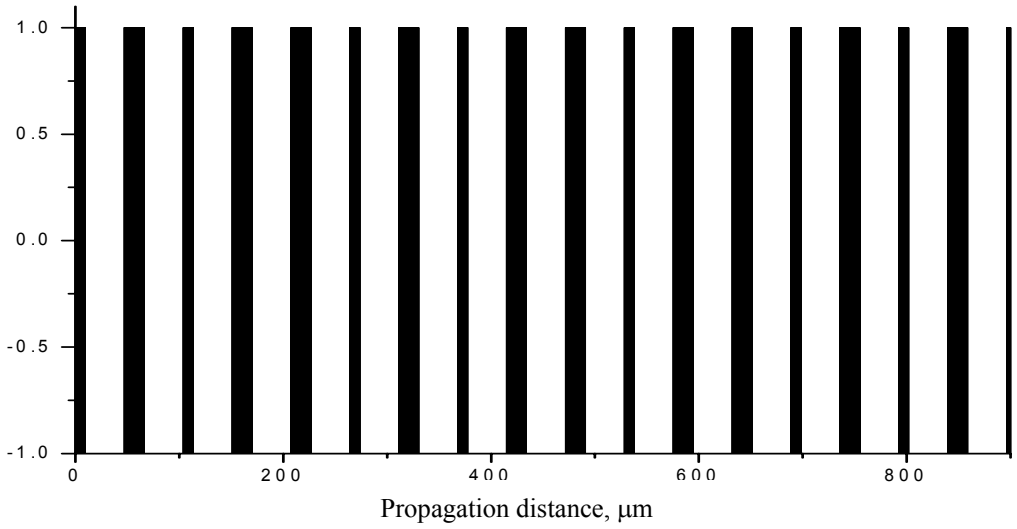

Fig. 82: Fibonacci lattice, an example of aperiodic poling. The Fibonacci lattice supports two second-order processes simultaneously.

The structure shown on Fig. 82 can be used as a mask for producing alternative poling. White and black stripes correspond to opposite poling directions. As a result, a space modulation of second-order nonlinear susceptibility can be achieved. Aperiodic (Fibonacci-type) poling supports the two addressed nonlinear processes along the whole interaction length (as shown on Fig. 83).

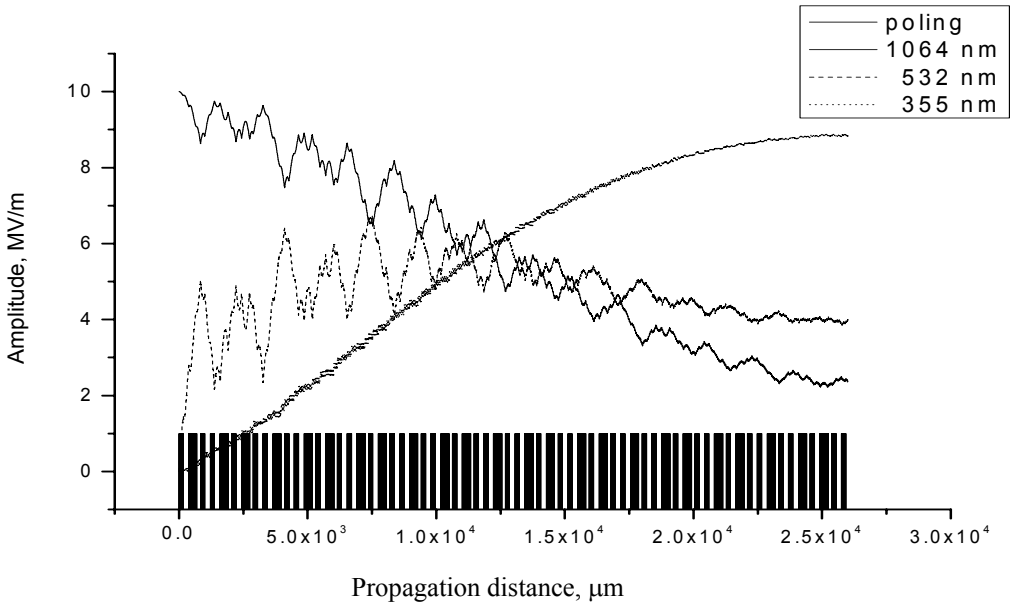

Fig. 83: Two selected second-order nonlinear processes (SHG, SFG) are simultaneously realized in a Fibonacci-type aperiodically poled structure. The electric field amplitudes of fundamental, SH and TH waves are plotted vs. propagation distance. The structure has a high efficiency of conversion (88.3%).

Nonlinear properties of PPQ-based planar waveguides

The high refractive index of polyphenylquinoxaline (PPQ) is a promising property for application in nonlinear waveguides and devices based on them. The refractive index contrast between core and cladding defines the amount of energy concentrated within the core. Hence for nonlinear applications a high refractive index core is preferable (Fig. 84(a,b); Fig. 85).

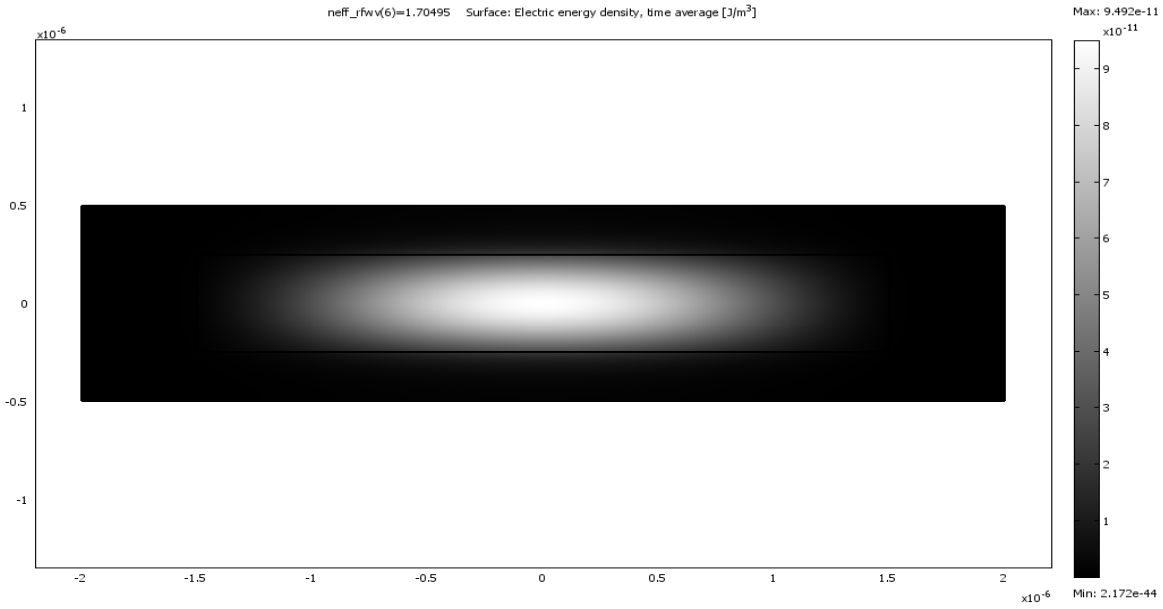

a)

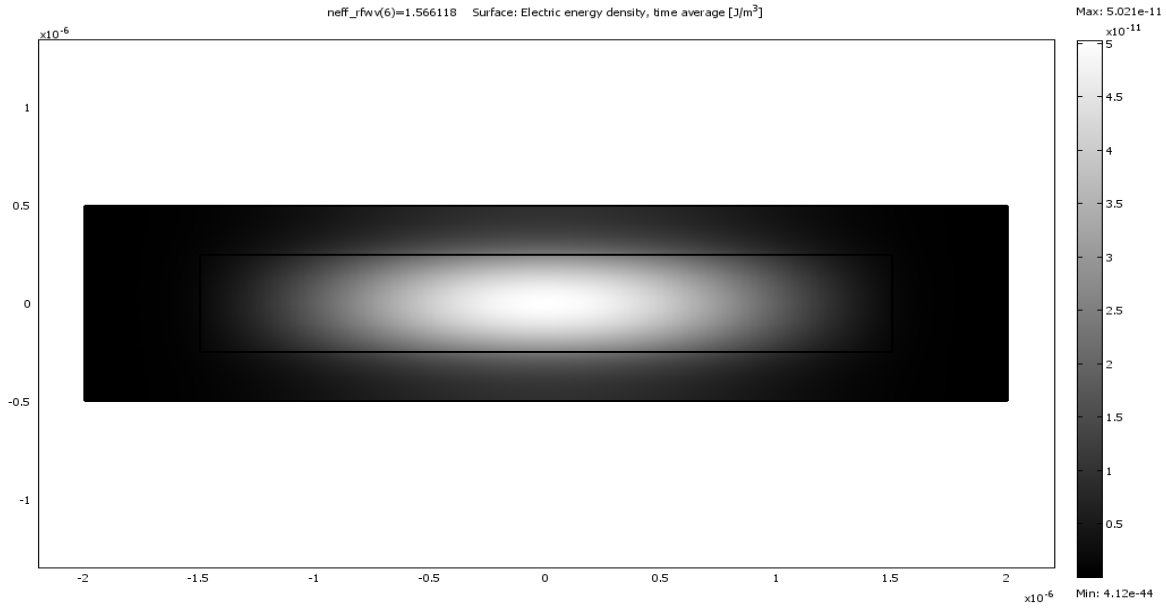

b)

Fig. 84: Electrical field energy distribution within a plane waveguide (cross-section). a) High contrast waveguide, n_{core}=1.76 (PPQ) $n_{cladding}$=1,515 (BK7 glass); b) Low contrast waveguide n_{core}=1.61 (Polycarbonate) $n_{cladding}$=1,515 (BK7 glass);

A difference of 0.1 in the index contrast leads to a notable increase of energy confinement in the core. Since only the core has a high nonlinear optical susceptibility, the efficiency is higher in case of a waveguide with high index contrast than in case of low index contrast (Fig. 85).

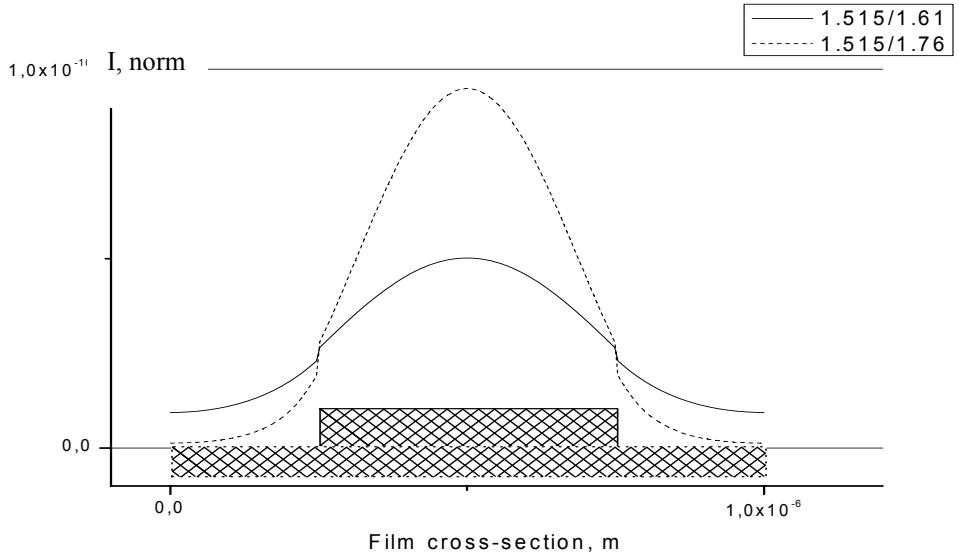

Fig. 85: Cross-section in the middle point of the waveguides shown in Fig. 84. The high contrast waveguide has its main part of energy concentrated in the core (dashed line), in contradiction to the low index contrast waveguide (solid line).

Precise measured dispersion curves allow the calculation of the coherence length of the SHG process (Fig. 86). The planar waveguide with a thickness that provides modal phase matching effectively converts the light with wavelength 1064 nm to its second harmonic with wavelength of 532 nm.

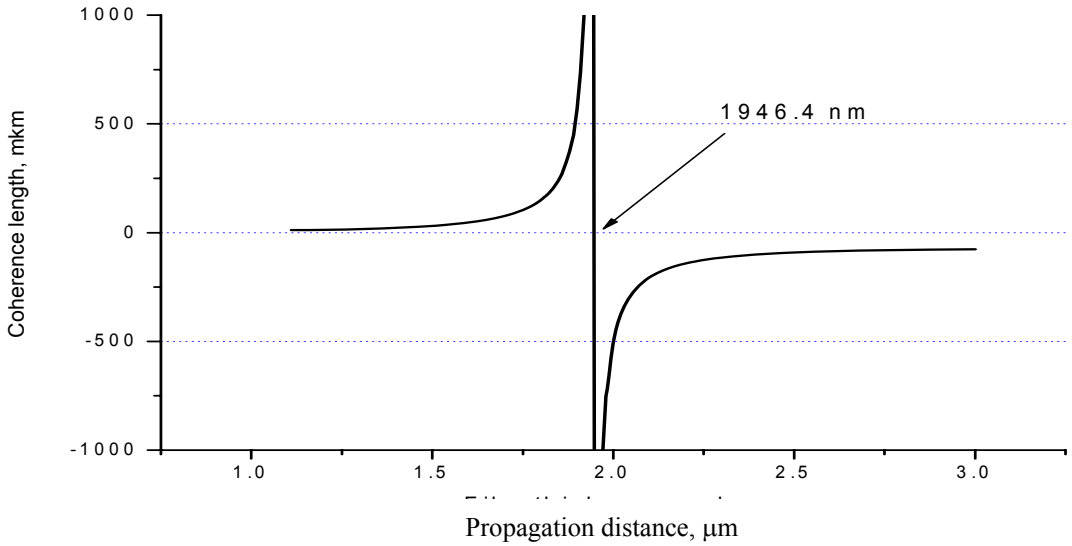

Fig. 86: Coherence length vs. film thickness for a PPQ-DR1 spin coated film for the case of modal phase matching TM1 (1550)->TM0 (775 nm). A thickness of 1946±25 nm provides a coherence length >1 mm. An infinite coherence length (at 1946 nm of film thickness exactly) means phase-matching (equivalent propagation speed) between two modes.

The procedure of poling induces a relatively strong (0.02..0.03) birefringence in the polymer guest-host film. This means that the dispersion curves should be measured with respect to the right polarization. The prism-coupling method allows measuring both TE and TM polarizations separately.

NLO devices based on periodic and aperiodic poling

Different kinds of rectangular waveguides

All mechanisms of light transformation in specially prepared nonlinear-optical structures can be exploited in a wide range of electro-optical and opto-optical devices. The waveguides can be prepared from polymer films by different methods (Fig. 87). *A ridge waveguide* is a strip of high refractive index material on top of a low refractive index cladding. The smoothness of air-core and core-cladding is playing a central role in scattering losses. In case of *a rib waveguide* the guiding strip is formed on top of the same material (for instance by plasma etching) and the core-cladding interface is not present. One requirement on the smoothness vanishes.

In case of *a strip-loaded waveguide* the guiding channel is formed by a strip of low refractive index transparent material deposited on top of a high refractive index film. An advantage of this waveguide is that the requirement of a smooth surface at air-film interface is omitted.

By modification of the refractive index of the polymer film one can create *an embedded guide*. Refractive index can be modified for instance chemically (etching) or optically

(bleaching). Since core and cladding have the same surface produced in one-step (for instance by spin-coating) the smoother air-film interface can be obtained.

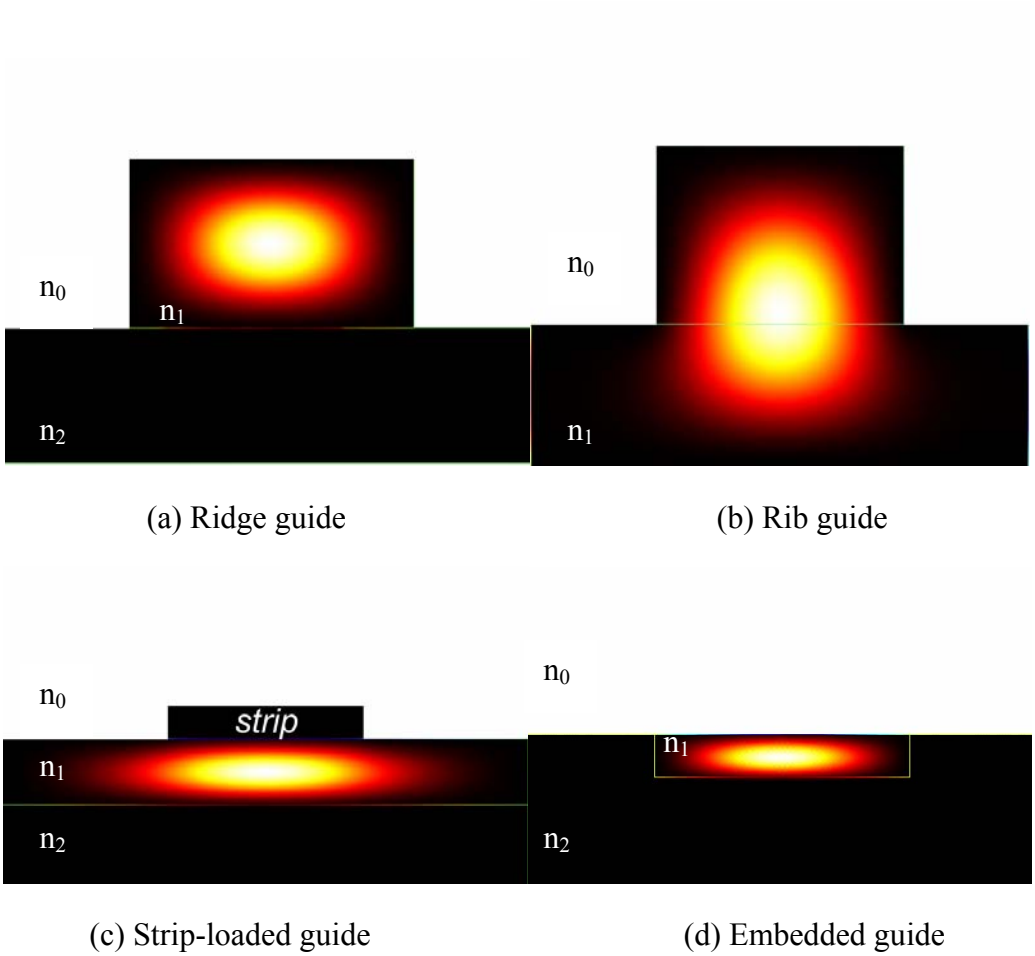

Fig. 87: Cross-section through rectangular waveguides formed by different techniques in/on polymer layers. The light energy density confined in the waveguide was calculated by finite element analysis. The bright areas correspond to high energy density

The device fabrication starts with a gold-coated fused silica substrate. Gold coating is performed by vacuum thermal deposition with subsequent annealing at 200 °C for 2 hours in vacuum. Spin-coating and curing of a 2–3 μm thick lower layer (lower cladding) by exposure to UV light for 10 min. As cladding material, EPO-CLAD negative photoresist (MRt GmbH, Berlin, Germany) which becomes insoluble after UV illumination was used. As second layer of the same material was deposited and illuminated through a contact mask. After exposition and following washing the negative image of the fabricated structure is forming the second layer. A 2 μm thick layer of PPQ2b-DR1 guest-host polymer was spun on and vacuum dried over 2 hours. The viscosity of the solution used for spin coating has to be low enough to fill the channels, obtained in the previous step. Then the next cladding layer of the EPO-CLAD was deposited. Aluminium poling electrodes were then fabricated by vacuum-deposition directly on top of the dried cladding by using a mask.

As can be seen on Fig. 88 the electrical field energy is localized in the space above the filled-channel waveguide. This reduces the influence of possible losses by the cladding. In addition, the penetration of the electrical field into the lower electrode is minimized.

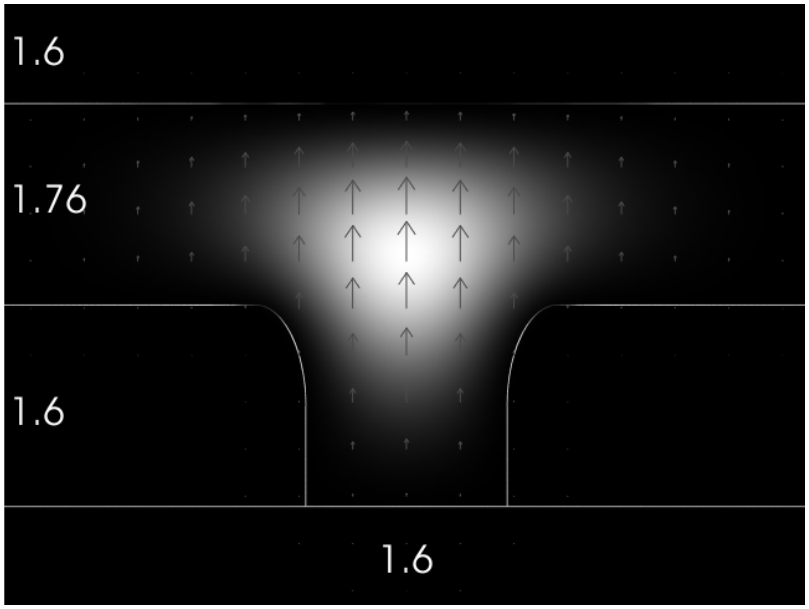

Fig. 88: Cross-section through a filled-channel waveguide. The electrical field energy (bright area)) is localized above the channel. Each layer is 2 μm thick. The channel width is also 2 μm. Arrows show the direction of the electrical field.

In integrated optical devices coupling between different waveguides can be realized by placing two channels close to each other so that the evanescent fields overlap. Varying the distance between both channels allows adjustment of the required coupling.

All-optical switching

An optical switching device allows direct light entering the input into two or more output channels. Switching of an optical signal can be realized via the intensity dependence at the coupling, which determines the output. More complicated devices (multiplexer, demultiplexer) include more than two inputs/outputs.

An easy way to realize all-optical switching is nonlinear self-action. In a medium with third-order nonlinearity, the refractive index and absorption coefficient of a light field present in the medium are modified by the strength of the light intensity. Because the field effectively acts on itself, this interaction is termed a self-action effect. However, the self-action can also be realized via second-order nonlinearities[104]. As mentioned above, the waveguide configuration can provide high power density over a long propagation distance. That makes it possible to accumulate a nonlinear phase shift.

In a second-order nonlinear waveguide, the phase shift can achieve a high value. However, this effect occurs only by using QPM technique. In a QPM waveguide, one can use dispersive media. During propagation the energy transfer between ω and 2ω waves occurs. Due to dispersion the 2ω wave propagates slower (normal dispersion) and after back-conversion into the fundamental a large phase shift occurs. Fig. 89 shows the calculated phase shift in a 5 mm long waveguide ($\chi^{(2)}$=10 pm/V). The QPM structures were optimized for a fundamental wavelength of 1064 nm. At this wavelength, the phase shift is zero because the QPM structure is optimized so that no back-conversion happens. Small detuning by wavelength (or by domain size of QPM grating) leads to a fast increase of the phase shift.

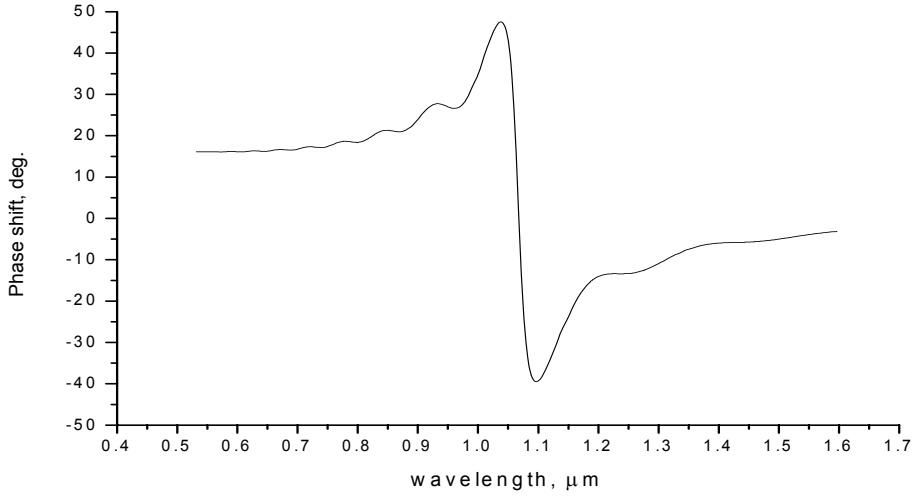

Fig. 89: Calculated nonlinear phase shift of the fundamental at the output of a 5 mm long QPM structure as a function of fundamental wavelength. The structure was optimized for maximum phase shift at a fundamental wavelength of 1064 nm.

In the present case, the maximum phase shift occurs when the domain size is equal to 1.025 of the coherence lengths. As shown in Fig. 90 (a), during propagation the fundamental wave is partially converted into the SH signal and back.

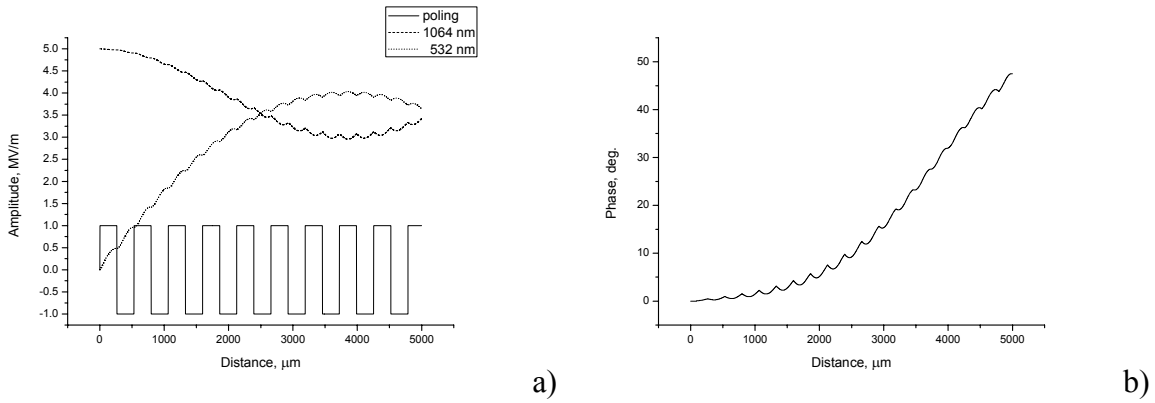

a) b)

Fig. 90: (a) Field amplitudes of fundamental and SH wave and (b) phase of the fundamental wave versus propagation distance in a QPM structure optimized to achieve maximum phase-shift of the fundamental. The domain size is 1.025 of the coherence lengths.

Devices that exploit intensity-modulated phase shift (Mach-Zehnder interferometer) require a phase shift of π induced in a length of about 1 cm or below. Often a smaller phase shift is sufficient as a base for light-modulation devices.

Optical limiting

One approach toward optical limiting makes use of materials whose optical transmittance decreases at high light levels. Such non-linear transmission function can be created using the SHG process. In this case the transmitted pump beam is depleted in a non-linear way due to energy conversion to the second harmonic. This device allows a linear transmission of light only if the intensity is less than a certain value (Fig. 91).

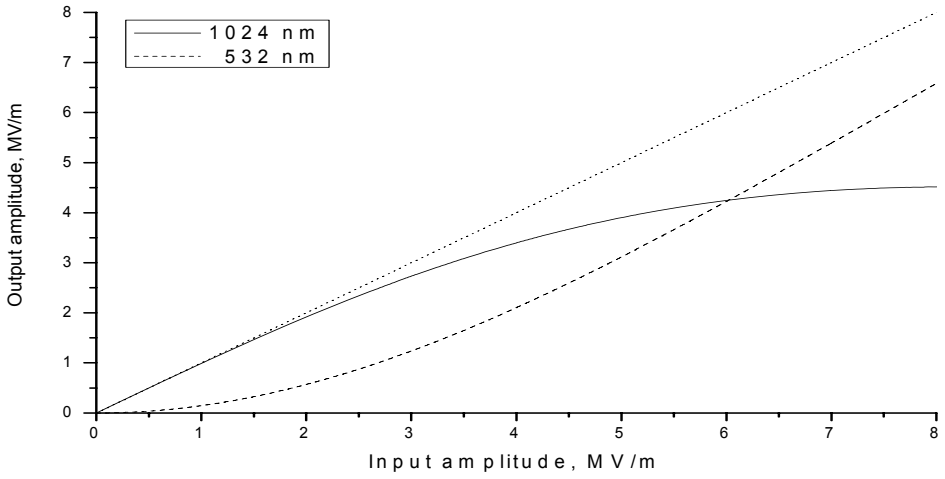

Fig. 91: Electrical field amplitude of fundamental (1064 nm) and SH (532 nm) wave at the output of a QPM structure optimized for optical limiting. The effect of SHG in the QPM structure limits the output intensity of the fundamental frequency at high intensities. With the growth of the input fundamental signal (abscissa), the output fundamental signal (solid line) deviates from a linear law (dotted line) because of energy conversion into the second harmonic (dashed line).

Light modulation

Light signal controlling by light is a fast way to manage information flows in telecommunication. Change of refractive index of nonlinear material can be used for modulation of the outcoming beam. The easiest way is to use an external electrical field for modulation. As shown above, the process of SHG in planar waveguides is sensitive to both thickness and refractive index of the core material. The applied electrical field is able to modulate the refractive index with high frequency so that the SHG signal will also be modulated (Fig. 92).

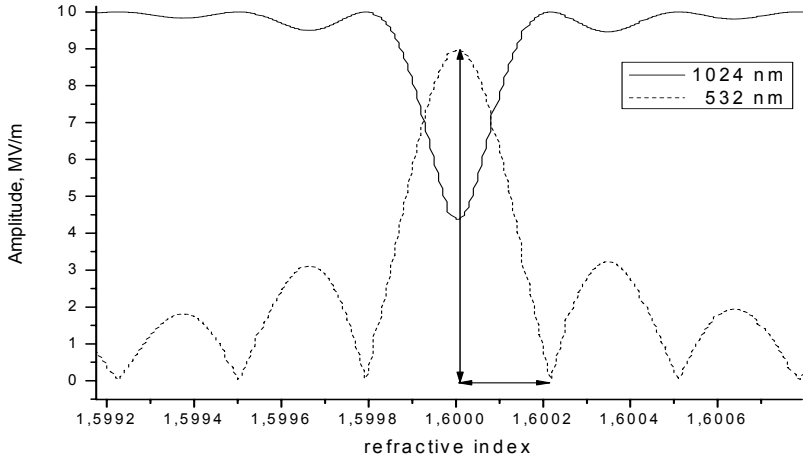

Fig. 92: Electric field amplitude of fundamental (1064 nm) and SH (532 nm) in an inverted waveguide as a function of refractive index (at 1064 nm). Small deviations (modulation) of refractive index of the waveguide core lead to proportional modulation of the SHG signal at the output.

For light modulation in integration optics the Mach-Zehnder interferometer (MZI) is widely used. We have chosen laser etching as a fast method of patterning.

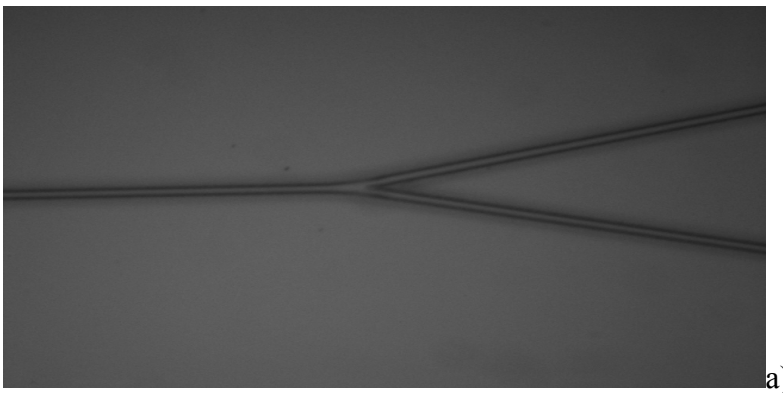
a)

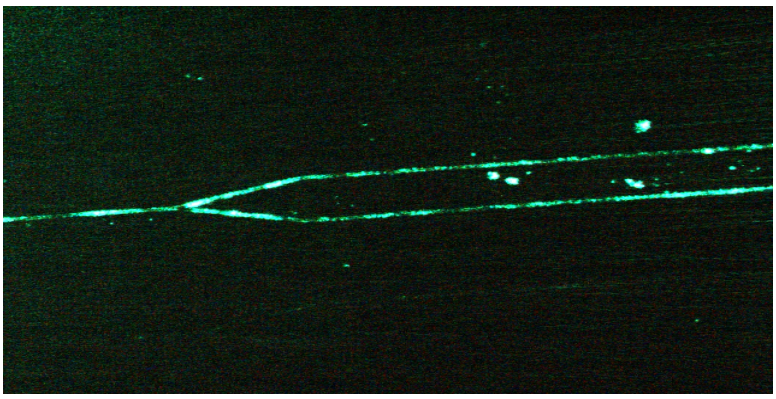
b)

Fig. 93: (a) Mach-Zehnder (MZ) interferometer prepared by means of laser etching, (b) photograph of light propagation within the MZ interferometer (visible by scattered light).

The phase delay induced in one of the arms of a MZI leads to interference at the output. This interference is observed as light modulation. If an applied AC electrical field is the source of phase modulation, then the MZI works as electro-optical modulator.

The intensity dependence of phase in cascaded QPM can be used to convert the MZI into an optical limiter. In this case, when the intensity achieves a certain level the destructive interference switches off the signal on the output.

Summary

Organic materials were investigated with respect to their linear and second-order nonlinear properties.

The present work followed three main directions: development of new organic materials with high nonlinear optical susceptibility, optimization of the preparation process with the aim to obtain films with high second-order nonlinearity and quality required for nonlinear applications, and theoretical analysis of wave propagation and wave coupling in optical waveguides.

Polymer films doped with different nonlinear chromophores were selected as a basis for building integrated optical elements. Preparation of multi-layer structures by means of various methods of film deposition was analyzed in detail. Diverse techniques were discussed and compared with respect to their advantages and disadvantages: spin-coating, dip-casting, and vacuum deposition. It was found that layers prepared by spin-coating have good homogeneity and their thickness can be easily controlled by regulation of the rotation speed of spin-coater. That is important for preparation of waveguides. However, the typical thickness of spin-coated films ranges between tens of nm and several μm. Films fabricated by dip-casting are thick in comparison to films prepared by use of spin-coating and can form a good buffer layer. The core layer can also be deposited in vacuum. In this work there was shown that thin layers created by using vacuum deposition can have second-order nonlinear properties due to the influence of a specially prepared substrate having the ability to orient deposited squarylium chromophores.

Since vacuum-deposition can easily be combined with other methods (like spin- or dip- coating), such layers are promising for use in integrated photonics and for multi-component nonlinear waveguides. In this work unexpected second-order nonlinear properties of films made of centrosymmetric squarylium dye molecules were found. The reason for the appearance of SHG in these films can be explained in terms of inter-molecular charge exchange between neighboring molecules, which leads to an asymmetric charge distribution in the π-electron system of these chromophore. Due to this break of symmetry SHG can be observed. This was, in addition, quantitatively described with the help of quantum chemical calculations.

Guiding and buffer layers were analyzed with the help of various contact and non-contact techniques. For instance the multi-wavelengths prism coupling is precise, self-made instrument that was build. The multi-wavelength device was necessary for full characterization of properties of guiding films. Such a device was constructed using several compact laser sources. The whole range (0.5-1.5 μm) was covered with a step of ca. 100 nanometers. This set of developed characterization set-ups, together with standard measurement techniques allows a full spectroscopic and morphological characterization of materials and films. In case of ultra-thin films, the complex refractive index can be measured by ellipsometry or plasmon resonance spectroscopy. Guiding polymer layers are better characterized by the prism-coupling method. The precision of determination of optical constants by means of the prism coupling technique is one to two orders of magnitude higher than obtained by ellipsometry. Modal dispersion measured with high precision provides essential information for calculation of modal- or quasi-phasematching conditions for various kinds of samples and devices.

In the present work, several methods of inducing nonlinearity in the prepared waveguides were applied. By placing the dye-doped polymer layer within the electrical field with simultaneous heating above their glass transition temperature, the dye molecules (dipoles) rotate along the field direction. Due to such orientation, the material obtains second-order nonlinear optical properties. During this procedure, the optimization of poling is possible. For that rea-

son, the poling dynamics were investigated in-situ. This means that the SHG signal was measured at the same moment when the electrical field was applied and the sample was heated above the glass transition temperature. Varying the field strength and temperature, the optimal poling conditions were found. Moreover, it was demonstrated that poling is possible below the glass transition temperature. That phenomenon can be used for "refreshing" the nonlinear properties of poled films but must also taken into account for estimation of the long-term orientational stability of the poled polymer layers. During exploitation due to natural dipole relaxation even at room temperature the orientational order and, hence, nonlinearity of doped films decreases. One can apply the electrical field and slightly heat up the film. As was shown even heating below glass transition temperature leads to reordering of dipoles and, connected to this, to an increase of the SHG signal.

Some aspects of high-intensity light propagation within strong nonlinear media were analyzed. After poling, dye-doped films demonstrate high second-order nonlinearity, in some cases even higher than inorganic crystals. When a light beam with high intensity propagates within a material with high second-order nonlinearity, second harmonic generation occurs. It is a well-known fact that the efficiency of conversion into second harmonic depends on light intensity. Considering the intensity distribution within the spatial profile of the propagating beam, the analysis of conversion into the second harmonic was performed in this work. The possibility of pulse shape distortion was found in some cases.

For development of nonlinear photonic devices, the light propagation within multilayer structures must be analyzed in detail. Having measured nonlinear properties of deposited multilayer structure and taking into account the measured linear properties of each layer, one can calculate propagation constants and describe the energy exchange between fundamental and second harmonic waves. Finite Elements Analysis was used for numerical computation of properties and for characterization of light propagation within different kinds of self-made waveguides. In addition, some aspects the electro optics such as distribution of DC or RF electrical field in integrated photonic elements were investigated. Often, conductive electrodes, placed near to the core of a waveguide, become a reason for additional losses. In this work, several configurations were found that provide a homogeneous electrical field but do not contribute to significant losses of propagating waves.

Together with the optimization of the waveguide geometry, the nonlinear optical properties of a single molecule can be optimized with the aim to improve efficiency of a photonic device. Using *ab-initio* and semi-empirical methods of quantum chemistry the charge transfer in donor-acceptor molecular system was described. Applying the so-called "two-level model", high-order hyperpolarisabilities responsible for molecular nonlinearity were calculated for a series of dyes. Additional to widely used organic NLO combinations of dye-polymer systems such as DR1-PMMA (Disperse Red 1; Poly-MethylMethAcrylate), the analysis of a series of newly synthesized π-conjugated dyes was performed. For practical testing, the dyes were incorporated with a certain concentration in a polymer matrix and oriented by corona poling. The obtained SHG signal contains information about the nonlinear susceptibility of material. A clear correlation between the measured nonlinear susceptibility and calculated molecular hyperpolarsability was found. In this way, several new dyes created in the project were investigated together with several types of polymers some of which (polyphenylquinoxaline derivates) were not used in NLO before. From more than twenty investigated nonlinear dyes, only three, which show sufficient nonlinearity and stability, have been tested. The same holds for the investigated polymers. Some of them, being suitable for use in the infrared range, show too high losses in the visible range.

Improvement of linear and nonlinear optical properties of dye-doped polymer films can be performed by proper selection of appropriate matrix polymers. As was shown in this work, the optimal polymer for poled films must be not only transparent but also have high glass

transition temperature and low conductivity even being doped with dye molecules. The solubility is also important for formation of smooth layer. Level of losses of material for nonlinear applications must be much lower than for convenient linear optics. In a low-loss medium, the light with higher intensity is able to propagate over a longer distance without significant reduction of intensity. Of course, organic materials in most cases cannot support propagation of very intense light. Even pure PMMA has a damage threshold of about 3 GW/cm^2. Introducing any kind of dopants notably reduces this value. As a rule, dye molecules introduce local micro- and nano- inhomogeneities into the polymer matrix. That leads to light energy scattering. A detailed analysis of dye-polymer miscibility can help to reduce this effect.
Quasi-phase matching (QPM) as a well-known method to reach high conversion ratios from the fundamental (F) to the SH wave was applied to create periodic poling patterns. So, periodically poled domains of a desired size have been prepared. This size fits exactly to the length of periodic energy exchange between the propagating waves. In this work also a new technique of poling, Fibonacci-type poling, was investigated in details. This technique was used for further optimization of light conversion in organic waveguides. As was described in this work, such technique can provide cascaded (i.e. involving two or more nonlinear processes) interaction over any propagation length. Several devices that utilize the concept are proposed. A Fibonacci super lattice can be developed so that energy conversion from the fundamental wave into the second harmonic occurs over the whole propagation distance. This means, in case of waveguide configuration, the efficiency of conversion continuously grows with waveguide length. A small effect induced by external influence (for instance Pockels effect) accumulates along propagation distances. Phase modulation with low driving voltage (several volts) can be achieved. Such electro-optic phase modulators can be used as a part of integrated interferometers for light switching. As an example, a device based on Mach-Zehnder interferometer, utilizing cascaded nonlinearity is described.
Finally, new applications of the well-known theory of second-order nonlinear optics were demonstrated in the frame of integrated photonics. Together with electro-optical devices, some opto-optical devices utilizing a cascading-based nonlinearity were also analyzed using finite elements analysis. For instance, frequency conversion into the third harmonic was realized with the help of two second-order nonlinear processes: SHG ($\omega+\omega\rightarrow2\omega$) followed by SFG ($2\omega+\omega\rightarrow3\omega$). A particular case is the generation of the second harmonic followed by back-conversion into the fundamental wave. As was shown in this work, due to spectral dispersion an intensity-dependent phase shift can be produced. In this case, a scenario similar to the third order nonlinear optical Kerr-effect is realized. Since second-order nonlinearities in poled dye-doped films can be very high, the efficiency of a cascaded process is higher than the direct generation of third harmonics using third-order nonlinearity.

This work demonstrates how cascaded second-order nonlinear processes can be utilized as a base for active elements for integrated photonics. Advantages and disadvantages of application of poled polymer films were discussed. Several new device concepts for all-optical switching and optical limiting were proposed. In addition, several aspects of electro-optical light modulation were discussed. Some problems connected to the presence of electrodes were analyzed in detail with the help of finite element analysis. Possible future developments using nonlinear phase shifts as a base for new ultrafast opto-optical and electro-optical switching devices were discussed.

References

(1) Saleh, B.; Teich, M.; Masters, B. *Journal of Biomedical Optics* **2008**, *13*, 049901.
(2) He, G. S.; Bhawalkar, J. D.; Zhao, C. F.; Prasad, P. N. *Applied Physics Letters* **1995**, *67*, 2433.
(3) Ji, F.; Zhang, B. G.; Li, E. B.; Li, H. F.; Zhou, R.; Zhang, T. L.; Wang, P.; Yao, J. Q. *Optics Communications* **2006**, *262*, 234.
(4) Yuan, W.; Kim, S.; Fetterman, H. R.; Steier, W. H.; Jin, D. L.; Dinu, R. *Ieee Photonic Tech L* **2007**, *19*, 519.
(5) Li, Y. G.; She, W. L. *Acta Phys Sin-Ch Ed* **2007**, *56*, 895.
(6) de Silva, J. P.; Geoghegan, M.; Higgins, A. M.; Krausch, G.; David, M. O.; Reiter, G. *Physical Review Letters* **2007**, *98*.
(7) Yildiz, U. H.; Sahin, E.; Akhmedov, I. M.; Tanyeli, C.; Toppare, L. *J Polym Sci Pol Chem* **2006**, *44*, 2215.
(8) Wang, F.; Yang, J. Y.; Chen, L. M.; Jiang, X. Q.; Wang, M. H. *Ieee Photonic Tech L* **2006**, *18*, 421.
(9) Shim, N.; Moon, B.; Lee, H. *React Funct Polym* **2006**, *66*, 1506.
(10) Yuan, W.; Kim, S.; Steier, W. H.; Fetterman, H. R. *Ieee Photonic Tech L* **2005**, *17*, 2568.
(11) Xu, G. Y.; Liu, Z. F.; Ma, J.; Liu, B. Y.; Ho, S. T.; Wang, L.; Zhu, P. W.; Marks, T. J.; Luo, J. D.; Jen, A. K. Y. *Optics Express* **2005**, *13*, 7380.
(12) Bortnik, B.; Hung, Y. C.; Tazawa, H.; Seo, B. J.; Luo, J.; Alex, K. Y. J.; Steier, W. H.; Fetterman, H. R. *Ieee J Sel Top Quant* **2007**, *13*, 104.
(13) Michalak, R. J.; Kuo, Y.; Nash, F. D.; Szep, A.; Caffey, J. R.; Payson, P. M.; Haas, F.; McKeon, B. F.; Cook, P. R.; Brost, G. A. *Ieee Photonic Tech L* **2006**, *18*, 1207.
(14) Paloczi, G. T.; Huang, Y.; Yariv, A.; Luo, J.; Alex, K. Y. J. *Applied Physics Letters* **2004**, *85*, 1662.
(15) Song, R.; Yick, A.; Steier, W. H. *Applied Physics Letters* **2007**, *90*, 191103_1.
(16) Armstrong, J. A.; Bloembergen, N.; Ducuing, J.; Pershan, P. S. *Phys. Rev.* **1962**, *127*, 1918.
(17) Lagatsky, A. A.; Brown, C. T. A.; Sibbett, W.; Holmgren, S. J.; Canalias, C.; Pasiskevicius, V.; Laurell, F.; Rafailov, E. U. *Optics Express* **2007**, *15*, 1155.
(18) Loza-Alvarez, P.; Ebrahimzadeh, M.; Sibbett, W.; Reid, D. T.; Artigas, D.; Missey, M. *J Opt Soc Am B* **2001**, *18*, 1212.
(19) Loza-Alvarez, P.; Reid, D. T.; Faller, P.; Ebrahimzadeh, M.; Sibbett, W. *J Opt Soc Am B* **1999**, *16*, 1553.
(20) [Anon] *Laser Focus World* **1997**, *33*, 9.
(21) Khanarian, G.; Mortazavi, M. A.; East, A. J. *Applied Physics Letters* **1993**, *63*, 1462.
(22) Ay, F.; Kocabas, A.; Kocabas, C.; Aydinli, A.; Agan, S. *Journal of Applied Physics* **2004**, *96*, 7147.
(23) Bohn, P. W.; Fell, N. F.; Hughes, K. D. *Abstracts of Papers of the American Chemical Society* **1991**, *202*, 70.
(24) Chen, K. X.; Chu, P. L.; Chan, H. P. *Optics Communications* **2005**, *244*, 153.
(25) de Ridder, R. M.; Driessen, A.; Rikkers, E.; Lambeck, P. V.; Diemeer, M. B. J. *Opt Mater* **1999**, *12*, 205.
(26) Zubia, J.; Irusta, U.; Arrue, J.; Aguirre, A. *Ieee Photonic Tech L* **1998**, *10*, 1578.
(27) Delahaye, E.; Tancrez, N.; Yi, T.; Ledoux, I.; Zyss, J.; Brasselet, S.; Clement, R. *Chem Phys Lett* **2006**, *429*, 533.

(28) Fiebig, M.; Pavlov, V. V.; Pisarev, R. V. *J Opt Soc Am B* **2005**, *22*, 96.
(29) Acharya, S.; Krief, P.; Khodorkovsky, V.; Kotler, Z.; Berkovic, G.; Klug, J. T.; Efrima, S. *New J Chem* **2005**, *29*, 1049.
(30) Berlouis, L. E. A.; Wark, A.; Cruickshank, F. R.; Antoine, R.; Galletto, P.; Brevet, P. F.; Girault, H. H.; Gupta, S. C.; Chavada, F. R.; Kumar, S.; Garg, A. K. *Semicond Sci Tech* **1998**, *13*, 1117.
(31) Hehre, W. *Accounts of Chemical Research* **1976**, *9*, 399.
(32) Pastore, G.; Smargiassi, E.; Buda, F. *Physical Review A* **1991**, *44*, 6334.
(33) Bingham, R.; Dewar, M.; Lo, D.; Ramsden, C.; Eilers, J.; O'Leary, B.; Duke, B.; Liberles, A.; Whitman, D.; Gordon, M. *Journal Cover* **1975**, *97*, 1285.
(34) Dewar, M.; Zoebisch, E.; Healy, E.; Stewart, J. *J Am Chem Soc* **1985**, *107*, 3902.
(35) Boyd, R. W. *Nonlinear Optics*; Academic Press, 2003.
(36) Singer, K.; Kuzyk, M.; Sohn, J. *Journal of the Optical Society of America B* **1987**, *4*, 968.
(37) Ohring, M. *The material science of thin films*; Academic Press, Inc: San Diego, 1991.
(38) Ohring, M. *The materials science of thin films*; Academic Press: Boston, 1992.
(39) Middleman, S.; Hochberg, A. K. *Process engineering analysis in semiconductor device fabrication*; McGraw-Hill New York, 1993.
(40) Sellmeier, W. *Pogg. Ann. Physik. Chem.* **1871**, *143*, 272.
(41) Booij, H.; Thoone, G. *Rheol Acta* **1982**, *21*, 15.
(42) Forouhi, A. R.; Bloomer, I. *Phys. Rev. B* **1986**, *7018*.
(43) Forouhi, A. R.; Bloomer, I. *Phys. Rev. B* **1988**, *1865*.
(44) Born, M.; Wolf, E.; Bhatia, A. B. *Principles of optics*; Pergamon Press New York, 1975.
(45) Lee, H. S.; Kang, T. D.; Lee, H.; Lee, S. K.; Kim, J. H.; Choi, D. H. *Journal of Applied Physics* **2007**, *102*.
(46) Simpson, G. J. *Abstracts of Papers of the American Chemical Society* **2006**, *231*.
(47) Plocinik, R.; Simpson, G. J. *Abstracts of Papers of the American Chemical Society* **2005**, *230*, U199.
(48) Flueraru, C.; Schrader, S.; Zauls, V.; Motschmann, H.; Stiller, B.; Kiebooms, R. *Synthetic Metals* **2000**, *111–112*, 603.
(49) Tompkins, H. G. *Thin Solid Films* **2004**, *455-56*, 772.
(50) Tompkins, H. G.; Tasic, S.; Baker, J.; Convey, D. *Surface and Interface Analysis* **2000**, *29*, 179.
(51) Tompkins, H. G.; Tiwald, T.; Bungay, C.; Hooper, A. E. *Journal of Vacuum Science & Technology A* **2006**, *24*, 1605.
(52) Nalwa, H. S.; Miyata, S. *Nonlinear Optics of Organic Molecules and Polymers*; CRC Press, 1996.
(53) Kajzar, F.; Swalen, J. D. *Organic Thin Films for Waveguiding Nonlinear Optics*; Gordon & Breach, 1996.
(54) Maker, P.; Terhune, R.; Nisenoff, M.; Savage, C. *PHYSICAL REVIEW LETTERS* **1962**, *8*, 21.
(55) Prasad, P.; Williams, D. **1991**.
(56) Wood, G. L.; Sharp, E. J. In *Electro-optics handbook*; Ronald, W. W., Ediger, M. N., Eds. 2000.
(57) Cattaneo, S.; Kauranen, M. *Optics Letters* **2003**, *28*, 1445.
(58) Cattaneo, S.; Vuorimaa, E.; Lemmetyinen, H.; Kauranen, M. *J Chem Phys* **2004**, *120*, 9245.
(59) Dmitriev, V. G.; L.V, T. *Applied Nonlinear Optics*; Fizmatlit: Moscow, 2004.

(60) TANAS, R. In *MODERN NONLINEAR OPTICS*; Second Edition ed.; Evans, M. W., Rice., P. a. S. A., Eds.; JOHN WILEY & SONS, INC.: 2001.
(61) Flueraru, C.; Grover, C. P.; Schrader, S. *Optical and Quantum Electronics* **2002**, *34*, 1119.
(62) Furukawa, Y.; Markgraf, S.; Sato, M.; Yoshida, H.; Sasaki, T.; Fujita, H.; Yamanaka, T.; Nakai, S. *APPLIED PHYSICS LETTERS* **1994**, *65*, 1480.
(63) Paschotta, R.; Consulting, R. P. P. *Encyclopedia of Laser Physics and Technology*; Wiley-VCH; John Wiley [distributor], 2008.
(64) Salaneck, W. R.; Stafström, S.; Bredas, J. L. *Conjugated polymer surfaces and interfaces. Electronic and chemical structure of interfaces for polymer light emitting devices.*; Cambridge University Press: Cambridge, 1996.
(65) Harris, D. C.; Bertolucci, M. D. *Symmetry and spectroscopy: an introduction to vibrational and electronic spectroscopy*; Oxford University Press, 1978.
(66) Hypercube, I.; Hypercube, Inc.: 2002.
(67) Oudar, J. L.; Chemla, D. S. *Optics Communications* **1975**, *13*, 164.
(68) J. Zyss, J. L.; Oudar, J. L. *Phys. Rev. A* **1982**, *26*, 2016.
(69) Oudar, J. L.; Chemla, D. S. *J. Chem. Phys.* **1977**, *66*, 2664.
(70) Bosshard, C.; Florsheimer, M.; Hulliger, J.; Bonnett, R.; Bosshard, C. B.; Kaatz, P.; Pretre, P. *Organic Nonlinear Optical Materials*; Taylor & Francis, 1995.
(71) Clark, R. J. H.; Hester, R. E. *Spectroscopy* **1993**.
(72) Augl, J. M.; Booth, H. J. *Journal of Polymer Science: Polymer Chemistry Edition* **1973**, *11*, 2179.
(73) Hergenrother, P. M.; Levine, H. H. *Journal of Polymer Science Part A-1: Polymer Chemistry* **1967**, *5*, 1453
(74) Stille, J. K.; Williamson, J. R. *Journal of Polymer Science Part A: General Papers* **1964**, *2*, 3867.
(75) Wrasidlo, W.; Augl, J. M. *Journal of Polymer Science Part B: Polymer Letters* **1969**, *7*, 281
(76) Wrasidlo, W.; Augl, J. M. *Journal of Polymer Science Part A-1: Polymer Chemistry* **1969**, *7*, 3393
(77) Wrasidlo, W. J.; Augl, J. M. *Polymer preprints* **1969**, *10*, 1353.
(78) OBrien, D.; Weaver, M. S.; Lidzey, D. G.; Bradley, D. D. C. *Applied Physics Letters* **1996**, *69*, 881.
(79) Yoshimura, D.; Seki, K.; Miyamae, T.; Ishii, H.; Hasegawa, S.; Okudaira, K. K.; Ueno, N. *Surface Review and Letters* **2002**, *9*, 407.
(80) Lee, K. S.; Bosshard, C. *Polymers for Photonics Applications I*; Springer, 2002.
(81) Tanabe, Y. *Macromolecular Science and Engineering: New Aspects*; Springer, 1999.
(82) Cook, M.; Watts, D. C.; Williams, G. *T Faraday Soc* **1970**, *66*, 2503.
(83) Williams, G.; Watts, D. C. *T Faraday Soc* **1970**, *66*, 80.
(84) Shlesinger, M. F. *Annu Rev Phys Chem* **1988**, *39*, 269.
(85) Weiss, G. H.; Bendler, J. T.; Shlesinger, M. F. *Macromolecules* **1988**, *21*, 521.
(86) Soesanto, T.; Williams, M. *The Journal of Physical Chemistry* **1981**, *85*, 3338.
(87) Ferry, J. *Viscoelastic properties of polymers*; John Wiley & Sons Inc, 1980.
(88) Scherer, G. **1986**.
(89) Andrews, J. H.; Khaydarov, J. D. V.; Singer, K. D.; Hull, D. L.; Chuang, K. C. *J. Opt. Soc. Am. B* **1995**, *12*, 2360.
(90) Poga, C.; Brown, T. M.; Kuzyk, M. G.; Dirk, C. W. *J. Opt. Soc. Am. B* **1995**, *12*, 531.
(91) Enokida, T.; Suda, Y.; Toyo Ink Mfg Co, Japan Jpn. Kokai Tokkyo Koho: 1994; Vol. JP 06220438.

(92) Ashwell, G. J.; Roberts, M. P. S.; Rees, N. D.; Bahra, G. S.; Brown, C. R. *Langmuir* **1998**, *14*, 5279.
(93) Gritsenko, K. P.; Dimitriev, O. P.; Glasirin, N. P.; Schrader, S.; Brehmer, L. In *European Conference on Organic Electronics and Related Phenomena 2001 - ECOER'01, 18 - 21 November 2001*; Wong, J. E., Albrecht, F., Oda, M., Neher, D., Schrader, S., Eds.; The University of Potsdam: Potsdam, Germany, 2001, p 210.
(94) Gritsenko, K. P.; Dimitriev, O. P.; Grinko, D. O.; Schrader, S.; Brehmer, L. In *Applications of Photonic Technology 5*; Lessard, R. A., Lampropoulos, G. A., Schinn, G. W., Eds.; SPIE—The International Society for Optical Engineering: Bellingham, WA, USA, 2002; Vol. 4833, p 487.
(95) Gritsenko, K. P.; Dimitriev, O. P.; Kachkovsky, A. D.; Kurdiukov, V. V.; Slominsky, Y. L.; Tolmachev, A. I.; Tanaka, T.; Schrader, S.; Brehmer, L. In *European Conference on Organic Electronics and Related Phenomena 2001 - ECOER'01, 18 - 21 November 2001*; Wong, J. E., Albrecht, F., Oda, M., Neher, D., Schrader, S., Eds.; The University of Potsdam: Potsdam, Germany, 2001, p 208.
(96) Gritsenko, K. P.; Dimitriev, O. P.; Kislyk, V. V.; Getsko, O. M.; Schrader, S.; Brehmer, L. *Colloids and Surfaces A: Physicochemical and Engineering Aspects* **2002**, *198-200*, 625.
(97) Gritsenko, K. P.; Slominski, Y. L.; Tolmachev, A. I.; Tanaka, T.; Schrader, S.; Brehmer, L.; Thierry, A.; Wittmann, J. C. In *Applications of Photonic Technology 5*; Lessard, R. A., Lampropoulos, G. A., Schinn, G. W., Eds.; SPIE—The International Society for Optical Engineering: Bellingham, WA, USA, 2002; Vol. 4833, p 482.
(98) Grytsenko, K. P.; Dimitriev, O. P.; Kislyk, V. V.; Getsko, O. M.; Schrader, S.; Brehmer, L. In *9th International Conference on Langmuir Blodgett Films, LB9, 28 August - 3 September 2000* Potsdam, Germany, 2000; Vol. 28.
(99) Ashwell, G. J.; Jefferies, G.; Rees, N. D.; Williamson, P. C.; Bahra, G. S.; Brown, C. R. *Langmuir* **1998**, *14*, 2850.
(100) Ashwell, G. J. *Adv Mater* **1996**, *8*, 248.
(101) Ashwell, G. J.; Handa, T.; Leeson, P.; Skjonnemand, K.; Jefferies, G.; Green, A. *J Mater Chem* **1998**, *8*, 377.
(102) Ashwell, G. J.; Bahra, G. S.; Brown, C. R.; Hamilton, D. G.; Kennard, C. H. L.; Lynch, D. E. *J Mater Chem* **1996**, *6*, 23.
(103) Mabaya, N.; Lagasse, P. E. *Microwave Symposium Digest, 1980 MTT-S International* **1980**, *80*, 329.
(104) DeSalvo, R.; Hagan, D. J.; Sheik-Bahae, M.; Stegeman, G. I.; van Stryland, E. W.; Vanherzeele, H. *Opt. Lett* **1992**, *17*, 28.

Appendix

In mathematics, the Jacobi elliptic functions are a set of basic elliptic functions that have historical importance with also many features that show up important structure, and have direct relevance to some applications (e.g. the equation of the pendulum). They also have useful analogies to the functions of trigonometry, as indicated by the matching notation *sn* for *sin*. The Jacobi elliptic functions occur more in practical problems than the Weierstrass elliptic functions. They were introduced by Carl Gustav Jakob Jacobi, around 1830.

The two basic functions are denoted , *sn(u,k)* and *cn(u,k)*, where *k* is known as the elliptic modulus. They arise from the inversion of the elliptic integral of the first kind,

$$u = F(\phi, k) = \int_0^{\phi} \frac{dt}{\sqrt{1 - k^2 \sin^2 t}}$$

where $0<k^2<1$, k is the elliptic modulus, and $\phi = am(u,k) = am(u)$ is the Jacobi amplitude, giving

$$\phi = F^{-1}(u,k) = am(u,k)$$

From this, it follows that

$$\sin\phi = \sin(am(u,k)) = sn(u,k)$$
$$\cos\phi = \cos(am(u,k)) = cn(u,k)$$

These functions are doubly periodic generalizations of the trigonometric functions satisfying:

$$sn(u,0) = \sin u$$
$$cn(u,0) = \cos u$$
$$sn(u,1) = \tanh u$$
$$cn(u,1) = \operatorname{sech} u$$

(Weisstein, Eric W. "Jacobi Elliptic Functions." From MathWorld--A Wolfram Web Resource. http://mathworld.wolfram.com/JacobiEllipticFunctions.html)